Molecular Determinants of Gating at the Potassium Channel Selectivity Filter

Julio F. Cordero-Morales

Caracas, Venezuela

Licentiate, Universidad Central de Venezuela, 2001

A Dissertation presented to the Graduate Faculty of the University of Virginia in

Candidacy for the Degree of Doctor of Philosophy

Department of Molecular Physiology and Biological Physics

University of Virginia

May, 2008

_____

_____

_____

_____

_____

DEDICATION

This thesis is dedicated to Valeria who is my source of motivation and inspiration. She is not only my wife but also the person that everyday teaches me and makes my life enjoyable. I have no words to express my appreciation to Valeria, whose dedication, love and persistent confidence inspired me during my PhD studies. I am deeply indebted to Valeria for her support, guidance, friendship and encouragement during this part of my life. For these and many more reasons, this thesis is dedicated to her and all my future accomplishments would be because of Valeria and my Family.

ACKNOWLEDGEMENTS

I would like to thank my grandparents (Francisco and Mercedes), Simon, and Ana for their support during my early steps of my biology studies. I would like to thank my Father (Julio), Ana, and my siblings (Francisco, Rafael, and Mariana) for their special support during my PhD studies. I would also like to acknowledge my family in-law for their support (Enrique, Lulu, Juan, Maria Gabriela, Daniela, Juan Andres, Arthur, Carla, Carlos Eduardo, Eduardo and Ana). I feel very happy to be part of this family.

I thank my undergraduate advisor, Pedro Romero, for seeding me the interest for ion channels and for his guidance towards Eduardo Perozo laboratory. I am grateful with my old-time friend Carlo for sharing with me my passion for biology and always been on my side.

I would like to express my sincere appreciation to my advisor, Eduardo Perozo for his guidance, friendship, teaching, encouragement and continuous support throughout the course of my pH studies. I am especially grateful for his willingness to always be there to listen, to talk about his and my ideas and to give advice either for my professional career or personal life. An important virtue that I learn from him is the means to think in different ways to approach a research problem that would be one of the most important knowledge that I would use in my scientific life. I feel that it was a privilege to have Eduardo as my advisor during my pH studies.

My special thanks to Vishwath Jogini, for his friendship, his constant desire to help me, for sharing and teaching me his knowledge in Molecular Dynamics and X-ray crystallography, for his willingness to spend time with me brain-storming about results

and new experiment, and for his enthusiasm to perform more and more experiments. One of the more interesting and enjoyable parts of my PhD was sharing it with Vish, and I feel that it was a privilege to interact with him during this time.

I thank my entire laboratory colleagues (former and current members) for their help and support during my PhD studies (Chris Ptak, Jesus Romero, Toi and Thep Sompornpisut, Yi-shuan Liu, Jie Wu, Carlos Gonzalez, Olivier Dalmas, and Jose Santos). In particular, I would like to thank Sudha Chakrapani for her friendship, her enthusiasm to hear my ideas, her continuous teaching about ion channel analysis, and making me grow as a scientist. I also thank, Luis Cuello for sharing and discussing his passion about ion channels. I gratefully acknowledge Marien Cortes for her support, her collaboration in my projects and for making the laboratory a nice place to work. I sincerely thank H. Raghuraman for sharing with me his passion about science and for educating me about fluorescence spectroscopy. I feel fortunate and grateful for sharing my PhD years with this group of excellent scientists.

Also, I would like to thank Benoit Roux for his valuable contribution and advice during this thesis. I thank Anthony Lewis and Steve Goldstein for providing access and experimental advice of two electrode voltage clamp system. I thank Marcos Sotomayor for his help in molecular dynamics, critical reading and discussion of chapter 4.

I thank all the Professors of the University of Virginia who taught me during the course work. I specially thank Dr. Nakamoto, not only for being my Professor, Advisor and for his help during my PhD studies, but also for his friendship. I also thank Dr. Bayliss for being part of my committee and more importantly for allowing

me to learn two electrode voltage clamp in his laboratory, which was an important technique used in this work. I would like to express my gratitude to Dr. Wiener and Dr. Szabo for their help during my thesis and been part of my committee. I feel lucky to have been learnt from this group of people and grow as a scientist by their side. I gratefully thank Pam Mullinex, Carol Yowell, Cathy Black, Laura Wright for their help during my PhD studies.

Finally, again I would like to thank everybody who was important in the development of this thesis.

TABLE OF CONTENTS

CHAPTER 1: Abstract, Introduction and Thesis Outline

CHAPTER 2: Molecular determinants of gating at the KcsA selectivity filter

CHAPTER 3: Voltage-dependent gating at the KcsA selectivity filter

CHAPTER 4: Molecular driving forces determining potassium channel slow inactivation

CHAPTER 5: A multipoint hydrogen bond network driving potassium channel

C-type inactivation

CHAPTER 6: Multiple gating modes in KcsA are determined by the selectivity filter dynamics

CHAPTER 7: Conclusions, Future Perspectives and References

LIST OF FIGURES AND TABLES

CHAPTER 1: Introduction

CHAPTER 2: Molecular determinants of gating at the K$^+$ channel selectivity filter

CHAPTER 3: Voltage-dependent gating at the KcsA selectivity filter

CHAPTER 4: Molecular driving forces determining potassium channel slow inactivation

CHAPTER 5: A multipoint hydrogen bond network driving potassium channel C-type inactivation

CHAPTER 6: Multiple gating modes in KcsA are determined by the selectivity filter dynamics

PUBLICATIONS

1) **Cordero-Morales J.F**., Jogini V., Chakrapani S., and Perozo E. (2008). A multipoint hydrogen bond network driving potassium channel C-type inactivation. (in preparation)

2) **Cordero-Morales J.F.**, Jogini V., Lewis A., Vásquez V., Cortes D.M, Roux B., and Perozo E. (2007). Molecular driving forces determining potassium channel slow inactivation. *Nature Structural and Molecular Biology*, 14(11): 1062-1069.

3) Chakrapani S., **Cordero-Morales J.F.**, and Perozo E. (2007). A quantitative description of KcsA gating. Macroscopic current I. *Journal of General Physiology* 130: 465-478.

4) Chakrapani S., **Cordero-Morales J.F.**, and Perozo E. (2007). A quantitative description of KcsA gating. Single channel current II. *Journal of General Physiology* 130: 479-496.

5) **Cordero-Morales J.F.**, Cuello L., Zhao Y., Jogini V., Cortes D.M., Roux B., and Perozo E. (2006). Molecular determinants of gating at the potassium channel selectivity filter. *Nature Structural and Molecular Biology* 13(4):311-318. (Journal Cover).

6) **Cordero-Morales J.F.**, Cuello L., and Perozo E. (2006). Voltage-dependent gating at the potassium channel selectivity filter. *Nature Structural and Molecular Biology* 13(4):319-321.

7) Blunck R., **Cordero-Morales J.F.**, Cuello L., Perozo E., and Bezanilla F. (2006). Detection of the opening of the bundle crossing in KcsA with fluorescence lifetime spectroscopy reveals the existence of two gates for ion conduction. *Journal of General Physiology*. 128(5):569-581.

CONFERENCES

1) **Cordero-Morales J.F.**, Jogini V., Chakrapani S and Perozo E. (2008). A multi-point hydrogen bond network driving KcsA C-type inactivation. *52th Annual Meeting of the Biohysical Society.* Long Beach, CA. (Poster).

2) Chakrapani S., **Cordero-Morales J.F.**, Cuello L and Perozo E. (2008). C-type inactivation from the perspective of permeant ions. *52th Annual Meeting of the Biohysical Society.* Long Beach, CA. (Poster).

3) Raghuraman H., **Cordero-Morales J.F** and Perozo E. (2008). Gating-related conformational changes in the outer vestibule of KcsA: A functional and spectroscopic analysis. *52th Annual Meeting of the Biohysical Society.* Long Beach, CA. (Poster).

4) Vásquez V., **Cordero-Morales J.F.**, Cortes D and Perozo E. (2008). Structural dynamics of MscS transmembrane segments in the open state. A site-direct spin labelling analysis. *52th Annual Meeting of the Biohysical Society.* Long Beach, CA. (Platform).

5) **Cordero-Morales J.F.**, Cortes D., Chakrapani S., Jogini V., Cuello L., Vásquez V., and Perozo E. (2007). Multiple gating modes in KcsA are determined by the selectivity filter dynamics. *51th Annual Meeting of the Biohysical Society.* Baltimore, MA. (Platform).

6) Cuello L., Chakrapani S., **Cordero-Morales J.F.**, and Perozo E. (2007). Molecular basis of the conformational coupling between K$^+$ channels activation and inactivation gates. *51th Annual Meeting of the Biohysical Society.* Baltimore, MA. (Platform).

7) Jogini V., **Cordero-Morales J.F.**, Roux B., and Perozo E. (2007). Structural changes associated with gating events at the KcsA selectivity filter: A molecular dynamics study. *51th Annual Meeting of the Biohysical Society.* Baltimore, MA. (Poster).

8) **<u>Cordero-Morales J.F.</u>**, Cuello L., Zhao Y., Jogini V., Cortes D.M., Roux B. and Perozo E. (2006). Molecular determinants of gating at the potassium channel selectivity filter. *50th Annual Meeting of the Biohysical Society.* Salt Lake City, UT. (Platform).

9) **<u>Cordero-Morales J.F.</u>**, Cuello L. and Perozo E. (2006). Voltage-dependent gating at the potassium channels selectivity filter. *50th Annual Meeting of the Biohysical Society.* Salt Lake City, UT. (Poster).

10) <u>Chakrapani S</u>., **Cordero-Morales J.F.**, and Perozo E. (2006). Kinetic analysis of gating mechanisms in KcsA using macroscopic and single-channel currents. *50th Annual Meeting of the Biohysical Society.* Salt Lake City, UT. (Poster).

11) <u>Blunck R</u>., **Cordero-Morales J.F.**, Cuello L., Perozo E., and Bezanilla F. (2006) Monitoring the opening of KcsA using single channel fluorescence spectroscopy. *50th Annual Meeting of the Biohysical Society.* Salt Lake City, UT. (Poster).

12) **<u>Cordero-Morales J.F.</u>** (Invited Speaker, 2006) Molecular determinants of gating at the K^{+} channel selectivity filter. International Symposium on "Membrane Proteins and Cellular Dynamics". University of Osnabruck. Germany. http://www.physik.uni-osnabrueck.de/de/1953.htm.

13) <u>Blunck R</u>., **Cordero-Morales J.F.**, Cuello L., Perozo E., and Bezanilla F. (2005). Detecting the opening of the bundle crossing in KcsA using fluorescence lifetime spectroscopy. *49th Annual Meeting of the Biohysical Society.* Long Beach, CA. (Poster).

14) **<u>Cordero-Morales J.F.</u>**, Cuello L., and Perozo E. (2003) Modulation of gating in KcsA by Voltage. *47th Annual Meeting of the Biohysical Society.* San Antonio, TX. (Poster).

AWARDS

1) **Cordero-Morales J.F.**, Jogini V., Chakrapani S and Perozo E. (2008). A multi-point hydrogen bond network driving KcsA C-type inactivation. *52th Annual Meeting of the Biohysical Society.* Long Beach, CA. (Poster). Student Research Achievement Award.

2) **Cordero-Morales J.F.**, Structural, Computational Biology and Biophysics 2007 Outstanding Graduate Student (University of Virginia).

ABBREVIATIONS

Å	Angstrom
CW-EPR	Continuous wave electron paramagnetic resonance.
DDM	n-Dodecyl-β-D-Maltopyranoside.
DM	n-Decyl-β-D-Maltopyranoside.
DPPC	Dipalmitoylphosphatidylcholine
EPR	Electron Paramagnetic Resonance spectroscopy
Fab	Fragment of antibody
Fo-Fc	Electron density maps
HEPES	4-(2-hydroxyethyl)-1-piperazineethanesulfonic acid
hERG	human ether-à-go-go related gene, voltage gated potassium channels
IPTG	Isopropyl-β-D-thiogalactopyranoside.
KcsA	Prokaryotic potassium channel from *Streptomyces lividans*
Kv	Voltage gated potassium channels
KvAP	Prokaryotic voltage gated potassium channel
Kv1.2	Voltage-gated K^+ channel from rat brain
MD	Molecular dynamics
MOPS	4-morpholine propanesolfonic acid
MthK	Prokaryotic calcium gated potassium channel
MTSES	2-sulfonatoethyl methanethiosulfonate sodium salt
NMG	N-methyl-glucamine
PBS	Phosphate-buffer saline

PDB	Protein Data Bank
PEG400	Polyethylene Glycol 400
PMF	Potential of Mean Force
PMSF	Phenylmethylsulfonyl fluoride
P_o	Open Probability
QA	Quaternary ammonium
RMSD	Root Mean Square Deviation.
S0-S4	Potassium ion binding sites within the selectivity filter
Shaker	Voltage gated potassium channels from *Drosophila melanogaster*
ShIR	Shaker Δ4-46 channel, lacking the fast N-type inactivation.
Spin label	(1-Oxyl-2,2,5,5-tetramethylpyrrolidin-3-yl) Methyl Methanethiosulfonate.
TBA	Tetrabutylammonium
TCEP	Tris-(2-Carboxyethyl)-Phosphine Hydrochloride.
TCYP	Tris-(2-Cyanoethyl)-Phosphine.
TEA	Tetraethylammonium
TM	Transmembrane.
WT	wild-type
z_{eq}	Equivalent charge

CHAPTER 1: Abstract, Introduction and Thesis Outline

1.1 ABSTRACT

KcsA is a prokaryotic proton-gated potassium channel from *Streptomyces lividan*s, whose open probability is modulated by transmembrane voltage but not by pH. Its gating is dominated at steady state by a previously unrecognized inactivation process that is mechanistically equivalent to the C-type inactivation associated with eukaryotic voltage-dependent K^+ channels. This inactivation is a wide spread regulation process in ion channels, however the molecular mechanism and conformational changes during this process are not well understood. In KcsA, the inactivation process is suppressed by the E71A mutation at the C-terminal region of the pore helix. In addition, two KcsA (E71A) crystal structures reveal large structural excursions of the selectivity filter during ion conduction and provide a glimpse of the range of conformations available to this region of the channel during gating. The hydrogen-bond network at the selectivity filter (Glu71-Asp80 and Trp67-Asp80) is the driving force that promotes filter instability through a compression of the selectivity filter parallel to the permeation pathway, which energetically biases it towards the inactivated conformation. This mechanism found in KcsA might serve as the basis for C-type inactivation in the K^+ channel family. Taken together, the results from this work provide a plausible framework to understand the molecular mechanism for C-type inactivation in K^+ channels.

1.2 INTRODUCTION

1.2.1 Potassium channels

All living cells are enclosed by the plasma membrane that acts as a barrier between the cytoplasm and the extracellular space. An exquisite ionic balance between these two compartments is accomplished by the presence of specialized proteins, such as ion channels, transporters, pumps and exchangers. Ion channels are macromolecular pores that allow the flow of ions with high selectivity through the cell membrane with a rate close to the diffusion limit (10^8 ions per second). Moreover, channels function are associated with regulation of electrical activity, signal transduction and osmotic balance among others. Their diversity in function is achieved by differences in ion conduction, selectivity and gating mechanism(Hille, 2001; Molleman, 2002).

Potassium channels are membrane proteins that catalyze the transfer of K^+ ions with high efficiency and selectivity through cell membranes. One way to classify K^+ channels is according to their membrane topology (two and six transmembrane segments, and two pore domain K^+ channels, Fig. 1). The most studied group comprises, the voltage dependent channels that contain a hydrophobic core with six transmembrane segments including the last two TM's which form the pore domain (Fig. 1, left panel). Voltage-dependent K^+ channels belong to a broad family, which also includes voltage-activated Na^+ and Ca^{++} channels, as well as inward rectifiers and cyclic nucleotide activated channels (Hille, 2001). In excitable cells, voltage-dependent K^+ channels help to set the membrane resting potential, to determine the action potential duration and to regulate periods of intense activity, among other functions. When these channels open, they shift the membrane potential of the cell towards the equilibrium potential of K^+ (–90 mV); in

contrast, the opening of Na^+ or Ca^{++} channels force the potential to positive levels (+40 mV or greater). Thus, one can imagine the cell as a dipole that is either positive or negative depending on the relative balance of ion channels, and whether or not channels are open at any given time. In higher organisms, K^+ channel malfunction can produce periods of electrical hyper-excitability, which in the heart can induce cardiac arrhythmias. For this reason, their study constitutes a high priority for pharmaceutical companies for the discovery of improved drugs (Brammar, 1999; Hille, 2001).
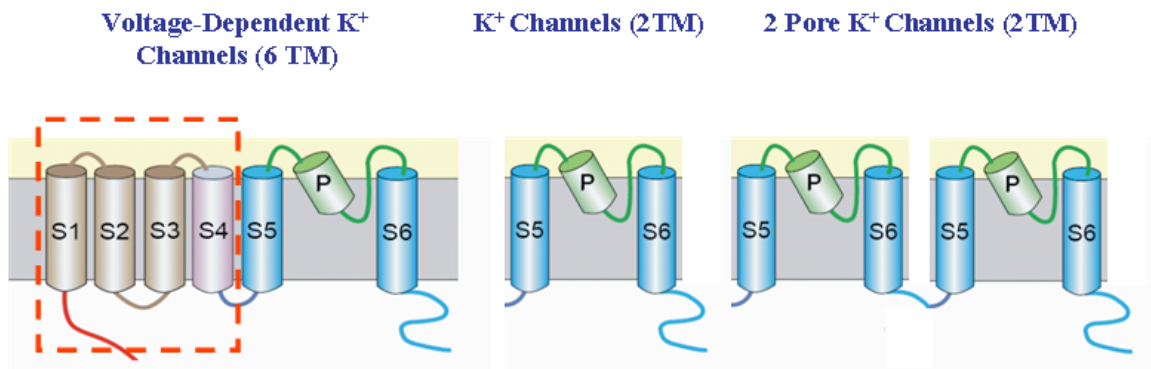
Figure 1 K^+ channels membrane topology

1.2.1.1 KcsA is a two transmembrane segments prokaryotic K$^+$ channel

The second family is formed by pore-forming subunits that have only two transmembrane segments including the pore domain (Fig. 1, middle panel). One of the members of the second family is KcsA, a K$^+$ channel from *Streptomyces lividans* activated by intracellular proton concentration (Fig. 2a,b and c), as demonstrated by macroscopic Rb$^+$ assays and single channel recordings (Cuello et al., 1998; Heginbotham et al., 1999). Moreover, KcsA activity is also modulated by transmembrane voltage (Fig. 2c) as there is a 50 fold increase in its open probability at steady state from +150 mV to -150 mV transmembrane voltage (Cuello et al., 1998). Later on, after the crystal structure determination of KcsA (3.2 and 2 Å resolution) many questions have been resolved, and at the same time new ones have emerged (Doyle et al., 1998; Zhou et al., 2001b).

The structure of KcsA comprises a pore formed by four identical subunits that surround a central ion conduction pathway (Fig. 2d and 3). Each subunit has two transmembrane segments, TM1 in the periphery of the channel, and TM2 lining the permeation pathway (Fig. 4a). Towards the extracellular side of the channel is the selectivity filter (Fig. 3 and 4a, highly conserved in the K$^+$ channel family), where ions are dehydrated by an extended chain that includes the so-called signature sequence (Heginbotham et al., 1994).

The high resolution structure of KcsA selectivity filter (2.0 Å) in the presence of high K$^+$ (200 mM KCl) is shown in Figure 3a. K$^+$ ions are stabilized by oxygen atoms from the protein backbone through an arrangement of eight oxygen atoms surrounding each K$^+$ ion. Additionally, the selectivity filter is stabilized by a hydrogen network, which includes hydrogen bonds between the carboxylic group of Glu71-Asp80 (carboxyl-

carboxylate), Trp67-Asp80, and a buried water bond to the amide nitrogen of Gly79 (Fig. 3c). Interestingly, the low K^+ structure of the selectivity filter (3mM KCl, 2.3 Å) is considerably different than the high K^+ structure (Fig. 3b). K^+ ions are missing at positions 2 and 3, and Val76 and Gly77 residues moved away from their original position. Moreover, the selectivity filter hydrogen bond network is reorganized, thus acquiring a new structure that might represent a non-conductive state (Zhou et al., 2001b).

Since its structural determination, KcsA has been the model for other ion channels with known and unknown structure, besides a vast amount of computational studies have been performed using its structure as a molecular model. Even though it has been very well studied from the structural and computational point of view, there are still many unanswered questions regarding its function that remain to be investigated. A few functional studies, in comparison to Shaker K^+ channel, have been carried out on this proton-gated K^+ channel and its function has been less correlated to other K^+ channels. A better description of the functional properties is required to complement the wealthy structural information that already exists and to be able to truly correlate structure and function.
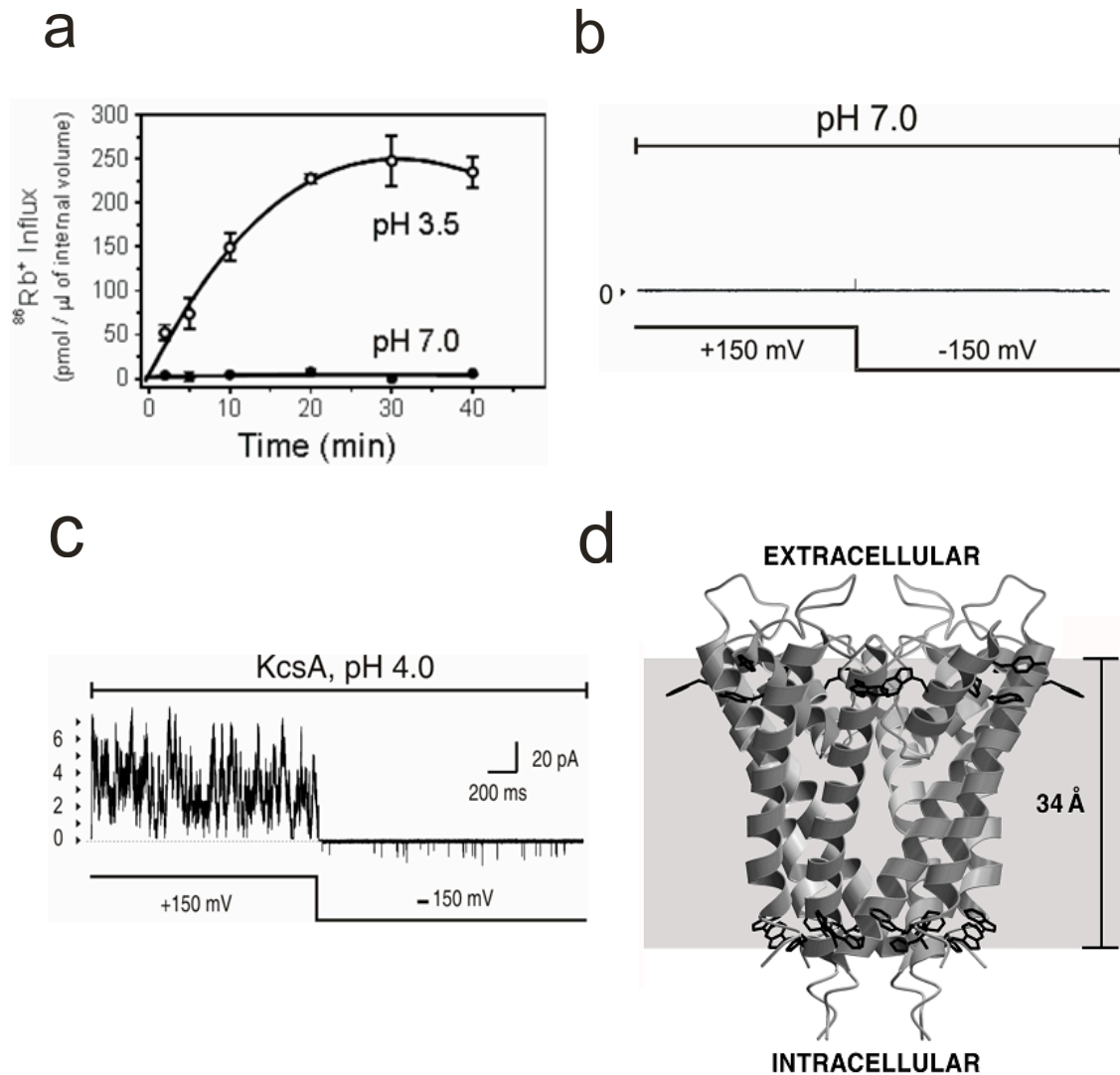
Figure 2 KcsA is a proton-gated potassium channel. a) Macroscopic Rb$^+$ influx from asolectin liposomes containing KcsA at acidic and basic pH. b and c) Representative single channel records of KcsA at different pHs and ± 150 mV transmembrane voltage. d) Ribbon representation of the KcsA crystal structure at 3.2 Å of resolution (Doyle et al., 1998).
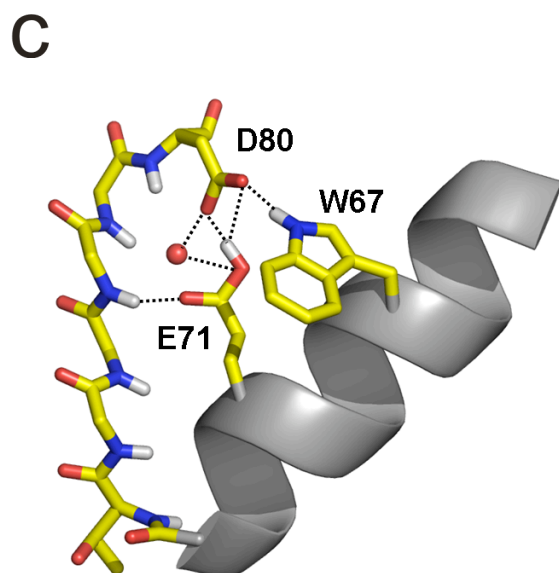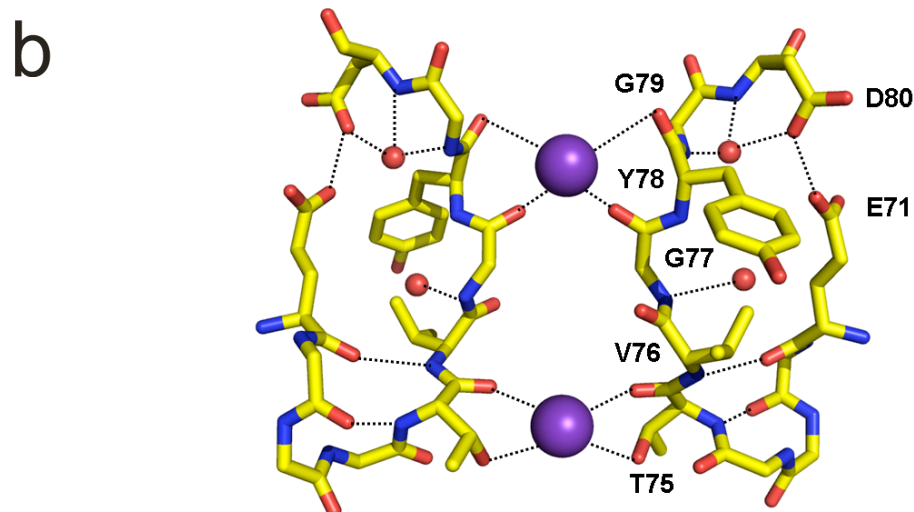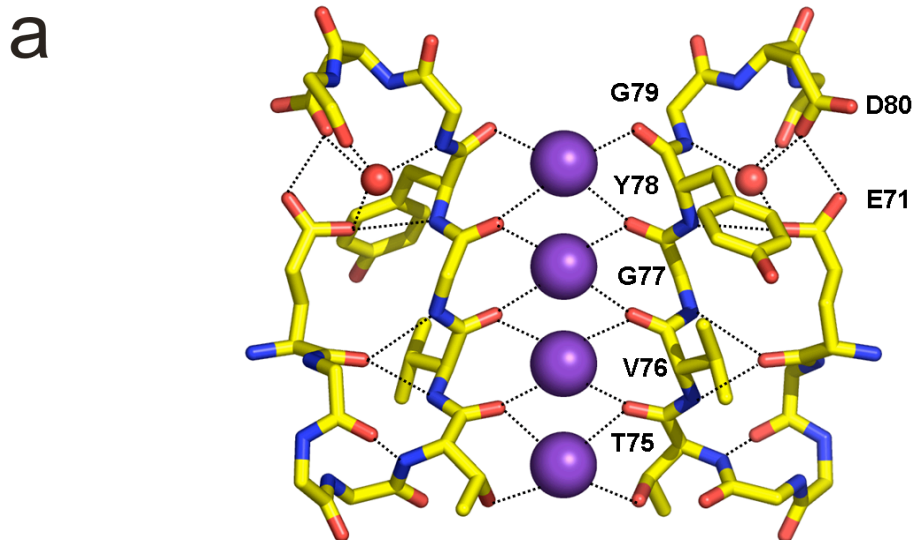
Figure 3 Crystal structure of the KcsA selectivity filter in high (200 mM KCl) and low K$^+$ (3 mM KCl). a and b) Two subunits of the KcsA selectivity filter structure are shown, with K$^+$ ions (purple spheres) in filter positions 1-4 (top to bottom). Each K$^+$ ion is located at the center of eight oxygen atoms. **c)** The selectivity filter is stabilized by a hydrogen network, which includes hydrogen bonds between the carboxylic group of Glu71-Asp80, Trp67-Asp80, and a buried water. Important hydrogen bonds (black dashed lines) and a buried water molecule (red sphere) are shown. (Zhou et al., 2001b).

1.2.2   Gating of potassium channels

1.2.2.1 Evidences for the existence of an intracellular gate in K$^+$ channels

Ion channel gating is defined as the process by which the pore undergoes conformational rearrangement along the permeation pathway that leads to the interconvertion between the conductive and non-conductive state of the pore. Ion channel gating responds to several stimuli, such as transmembrane voltage, extracellular and intracellular ligands, membrane bound ligands, and mechanical forces. These stimuli induce protein movement at specific regions (gates) of the channel that finally leads to ion conduction. The presence of a gate located in the intracellular region of potassium channels comes from the unique work of Armstrong in giant axons (1971), where he was able to suggest the existence of a gate by measuring the accessibility to quaternary ammonium (QA) compounds in the open and closed states (Armstrong, 1971). Later on, molecular and structural studies confirmed Armstrong's results that internal QA ion binds at the internal entrance of the selectivity filter (Choi et al., 1993; Zhou et al., 2001a).

In addition, similar accessibility experiments in Shaker K$^+$ channel confirmed the presence of an intracellular gate by introducing cysteines at various positions along the pore and testing their ability to be chemically modified when the channels are open or closed by the movement of an intracellular gate (Liu et al., 1997). These experimental evidences were confirmed by the crystal structure of KcsA (Fig. 4a), that showed a helix bundle crossing at the intracellular side of the channel presumably representing the intracellular gate (Doyle et al., 1998). The final demonstration of the intracellular gate in KcsA was made by Perozo and colleagues (1999) using electron paramagnetic resonance spectroscopy (EPR). They were able to monitor the conformational changes in the helix

bundle crossing (Fig. 4b) upon opening by intracellular acidification (Perozo et al., 1999). In addition to the EPR results, the crystal structure of MthK (a prokaryotic Ca^{++} gated K^+ channel) in the open state, constituted the final evidence that K^+ channels open by widening of the cross bundle section (Jiang et al., 2002). These studies, among many others, confirmed the basis for the presence of a lower gate controlling ion conduction in K^+ channels.
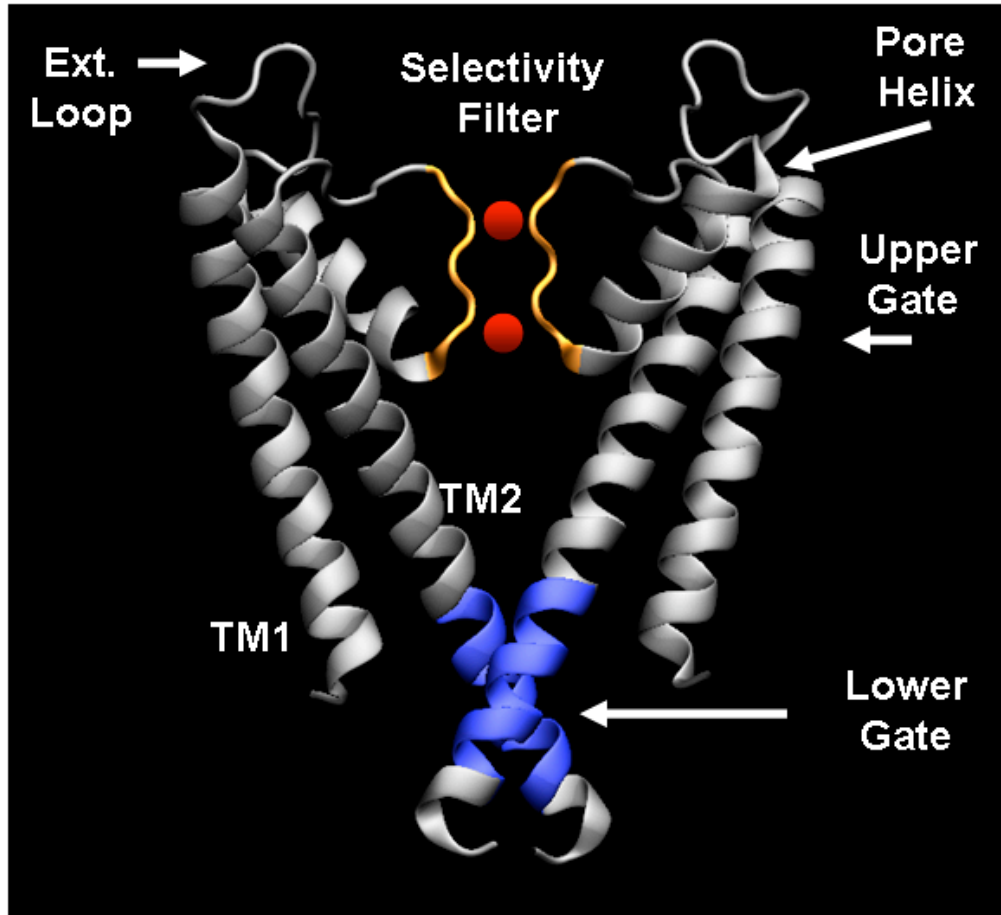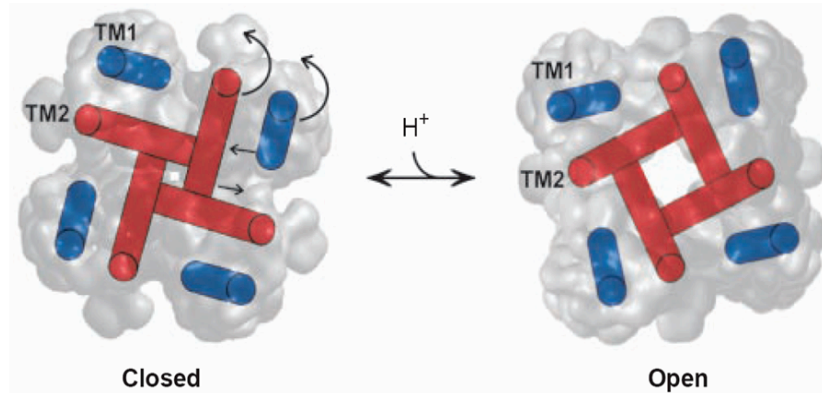
Figure 4 Location of the gates in K$^+$ channels. a) KcsA crystal structure at 3.2 Å resolution, showing the cross bundle section (blue) representing the lower gate, the selectivity filter (yellow) representing the upper gate , K$^+$ ions (red) and TM1, TM2 and pore helix (gray). Ribbon representation of only two subunits of the tetramer (Doyle et al., 1998). b) Model from EPR of KcsA opening. Initiated by a proton-dependent step, TM2 rotates in a counterclockwise direction and away from the permeation pathway, opening the channel. TM1s are represented by blue cylinders and TM2s are red.

1.2.2.2 Evidences for the presence of two gates in K$^+$ channels

Compelling evidence suggests that in addition to the main gate located at the cross bundle section of K$^+$ channels (discussed above), the selectivity filter plays a critical role in gating, acting as a second gate (Bruening-Wright et al., 2002; Claydon et al., 2003; Sun et al., 1996). One of the first indications came from the effect of certain permeant ions on gating (Demo and Yellen, 1992; LeMasurier et al., 2001; Spruce et al., 1989; Swenson and Armstrong, 1981). Ions with longer residency times in the selectivity filter (Rb$^+$ and NH$_4^+$) tend to stabilize the open conformation through a "foot in the door mechanism". Furthermore, one of the strongest indications for a gating mechanism at the selectivity filter is the occurrence of subconductance levels with altered selectivities (Chapman et al., 1997; Zheng and Sigworth, 1998). Additionally, mutations at or near the selectivity filter (Liu and Joho, 1998; Lu et al., 2001) and at the pore loop (Proks et al., 2001; Sun et al., 1996) revealed rapid gating transitions, pointing towards this region as an important contributor to the gating process.

On the other hand, X-ray crystallography study on KcsA suggested that two different conformations of the selectivity filter (high and low K$^+$ concentrations, Fig. 3) could account for the channel flickering and the permeant ion effect on gating (Zhou et al., 2001b). However, a clear understanding of the role of the selectivity filter during activation and inactivation gating requires additional structural and functional approaches.

1.2.3 Potassium channel activation

The molecular basis of ion channel activation requires understanding of the energy transduction mechanism that converts the stimuli (i.e. transmembrane voltage, ligand binding, or mechanical force) into protein movement that finally lead to ion conduction. The landmark work of Hodgkin and Huxley in giant squid axons set the ground state on ion channel research (Hodgkin and Huxley, 1952). They have proposed that K^+ channel gating requires the transition of four independent particles, since the rates of these transitions were exponentially dependent (n=4) on transmembrane voltage. This early idea was in agreement with the later finding that K^+ channels were composed of four identical subunits, each subunit contributing a voltage-sensor towards the activation process (MacKinnon, 1991). From there on, several studies have been directed towards understanding the activation gating in voltage-dependent K^+ channels.

Currently, we know that voltage-dependent potassium channels are formed by four identical subunits, each subunit comprises six transmembrane segments, S1–S6, the first four, S1–S4, constituting the voltage-sensor domain, and the last two, S5 and S6 (Fig. 1), forming the pore (Jiang et al., 2003; Long et al., 2005a; MacKinnon, 1991). Previous site-directed mutagenesis experiments demonstrated the role of the S4 segment containing charged arginine with additional participation of counter-charge bearing helices (S2 and S3) in the voltage sensing process (Aggarwal and MacKinnon, 1996; Seoh et al., 1996). The activation of Shaker K^+ channel is one of the most extensive voltage dependent processes studied so far (Bezanilla, 2000). It involves the movement of 12-13 electronic charges across the electric field, which corresponds to the conformational changes of the voltage sensor that is finally coupled to the pore domain,

thus leading to ion permeation. These conformational changes can be revealed by measuring the gating charge in the absence of ionic current as shown in Na^+ channels (Armstrong and Bezanilla, 1973) and K^+ channel (Bezanilla et al., 1991).

Several works have suggested that voltage-dependent K^+ channel pass through several closed states before entering into the open state, since comparison of the voltage sensor changes (Q-V relationship) and pore opening (Po-V relationship) revealed that the voltage sensor undergoes conformational changes before pore opening (Bezanilla, 2000). In addition, conformational changes before channel opening also have been suggested to occur in the S4-S5 linker (Long et al., 2005a; Long et al., 2005b) and the S6 (Liu et al., 1997). Even though there are ample functional and structural studies, Kv channel activation mechanism still is a field with great deal of controversy (Chanda et al., 2005; Cuello et al., 2004; Gandhi et al., 2003; Jiang et al., 2003; Long et al., 2005a; Long et al., 2005b; Posson et al., 2005; Ruta et al., 2005).

On the other hand, the molecular basis of KcsA proton-activation has been less studied. At basic intracellular pH, the second transmembrane segment of each of the four channel subunits come together as a helix bundle (Fig. 4a) and it has been suggested to form a barrier for permeating ions, thereby acting as the primary gate for the channel (lower or activation gate) (Liu et al., 2001; Perozo et al., 1999). Although the precise location of the pH-sensor is still unknown, a recent nuclear magnetic resonance (NMR) study has shown that residue H25 at the interface of the two transmembrane segments in the intracellular region of the channel undergoes conformational changes in response to pH change. From this and other observations, the authors associated this residue with the

pH gating process in KcsA (Takeuchi et al., 2007). However, in the absence of conclusive functional evidences its role as a pH-sensor still remains speculative.

Furthermore, recent Monte Carlo normal mode analysis showed opening of KcsA involves rotation and unwinding of the TM2 bundle when residues at the intracellular region are protonated (Miloshevsky and Jordan, 2007). Although, there are few studies of the pH activation of KcsA, results seem to indicate that residues at the end of TM2 (E118 and E120) and TM1 (H25) play a major role in pH sensitivity.

1.2.4 Potassium channel inactivation

Ion channel inactivation is an effective mechanism to control the duration of the conductive state through structural rearrangements along the permeation pathway (Hoshi et al., 1991; Liu et al., 1996). This mechanism is a fast process, initially seen in Na^+ channels and later on observed in many others channels (Hodgkin and Huxley, 1952). This process plays fundamental role, for instance in voltage-gated K^+ channels, it contributes to the repolarization of cardiac myocytes. Inactivation plays a key role in early stages of repolarization through I_{to} (transient outward rectifier K^+ currents) and later through IKr (hERG). During the initial phases of the action potential, IKr currents are inactivated, and then during the repolarization phase hERG recovers from inactivation, thus allowing outward K^+ currents and the subsequent repolarization of cardiac myocytes. Therefore, the molecular basis for the inactivation mechanism is crucial to understand general physiology (Keating and Sanguinetti, 2001). Although this process is highly variable in many of its properties among channels, two general mechanisms have been proposed, the N- and C-type inactivation.

1.2.4.1 N-type inactivation

N-type inactivation is a process that involves blocking of the intracellular region of the channel due to hydrophobic and electrostatic interactions of a short peptide (20 amino acids) located within its N-terminal region (Fig. 5, left panel). This block mechanism was first suggested by internally perfusing axons with pronase, a proteolytic enzyme that cut a peptide chain that links the ball to the inner region of the Na^+ channel (Armstrong and Bezanilla, 1973). After the treatment with pronase, Na^+ channels failed to inactivate. This process is referred as fast inactivation due to its fast kinetics, in the order of milliseconds. Later on, the fast inactivation in Kv channels (Shaker) was also shown to be removed by deletion of the ball and chain at the N-terminal region, and then recovered by adding the soluble N-terminal peptide (Hoshi et al., 1990). These results clearly suggested that the N-type inactivation is a general mechanism in ion channels.

1.2.4.2 C-type inactivation

The second mechanism of inactivation (Fig. 5, right panel) involves rearrangements of the pore domain that leads to constriction of the permeation pathway (Hoshi et al., 1991). This is referred as the slow inactivation, due to its slow kinetic behavior in comparison to the fast N-type inactivation. As this inactivation was affected by mutations near the C-terminal region of the channel it was termed C-type inactivation (Hoshi et al., 1991), although it was also found that mutations in the pore region affected this type of inactivation and then, the term P-type inactivation was also coined (De Biasi et al., 1993). Mechanisms underlying C-type inactivation have been widely studied, but yet the range of conformational changes during this process that leads to the closure of the permeation

pathway is still unknown, mostly due to a limited understanding of the molecular forces that drive the pore to its inactivated conformation, and the lack of structural information.

Liu and collaborators (1996), introducing cysteine residues at the outer mouth of Shaker K^+ channel and by measuring state-dependent changes in accessibility to chemical modifications, were able to demonstrate that during C-type inactivation there is a local rearrangement and constriction of the channels at the outer mouth (Liu et al., 1996). Similar changes were structurally observed in the crystal structure of KcsA in low K^+ (3 mM, Fig. 3b), which represent the structure of the pore in a non-conductive state (Zhou et al., 2001b). These results show functional and structural evidence of the conformational changes that might occur during the gating of K^+ channel.

1.2.4.3 Interaction of N- and C-type inactivation

The kinetics of C-type inactivation can be highly influenced by N-type inactivation. Interaction between C- and N-type inactivation has been suggested to occur by two pathways (Fig. 6); one is due to the block of the permeation pathway by the N-terminal region (N-type inactivation), which promotes the development of C-type inactivation (Fig. 6, left panel). The work by Baukrowitz and collaborators (1995), concluded that after the intracellular mouth of the pore domain is occluded by the binding of the N-terminal domain, K^+ ion conduction stops and as the last external ion leaves the pore the channels enters into a non-conducting conformation (Baukrowitz and Yellen, 1995). The other pathway is by allosteric modification (Fig. 6, right panel) that occurs when the N-terminal inactivating peptide binds to the channel and induces a sequence of

conformational changes that leads to the constriction of the permeation pathway (Rasmusson et al., 1998).
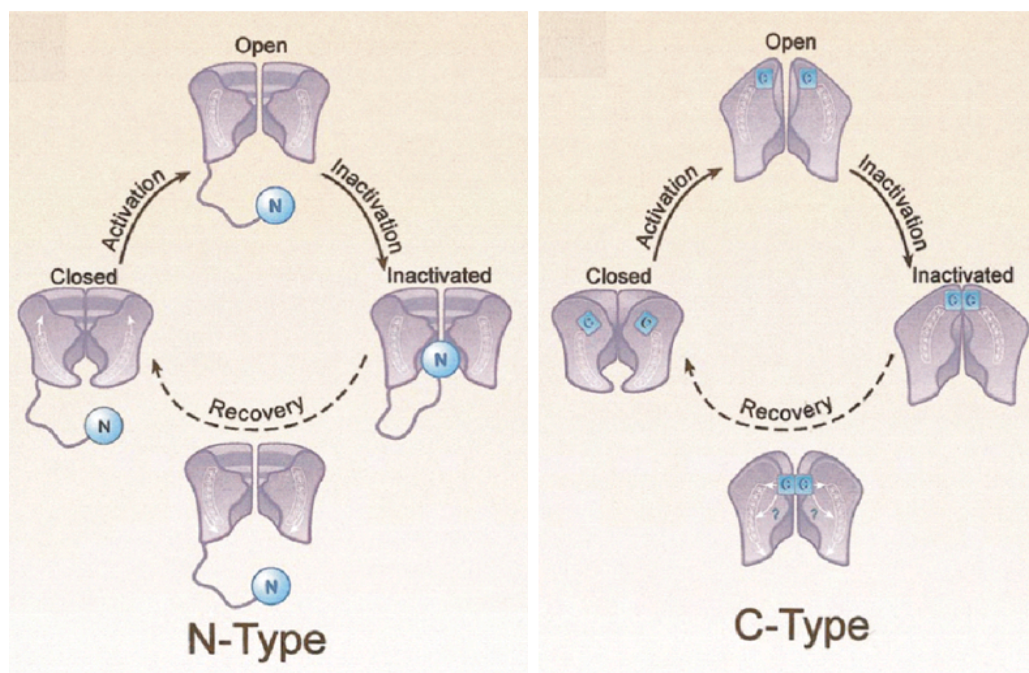
Figure 5 Schematic representations of N- and C-type inactivation mechanism. Each diagram shows the biophysical state of a putative channel during gating (Rasmusson et al., 1998).
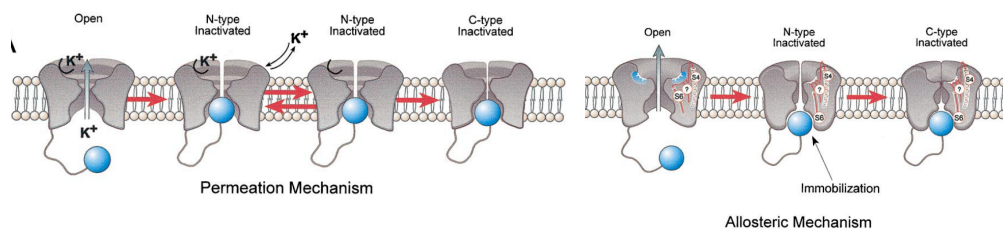
Figure 6 Stimulation of C-type inactivation by N-Type inactivation. Two possible mechanisms (Rasmusson et al., 1998).

1.2.4.4 Regulation of C-type inactivation

C-type inactivation is a variable process among ion channels mostly due to the different degree of modulation. Lopez-Barneo and colleagues (1993), in an elegant and classical work, were able to demonstrate that extracellular K^+ concentration modulate C-type inactivation in Shaker K^+ channel. Decreasing the extracellular K^+ leads to a dramatic increase in the rate of inactivation, suggesting that extracellular potassium might avoid or decrease the conformational changes during the transition from the conductive to the non-conductive state of the channel (Lopez-Barneo et al., 1993).

Likewise, several groups support the role of the permeant ion as a critical factor in the modulation of C-type inactivation (Demo and Yellen, 1992; LeMasurier et al., 2001; Lopez-Barneo et al., 1993; Shapiro and DeCoursey, 1991; Spruce et al., 1989; Swenson and Armstrong, 1981). Ions with longer occupancy in the selectivity filter (Rb^+, Cs^+, NH_4^+) tend to slow-down entry into the inactivated state through a "foot in the door mechanism" in which the resident ion stabilizes the conductive conformation. Moreover, binding of the blocker Tetraethylammonium (TEA) in the extracellular region leads to dramatic decrease of C-type inactivation suggesting that not only K^+ ions can impede the conformational changes leading to inactivation but also extracellular blockers (Choi et al., 1991; Lenaeus et al., 2005; Lopez-Barneo et al., 1993).

1.2.4.5 Why study the inactivation process?

Inactivation is a molecular process that exists in many types of channels and it plays a fundamental physiological role (Hille, 2001). Mechanisms underlying C-type inactivation have been extensively studied, but yet the range of conformational changes during this process is still unknown.

For instance, hERG inactivation is very fast and voltage dependent, as a consequence the channel behaves like an inward rectifier (Smith et al., 1996). Mutations and blockage of hERG are the most frequent causes for malfunctions in human cardiac myocytes (Marban, 2002). hERG is the most sensitive K^+ channel to a large variety of drugs, since acquired LQTs are caused by treatment with medications that block this channel, such as class III antiarrhythmic drugs or certain antihistamines (Keating and Sanguinetti, 2001). These unwanted side effects sometimes, but not always, are associated with overdose which could be exacerbated inducing ventricular fibrillation and sudden death (Hoffmann and Warner, 2006; Marban, 2002; Roden and Balser, 1999; Sanguinetti, 1999). Interestingly, hERG sensitivity to drugs is enhanced when the channels are C-type inactivated, suggesting that the affinity of the drugs are higher when the channel undergoes structural rearrangements from the conductive to the non-conductive state (Ficker et al., 1998).

Pharmaceutical companies invest lots of resources trying to develop new drugs that avoid the side effects on hERG by using high throughput assays that allow fast screening of different drugs. However, due to a limited understanding of the molecular forces that drives the pore to its inactivated conformation and the lack of structural information, these companies fail to develop more efficient drugs.

On the other hand, it has been shown that inactivation in hERG is removed by mutating Ser620 (Ficker et al., 1998) and this residue is equivalent to the critical Glu71

that also modulates inactivation in KcsA (Chapter 2). Inactivation in hERG is also enhanced when Ser631 is changed to alanine (Zou et al., 1998), corresponding to Thr449 in Shaker (Lopez-Barneo et al., 1993) and Tyr82 in KcsA, which have similar responses (Chapter 2). It is clear that a detailed understanding of the inactivation mechanism in KcsA is not limited to the prokaryotic channel family but gives important inroads as of how inactivation gating occurs in several other channels that can have huge impact on human health.

In this thesis, we studied the functional and structural properties of KcsA, a potassium channel from *Streptomyces lividans* in an attempt to understand the molecular mechanism of gating of this pH activated prokaryotic channel. Moreover, using a multidisciplinary approach together with selected prokaryotic and eukaryotic potassium channels (KcsA, Shaker and Kv1.2) this work gathers new information deciphering a common mechanism of C-type inactivation in the K^+ channel family.

1.3 THESIS OUTLINE

This thesis combine a multi-disciplinary approach to understand the mechanism of activation and inactivation in K^+ channels. Because of the complexity of ion channel gating, we decided to study this problem using EPR spectroscopy, X-ray crystallography, computational and electrophysiological methods. KcsA, a potassium channel from *Streptomyces lividans* (Schrempf et al., 1995) is an ideal candidate for this study because of an amenable biochemical preparation which yields milligrams of a very stable protein (Cortes and Perozo, 1997). Two studies were determinant on the development of this thesis, Cuello and collaborators (1998) were able to demonstrate that KcsA becomes active by acidification of the media (Cuello et al., 1998) and, Doyle and collaborators (1998) solved the first crystal structure of a potassium channel (Doyle et al., 1998).

Taking advantage of these previous results, we have demonstrated (Chapter 2) the existence of a C-type inactivation process in or around the selectivity filter of KcsA. Further structure-function experiments led us to identify residues playing a critical role in inactivation and helped uncover a mutant that essentially abolishes inactivation (E71A). Two KcsA (E71A) crystal structures reveal large structural excursions of the selectivity filter during ion conduction. These set of evidences from KcsA, point to the selectivity filter as the region with major influence on gating and suggest the possible conformational rearrangement of the potassium channel selectivity filter during the gating process.

In the chapter three, we focused our attention to the molecular basis of voltage dependent gating in KcsA. Earlier electrophysiogical experiments suggested that KcsA gating, which lacks a "standard" voltage sensor, is influenced by transmembrane voltage

(Cuello et al., 1998; Heginbotham et al., 1999). Through site-directed mutagenesis we demonstrated that voltage-dependent gating in KcsA takes place at the selectivity filter. We identified the voltage sensor as the pore helix residue Glu71, any neutralizing mutation at this region renders KcsA gating voltage-independent. A mechanism for voltage-dependent gating at the selectivity filter is proposed based on the reorientation of the carboxylic moiety of Glu71 and its influence on the conformational dynamics of the selectivity filter.

As a continuation of our studies of gating, we studied the hydrogen-bond network at the selectivity filter (Glu71-Asp80, Trp67-Asp80). In chapter four and five, we found that these interactions are the driving forces that promote instability through a compression of the selectivity filter parallel to the permeation pathway, which energetically biases it towards the inactivated conformation. This mechanism found in KcsA might serves as the basis for C-type inactivation in the K^+ channel family.

In an attempt to understand the mechanistic basis behind the stabilization of open state by E71A, we functionally characterized a series of side chain substitutions, varying charge and side chain volume at position 71. In chapter six, we demonstrated that the different flickering behavior at the single channel level in WT KcsA occurred mostly through fast fluctuations at the selectivity filter. As shown from the kinetic analysis of various Glu71 mutants, once inactivation is eliminated, it is possible to unmask several of these kinetic modes of gating, depending on the side chain at position 71.

CHAPTER 2: Molecular determinants of gating at the KcsA selectivity filter

2.1 ABSTRACT

In this chapter, we show that in the potassium channel KcsA, proton-dependent activation is followed by an inactivation process similar to C-type inactivation, and this process is suppressed by the E71A mutation in the pore helix. EPR spectroscopy demonstrates that the inner gate opens maximally at low pH regardless of the magnitude of the single channel open probability, implying that stationary gating originates mostly from rearrangements at the selectivity filter. Two E71A crystal structures obtained at 2.5 Å reveal large structural excursions of the selectivity filter during ion conduction and provide a glimpse of the range of conformations available to this region of the channel during gating. These data establish a mechanistic basis for the role of the selectivity filter during KcsA gating.

2.2 INTRODUCTION

The activity of ion channels is governed by mechanisms that allow the selective conduction of ions across the membrane, and control the onset and duration of the conductive state (gating). At the single channel level, gating is characterized by transitions between conductive and non-conductive conformations, via structural rearrangements along the permeation path (Mackinnon, 2004; Yellen, 2002). We have studied the prokaryotic K^+ channel KcsA (Schrempf et al., 1995) from *Streptomyces lividans,* in an attempt to develop a mechanistic understanding of the molecular events that underlie gating in K^+ channels. KcsA is activated by protons (Cuello et al., 1998) acting on the intracellular side of the channel (Heginbotham et al., 1999). Additionally, open probability (P_o) is modulated by transmembrane voltage, in spite of the absence of a

canonical voltage sensor. EPR spectroscopic experiments have shown that KcsA gating is associated with a movement of at least 9 Å at the base of the TM2 inner helix bundle (Liu et al., 2001; Perozo et al., 1998; Perozo et al., 1999). This type of movement is related to the conformational changes described in voltage-dependent and inward-rectifier K^+ channels by indirect methods (Hackos et al., 2002; Jin et al., 2002; Liu et al., 1997; Loussouarn et al., 2001) and may correlate with the open conformations observed in the crystal structures of MthK and KvAP (Jiang et al., 2002; Jiang et al., 2003).

Paradoxically, even when maximally activated KcsA opens with a very low P_o under steady state conditions (from < 0.03 to 0.2 (Cuello et al., 1998; Heginbotham et al., 1999; Meuser et al., 1999)). Yet, if the EPR-determined movement of the inner helices is indeed a reflection of the structural changes in the close-to-open transition, why does KcsA exhibits such a low P_o? We have suggested that this paradox could be resolved if the low P_o was due to other structural elements in KcsA (e.g. the selectivity filter) acting in concert with the opening of the inner helix bundle (Liu et al., 2001). Several pieces of evidence point to the selectivity filter as a region with a great deal of influence over the gating behaviour of K^+ channels, including the effect of certain permeant ions on gating (Demo and Yellen, 1992; Shapiro and DeCoursey, 1991; Spruce et al., 1989; Swenson and Armstrong, 1981), the effect of unnatural amino acid mutagenesis at the selectivity filter (Lu et al., 2001), and the role of subconducting states and specific P-loop mutants on single channel gating kinetics (Alagem et al., 2003; Chapman et al., 1997; Proks et al., 2001; Zheng and Sigworth, 1997). Gating of K^+ channels at the level of the selectivity filter has been traditionally associated with C-type inactivation, a slow process by which the channel enters a non-conductive conformation, and is sensitive to external K^+

concentration (Hoshi et al., 1991; Kiss et al., 1999; Liu et al., 1996; Lopez-Barneo et al., 1993).

Here, we have discovered a process that explains the low open probability gating in KcsA through putative molecular rearrangements within the selectivity filter. This process appears to be related to C-type inactivation in voltage-gated (Kv) channels. Thus, this chapter deals with two key issues regarding the molecular basis of inactivation gating in K^+ channels: defining the role of different structural elements in stationary and non-stationary gating and establishing the structural basis that underlies gating at the selectivity filter.

2.3 EXPERIMENTAL METHODS

2.3.1 Materials

The vector pQE32 was bought from QIAGEN (Valencia, CA). The IPTG, and the detergents DM and DDM (solubilization grade) were obtained from Anatrace (Maumee, OH). Talon cobalt resin was bought from Clontech (Mountain View, CA). The reducing agent TCEP was purchased from Pierce (Rockford, IL). The reducing agent TCYP was bought from Molecular Probes (Carlsbad, CA). The spin label was purchased from Toronto Research Chemicals Inc. (North York, On, Canada). The asolectin was bought from Avanti Polar Lipids Inc. (Alabaster, AL). All other reagents were purchased from Sigma or Fisher. KcsA monoclonal antibody hybridoma cell line was kindly donated by Prof. R. MacKinnon (Rockefeller University, NY). The QuickChange site direct mutagenesis kit was obtained from Stratagene (La Jolla, CA). T7 mMessage mMachine kit was bought from Ambion Inc. (Austin, TX).

2.3.2 Mutagenesis and channel biochemistry

The mutations were made using a QuickChange site direct mutagenesis kit (Stratagene, La Jolla, CA). A pQE32 vector containing KcsA with the RGS-(6 x His) epitope at the N-terminus was used for *E.coli* protein expression and purification as described previously (Cortes and Perozo, 1997; Perozo et al., 1998). Membranes containing KcsA were solubilized in PBS (1X) containing dodecyl maltoside (DDM, 10 mM) at room temperature, spun-down at 100000 x g for 1 h and purified with a Co^{2+}-based metal-chelate chromatography resin (Talon resin Clontech, Palo Alto, CA) and gel filtration chromatography in a Superdex 200 column. Purified protein was reconstituted in pre-formed asolectin liposomes at several lipid:protein ratios by the dilution method (Cortes and Perozo, 1997). For EPR measurements, purified mutants were spin labelled in the presence of TCYP and TCEP with methanethiosulfonate spin label (Toronto Research) at a 10:1 label:channel molar ratio and reconstituted in asolectin vesicle by dilution in PBS (1X) pH 8 followed by additional detergent extraction with biobeads (Cuello et al., 1998).

2.3.3 Liposome patch-clamp

Electrophysiological measurements on proteoliposomes were performed using patch clamp technique following the method as previously described (Cortes et al., 2001; Delcour et al., 1989). Single channel records were obtained from 1:5,000-10,000 protein to lipid ratio and macroscopic currents were measured at a 1:100 (mass:mass). The liposome suspension was centrifuged for 1 h at 100,000g and the pellet (about ~10 mg of lipids) was resuspended in 60 μl of rehydration buffer. The proteoliposomes were dried overnight in a desiccation chamber under vacuum for about 12 hours, and subsequently rehydrated with

20 µl of buffer, yielding liposomes of different size suitable for patch-clamp after a few hours. Unless explicitly stated, patch clamp measurements were done in symmetrical conditions: 200 mM KCl and 5 mM 4-morpholine propanesolfonic acid (MOPS) buffer, pH 4.0 at room temperature. Bi-ionic (K^+/Na^+) experiments for selectivity measurements were obtaining using 1.2 s ramps protocols between -200/+200 mV. Single channel currents were recorded with an Axopatch 200B, and currents were sampled at 40 kHz with analog filter set to 5 kHz (–3 dB). Pipette (borosilicate, 100 µl) resistances were 1.7-2 MΩ. Macroscopic currents were recorded after a pH jump using an RCS-160 fast solution exchanger (Biologic) fed by gravity. Single channel analyses were done using pCLAMP 9 (Axon Instruments, Inc.). Idealization of the currents was done through the half-amplitude threshold algorithm at 2 kHz.

2.3.4 EPR spectroscopy

X-band CW-EPR spectra were obtained from spin labeled and reconstituted channels as described in ref. (Perozo et al., 1998) using Bruker ELEXYS spectrometer equipped with a loop-gap resonator under the following conditions: 2 mW incident power, 100 kHz modulation frequency and 1 G modulation amplitude. All spectra were obtained at room temperature.

2.3.5 Purification of a KcsA-Fab complex

KcsA was purified in DM and the C-terminus truncated (Δ125) channels were obtained by chymotrypsin proteolysis. IgG was purified from mouse hybridoma cell culture supernatant using protein A affinity chromatography (University of Virginia, The lymphocyte culture center). Fab fragment of the antibody was obtained by papain proteolysis followed by Q-sepharose chromatography. KcsA$_{Δ125}$ was mixed with Fab (1:4

ratios) and then purified on a Superdex 200 column with 50 mM Tris buffer, 150 mM

KCl and 5 mM DM, pH 7.5.

2.3.6 X-ray crystallography

The KcsA mutant protein E71A was crystallized (in collaboration with Benoit

Roux and Vishwanath Jogini) in the presence of an antibody Fab fragment following

published protocols (Doyle et al., 1998; Zhou et al., 2001b). Beam-like crystals of KcsA-

Fab complex appeared after a week in a sitting drop containing 20–25% PEG400 (v/v),

50 mM magnesium acetate, 50 mM sodium acetate (pH 5.4-5.6) at 20 °C. Crystals

diffracted to Bragg spacing of 2.5 Å for the KcsA/Fab complex crystals. Data collection

and refinement statistics are given in Table 1. Data were obtained at the X4a and X29

beamlines of the National Synchrotron Light Source and processed with Denzo and

Scalepack (Otwinowski and Minor, 1997). E71A structures were solved by molecular

replacement using the WT KcsA-Fab complex structure as search model (1K4C).

Refinement of the structures was carried out through multiple cycles of manual

rebuilding using the program O (Jones et al., 1991) and refinement using CNS (Brunger

et al., 1998). B-factor refinement was carried out using the script of individual B-factor

refinement (bindividual.inp) in CNS with default settings and maximum likelihood

refinement target using amplitudes. In the first round of refinement the B-factors for all

atoms were reset to the value of 50.0 (Zhou et al., 2001b). One-dimensional electron

density profiles along the central axis of the selectivity filter were obtained as described

(Zhou et al., 2001b).

2.3.7 Figure preparation

All the molecular graphic figures in this work were made using Pymol (DeLano, W.L. The PyMOL Molecular Graphics System (2002) http://pymol.sourceforge.net/) and VMD developed with NIH support by the Theoretical and Computational Biophysics group at the Beckman Institute, University of Illinois at Urbana-Champaign. (http://www.ks.uiuc.edu/) (Humphrey et al., 1996).

2.4 RESULTS

2.4.1 An inactivation event during KcsA gating

Functional characterization of KcsA has been impaired due to the presence of a low open probability, thus making difficult the analysis of single channels recordings and the possibility to generate kinetic models to explain its gating properties. Previous results using CW-EPR demonstrated that proton dependent activation takes place through a rearrangement of the TM2, since they shift apart from the permeation pathway (Perozo et al., 1999). Taking into consideration these ion channel properties, several hypotheses could explain the low Po of KcsA: TM2 movements are only partial and require further movements to reach maximal Po, TM2 movements are not associated with gating, Inefficient coupling between proton binding and gate opening, TM2 movements are maximal and associated to gating, but ultimate control of open probability lies elsewhere.

To characterize the kinetic properties of pH-activated KcsA, we studied its single channel behaviour by liposome patch clamp methods from purified preparations reconstituted at very low protein-to-lipid ratios. Figure 7a shows a representative 1 min section of a long single channel recording obtained under symmetric K^+ concentrations (200 mM KCl, pH 4.0). At steady-state, KcsA gating is dominated by very long silent

periods ($\tau > 25$ s), interrupted by bursts of openings of highly variable kinetics (mean open times vary between 5 - 100 ms). Open probability varies between 0.05 and 0.15 (n >40 patches). KcsA dwell-time distributions reveal a complex, multi-exponential behaviour (Fig. 7b), which for the open times is mostly populated by transitions in the 5-20 ms regime and for the closed times by intra-burst closures with time constants of 0.5-10 ms.

Kinetic variability appears to be a hallmark of KcsA gating. This variability appears to occur in a non-random fashion, as recognized by the existence of a linear relationship between mean open and mean closed times across a large set of individual patches (Fig. 7c). This relationship suggests that for patches with a wide range of kinetics, long open times are typically associated with very long closed periods. We reasoned that this phenomenon could be explained by associating the long silent times in KcsA not with a resistance to open at low pH, but with the presence of a previously unrecognized inactivated state.

This inactivation process is best revealed under non-stationary conditions. Thus, we performed pH jump experiments using KcsA reconstituted at high protein to lipid ratios in order to study the time course of macroscopic currents. At depolarized voltages and in symmetric K^+ solutions (200 mM), changing the bath pH from 7.5 to 4.0 produced large, highly reproducible K^+ current transients as shown in Figure 8a. These transients are characterized by a relatively fast activation time course (t ~ 10-20 ms), followed by an exponential decay with a single time constant between 0.5 and 1.5 s relaxing to a steady state current that represents only 5-10 % of the peak current value. In addition, recent preliminary analyses of KcsA expressed in mammalian cells have demonstrated a

similar behavior (Gao et al., 2005). Consequently, the EPR spectroscopic change detected at low pH (Fig. 8b) is dominated by conformations in which the intracellular gate is structurally open, but the channel is functionally inactivated. This inactivation mechanism explains the low open probability in KcsA at steady state after pH activation (likely to be very efficient).
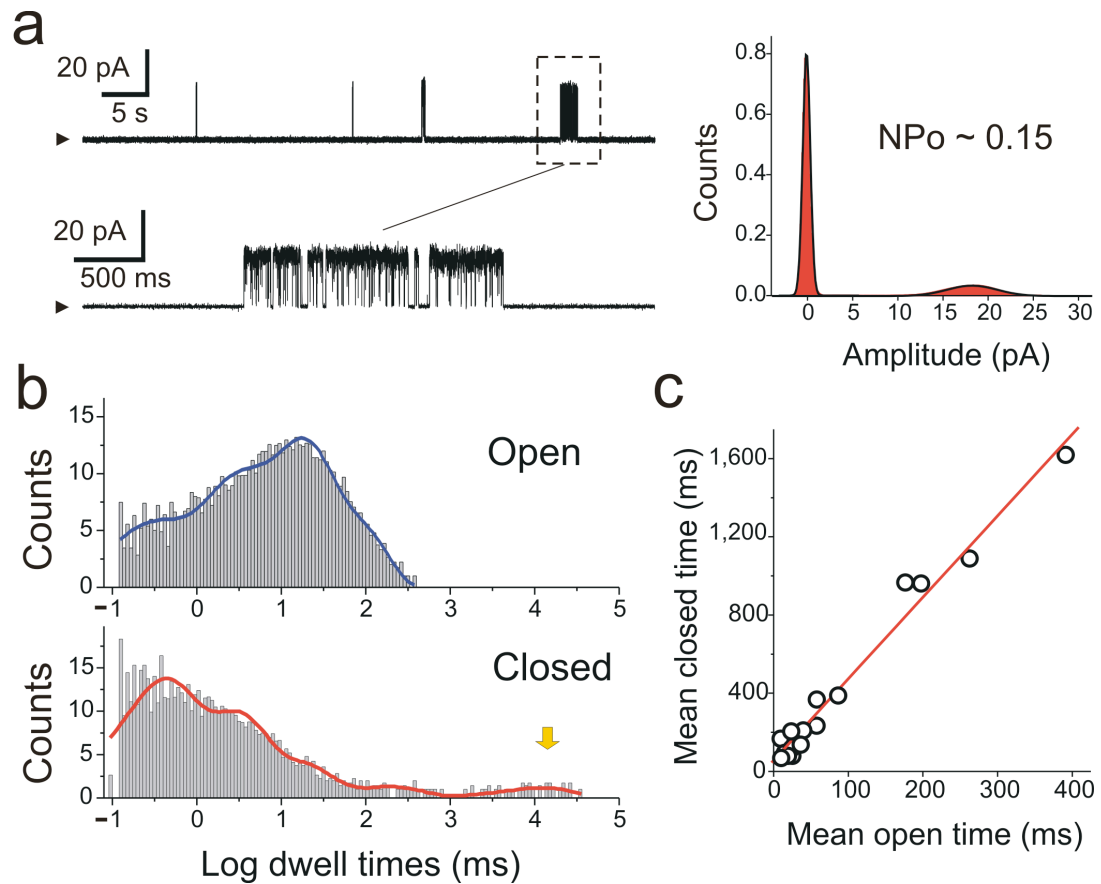
Figure 7 KcsA activity is dominated by long closed time periods. a) Single channel recordings of KcsA obtained in symmetric K^+ (200 mM, pH 4) are dominated by long closures. Traces shown in a slow time base (top) and as a higher resolution detail (bottom). The all-points histogram is shown in the right panel. Gaussian fits to the individual peaks were used to determine the nominal open probability (NPo = 0.15). b) Dwell-time distributions at +150 mV and pH 4.0 for a representative single channel recording of KcsA. c) A striking linear correlation exists between mean open and closed times for KcsA gating as well as for the wide-range variation in the individual patches.
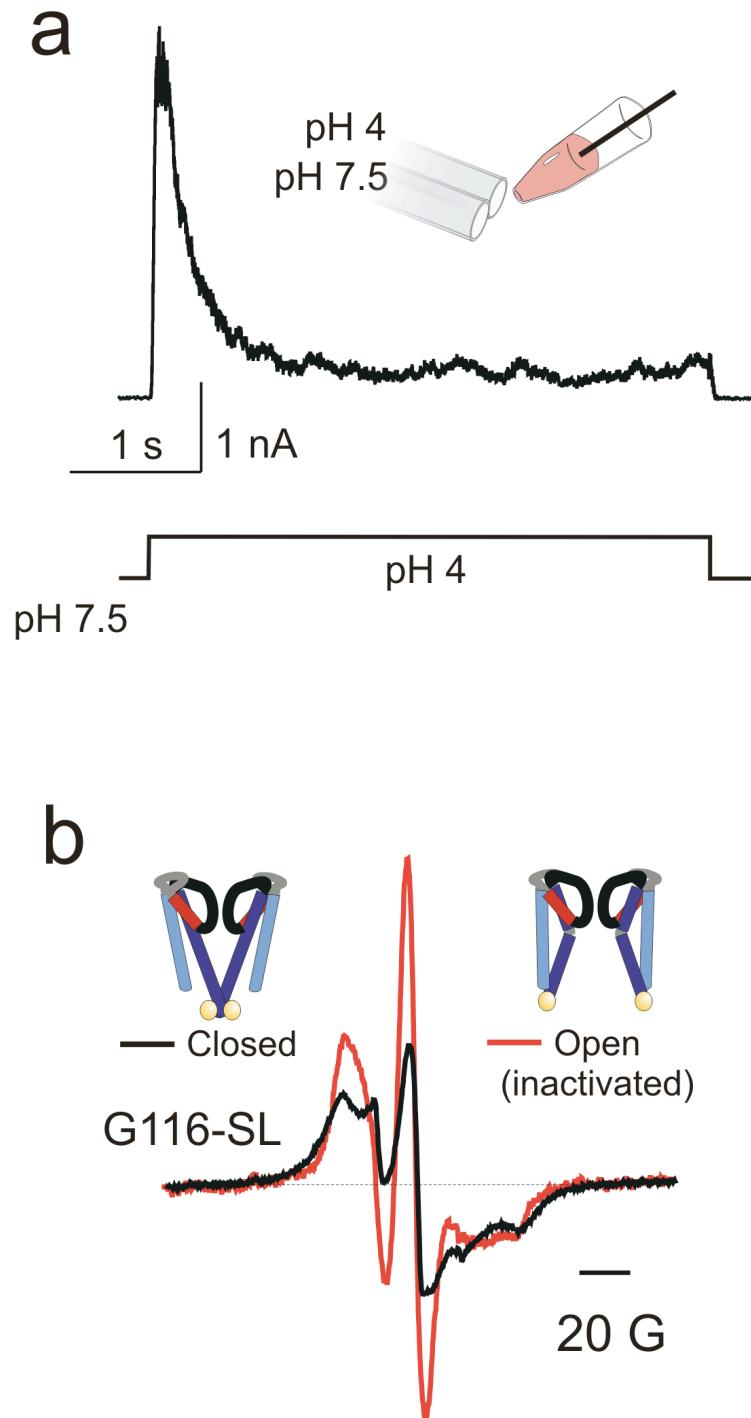
Figure 8 KcsA is inactivated under steady-state conditions. a) Rapid pH jump reveals the presence of a time-dependent inactivation process. b) Opening of the intracellular gate of KcsA monitored by CW-EPR from spin-labels attached at residue G116C-SL. Shown are CW-EPR spectra obtained after equilibrating reconstituted channel in pH 7 (black trace) or pH 4 (red trace) solutions.

2.4.2 The inactivation gate is located at the selectivity filter

We next aimed to identify the regions of KcsA responsible for the inactivation process. We focused our attention on the P-loop (Fig. 9a), by performing an alanine scan at the pore helix (residues 60-73) and the extracellular vestibule of the pore (residues 82 and 84), analyzing the steady-state single channel properties of each stable mutant at low pH (Fig. 9b). We avoided residues involved in ion conduction (74-81) and rejected mutants for which the oligomeric hydrodynamic properties deviated from a monoexponetial peak like WT behaviour (Fig. 10a).

An overview of the single channel traces reveals that the majority of the investigated alanine mutants display gating behaviours similar to that of the WT channel. As in WT-KcsA, most of the mutants display low open probabilities, very long closures and mean open times that varied between 5-30 ms (Fig. 10b-d). However, we identified three P-loop mutants that fundamentally affected KcsA gating: R64A, E71A and Y82A. In all cases, channels were fully selective against Na^+ under bi-ionic conditions (no Na^+ currents were detected), although we found slight shifts in the apparent reversal potential (Fig. 10e) for E71A (more selective) and Y82A (less selective) relative to the WT.

By far, the most dramatic functional effect was observed by placing an alanine at position Glu71, which consistently showed extremely high open probabilities ($P_o \sim 0.95$). More importantly, this was the only mutant that completely abolished the characteristic long closures associated with the low P_o in KcsA (Fig. 10c), rendering this mutant constitutively open at low pH.
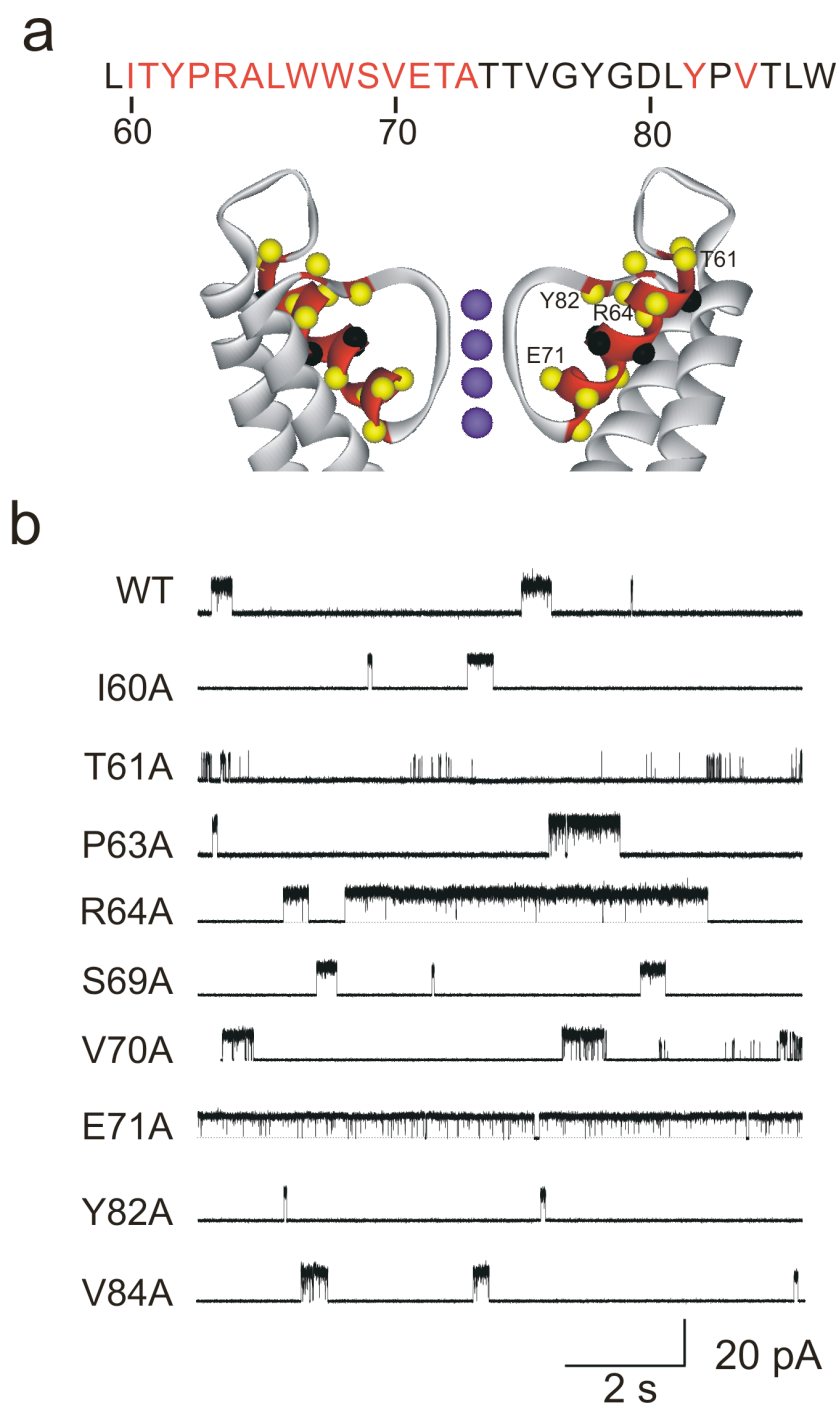
Figure 9 A pore-loop alanine scan identifies residues critical for the inactivation event. a) P-loop sequence with the alanine mutations in red and location of the mutated residues in the KcsA structure (yellow spheres). Residues in black represent positions for which data were not obtained. b) Representative single channel traces of the alanine mutants obtained at pH 4 and +150 mV in symmetric K$^+$ solutions.
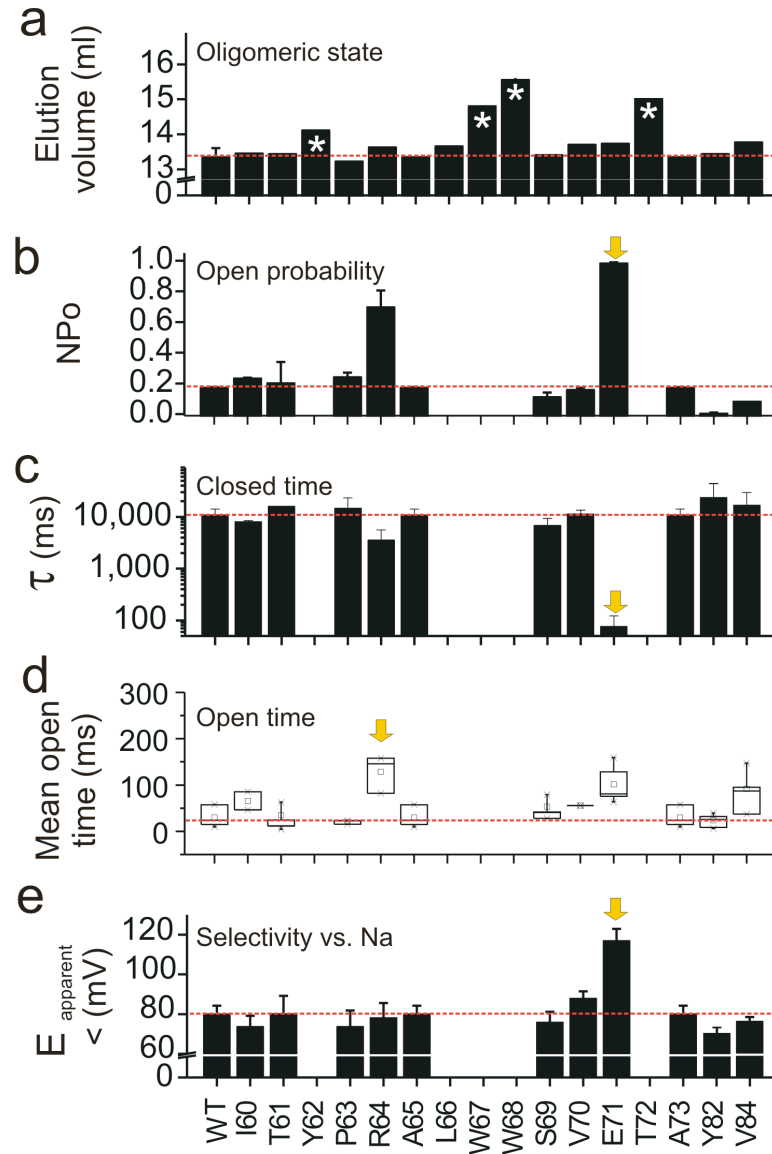
Figure 10 Analysis of the pore-loop alanine scan a) Hydrodynamic properties of the alanine mutants evaluated from the peak elution volume of the KcsA tetramer in a Superdex 200 gel filtration column. b) Nominal open channel probability evaluated from Gaussian fits of all-points-histograms. c) Dominant (slowest) closed time constant as determined from nominally single channel traces. d) Box plot of mean open times. In all cases (plots a-e), the dotted red line represents the mean value of WT KcsA. e) Selectivity vs. Na$^+$ estimated from single channel I-V ramps under bi-ionic conditions. No detectable Na$^+$ currents were seen in any of the mutants. E$_{apparent}$ is the potential at which K$^+$ currents can last be resolved. Error bars represent the standard deviation from the mean.

The E71A mutation also flattens the mean open vs. mean closed time relationship (Fig. 11a, red circles) relative to that in WT-KcsA (black squares) and as expected, produces non-inactivating macroscopic currents in pH jump experiments (Fig. 11b, red trace). The high-resolution KcsA structure (Zhou et al., 2001b) showed that Glu71 forms a strong carboxyl-carboxylate interaction with position Asp80 at the end of the GYGD signature sequence. This interaction is present in other bacterial channels (Kuo et al., 2003), and related electrostatic interactions exist in inward rectifiers (Yang et al., 1997a), but it is not normally found in eukaryotic voltage-gated channels. Although this interaction has important consequence for thermal stability in KcsA (Choi and Heginbotham, 2004), its precise functional role has been less obvious.

Substituting an alanine at position Arg64 increases the steady state P_o to about 0.65. This increase in single channel activity is the consequence of a relatively small decrease in the dominant closed dwell time (Fig. 10c) and an overall increase in the mean open time (Fig. 10d). After pH jumps, macroscopic currents show that the inactivation process is still present in R64A, but it proceeds at an intermediate rate between WT-KcsA and E71A (Fig. 11b, blue trace). In contrast, substitution of Tyr82 for alanine decreases open probability ($NP_o \sim 0.01$) relative to WT-KcsA by lengthening the long closures, and thus further stabilizing the inactivated state (Fig 10c). This is shown in Figure 11b, where macroscopic inactivation is both considerably faster and more complete after a rapid pH jump (green trace).

The present alanine scan has helped identify three KcsA mutants that display a wide variety of steady-state open probabilities. We have taken advantage of this set of mutants to evaluate the relative contributions of the selectivity filter and the inner helix

bundle gate to steady state gating. To this end, we introduced the E71A or Y82A mutations on a KcsA background with mutation G116C. This cysteine serves as a spin labelling site to report on the pH-dependent conformational changes in TM2 (Perozo et al., 1998; Perozo et al., 1999). Comparison of the CW-EPR spectra for spin-labelled G116C, E71A/G116C and Y82A/G116C mutants at pH 7.5 and 3.5 revealed strikingly similar spectral changes (Fig. 11c, left). Furthermore, the magnitude of the opening at the helical bundle crossing (estimated from the dipolar spectral amplitude ratio) shown as a box plot on Figure 11c (right panel) does not change in spite of the fact that these channels gate with two orders of magnitude difference in steady state NP_o (diamonds). This result argues convincingly that once activated by protons, the TM2 gate fully opens at low pH in spite of widely differing patterns of single channel behaviour and that most of the steady-state gating activity in KcsA takes place at the selectivity filter.
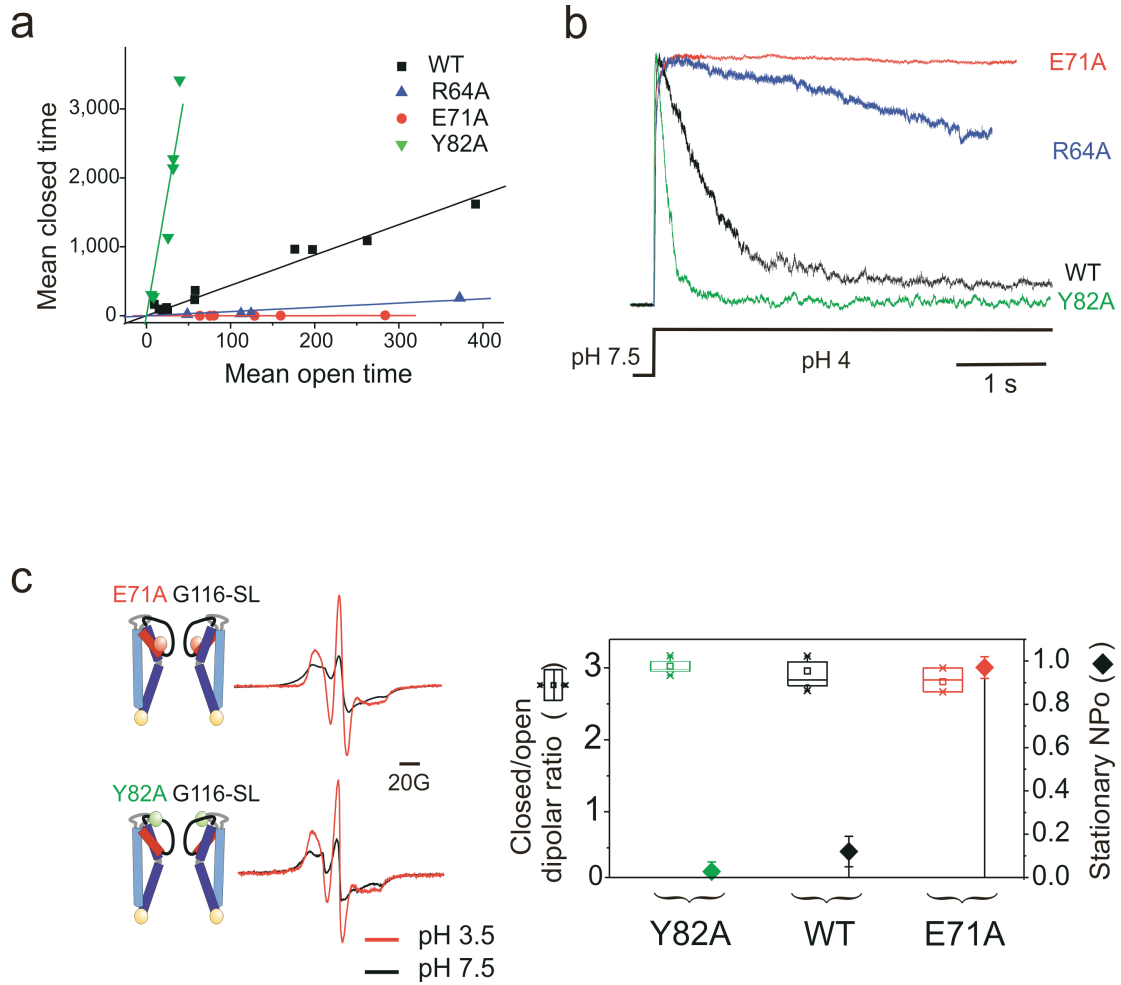
Figure 11 Pore loop mutants influence the rate and extent of inactivation. a) The mean open vs. mean closed times plot for E71A looses the linear correlation seen in WT KcsA. b) Macroscopic currents from rapid pH jumps show the almost complete elimination of the time-dependent inactivation process in E71A, a sharp reduction of inactivation for R64A and an enhancement of the rate and extent of inactivation for Y82A. c) The magnitude of the conformational rearrangement at the intracellular gate does not govern the steady state open probability. Gating changes were monitored by CW-EPR from spin-labels attached at residue G116C in WT channels and in mutants with very low (Y82A) and very high (E71A) P_o. Left panel, CW EPR spectra of the spin-labeled double mutants E71A/G116C and Y82A/G116C at neutral (black trace) and acidic (red trace) pH conditions. Right panel, the extent of intracellular gate opening derived from the amplitude ratio of spectra (dipolar ratio Ω, Box plot) is identical in WT, Y82A and E71A, in spite of large differences in P_o associated with the gating of each mutant (diamond symbol). Error bars represent the standard deviation from the mean.

Several lines of evidence point to a mechanistic equivalence between KcsA inactivation mechanism and the C-type inactivation process associated with voltage-dependent K^+ channels. Residue Tyr82 in KcsA is functionally equivalent to Thr449 in Shaker; mutation of the latter to alanine dramatically accelerates C-type inactivation (Lopez-Barneo et al., 1993), as observed in KcsA (Fig. 11b). Furthermore, mutations of Ser620 in hERG (equivalent to position Glu71 in KcsA) have a large impact on the rate of C-type inactivation (Ficker et al., 1998). These trends also agree with the known changes in K^+/Na^+ selectivity found in C-type inactivating channels (Kiss et al., 1999) and the alanine mutants that relieve or promote inactivation (Fig. 10e).

Moreover, one of the hallmarks of C-type inactivation is its dependence on external K^+ concentration (Lopez-Barneo et al., 1993). pH jump experiments carried out in the presence of extracellular NMG (195 mM) and with K^+ (5 mM) show that the rate of inactivation proceed faster than in symmetric 200 mM K^+ (Fig. 12). This result points to the well-known role of the external K^+ binding site in stabilizing the conductive conformation of the pore.
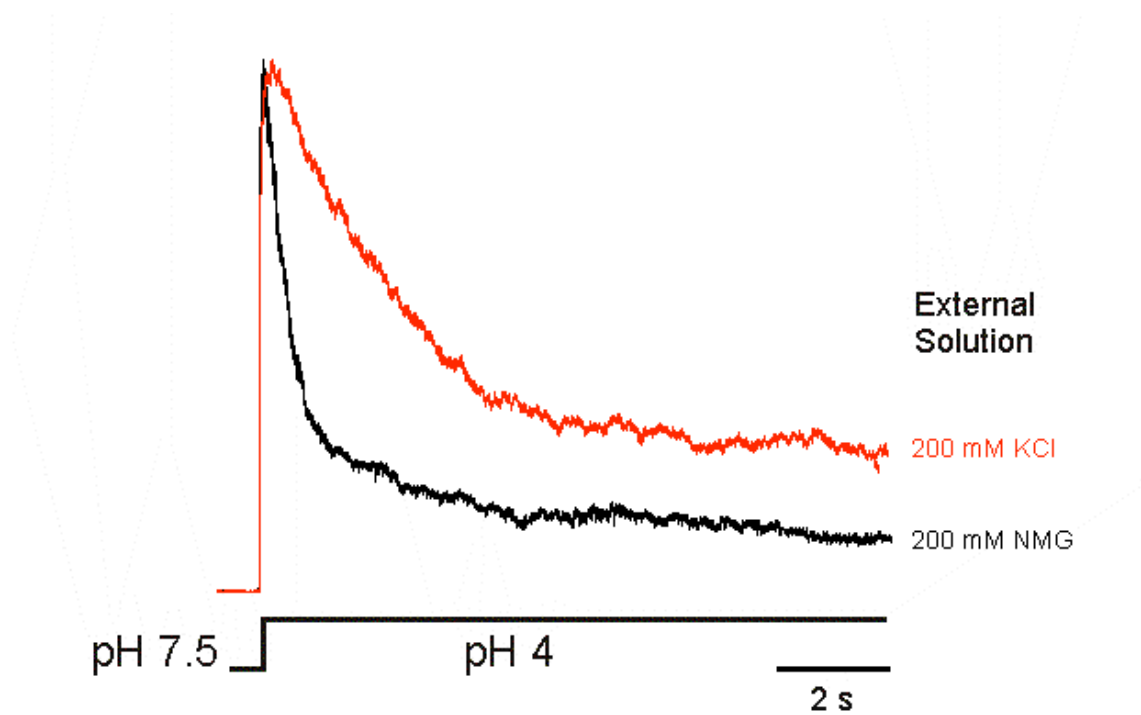
Figure 12 Inactivation kinetics depends on the extracellular K$^+$ concentration. KcsA macroscopic currents activated by a rapid pH jump were obtained in 200 mM K$^+$ (intracellular) and a pH change from 7.5 to 4.0. The external solution contained either 200 mM K$^+$ or 195 mM N-Methyl-Glucamine (NMG) + 5 mM K$^+$.

2.4.3 Two crystal structures of the E71A mutant of KcsA

In order to establish whether the large increase in open probability is reflected on the conformation of the filter, we determined (in collaboration with Benoit Roux and Vishwanath Jogini) the atomic structure of the E71A mutant. The structure in complex with a Fab antibody was solved by molecular replacement using the WT-KcsA/Fab structure (Zhou et al., 2001b) as the search model (PDB ID=1K4C). Of multiple diffracting crystals examined (resolution up to 2.5 Å), two X-ray structures of E71A/Fab were determined (Table1). One structure is similar to WT-KcsA (Fig. 13a), while the other displays substantial conformational changes in three regions of the pore (selectivity filter backbone, Asp80 at the outer end of the pore, and Trp67 along the pore helix, (Fig. 13b).

We refer to these two X-ray structures as the "flipped" and "non-flipped" conformations, according to the extent to which the side chain of residue Asp80 moves upward relative to its position in the WT structure (see below). The final models for these two structures were refined to free and crystallographic R factors of 24.2/26.3% (flipped E71A) and 24.3/25.6 % (non-flipped E71A), respectively. The model of the flipped Fab-E71A complex contains 534 amino acid residues, 43 water molecules, one partial lipid and 6 K^+ ions. The non-flipped model also contains 534 amino acids, 32 water molecules, two partial lipids and 7 K^+ ions.
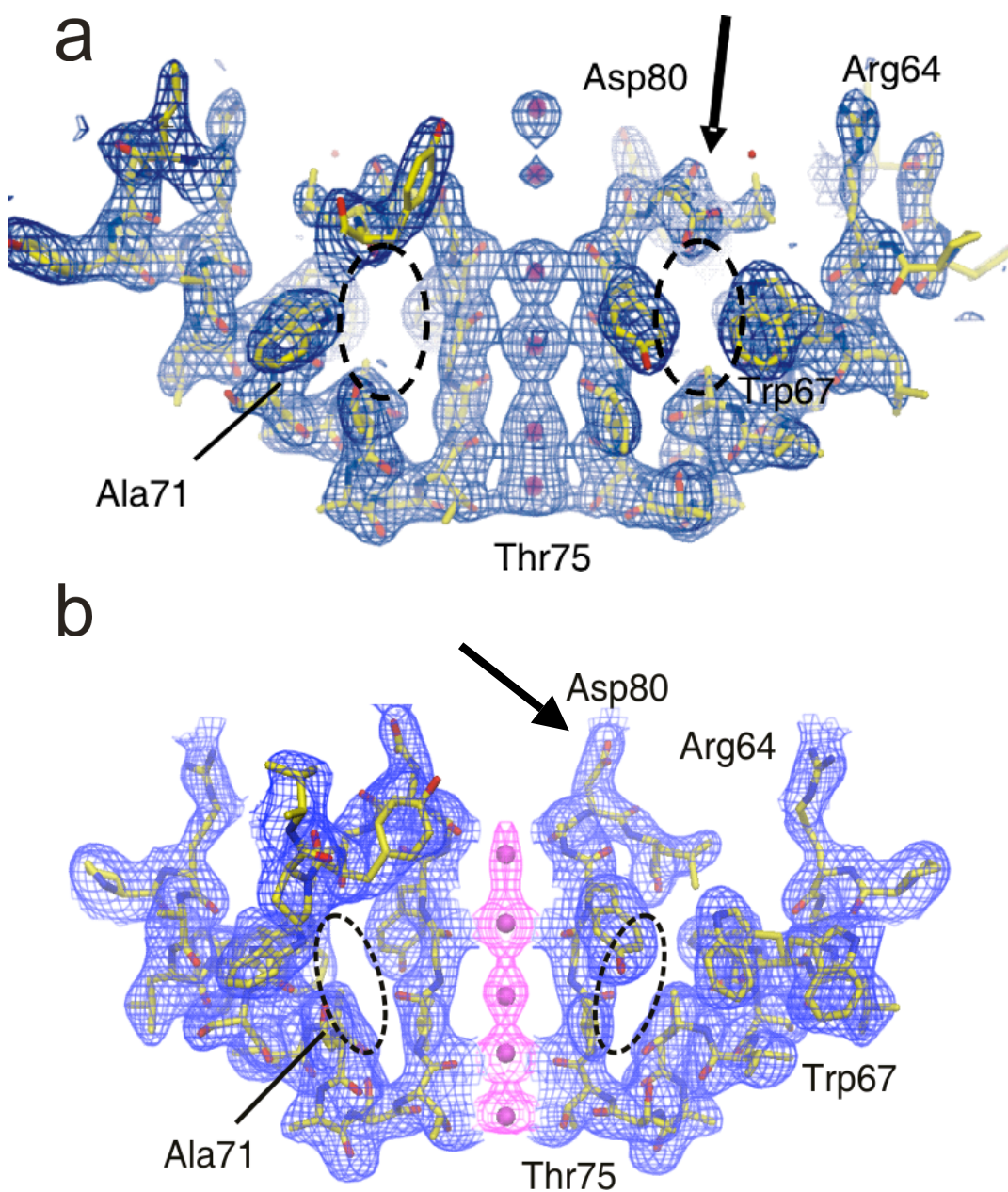
Figure 13 Two crystal structures of the non- inactivating E71A mutant. a) E71A structure with no significant changes in relation to the WT channel. b) E71A structure with residue Asp80 flipped upwards. The polypeptide chain is shown in a stick representation and the blue mesh corresponds to the 1σ contour of the 2Fo-Fc electron density map for the protein and 2σ contour for the ions (magenta mesh). The cavity created by the absence of the Glu71 side chain is highlighted by black dotted ovals. Data collection and refinement statistics are given in Table 1.

Superposition of the two E71A and WT-KcsA structures reveals the details of the conformational rearrangements found in the mutant (Fig. 14a). The RMSD of the flipped E71A, relative to the WT structure, is 1.21 Å for the backbone of residues 62-82 (1.61 Å when the side chains are included). The non-flipped conformation is quite similar to WT, with only small structural changes around the selectivity filter (backbone RMSD of 0.25 Å relative to WT for residues 62-82). Nonetheless, a slight upward displacement of the carboxylate side chain of residue Asp80 of ~0.5 Å toward the extracellular side is observed. In contrast, the carboxyl side chain of Asp80 moves upward by ~8 Å in the flipped conformation (Fig. 14a, upper inset). Perhaps as a consequence of this large reorientation, the backbone of residues 75-81 show major reorientations, particularly for residues 79-80 where the backbone is displaced upward over 2 Å, and residues Val76 and Tyr78 where backbone carbonyls reorient away from the fourfold axis of symmetry. Changes in the backbone of the pore helix appear minimal, though electron density corresponding to two distinct rotamers for Trp67 is clearly observed.

The structural rearrangements observed in the flipped E71A structure have an impact on the position and occupancy of the ions in the selectivity filter. Figure 14b, top panel shows the electron density for the ions in the pore for the flipped (left) and non-flipped conformations (right). In the flipped conformation, the ions in the S1-S3 binding sites appear displaced by about 1.5 Å towards the extracellular side of the pore, with one additional ion density present between residues 78 and 79. Moreover, there is little or no density corresponding to the external ion binding sites (S0 and S_{ext}) (Zhou et al., 2001b). One-dimensional electron density profiles along the pore axis (Fig. 14b, bottom panel) for the two crystal conformations of the E71A mutant confirm that ions in the non-flipped

structure match the positions and occupancy of those in the WT structure. However, the ion occupancy in the flipped structure shows a higher occupancy of S1 relative to S2:S4). This result is somewhat unexpected, given that the largest distortions in the selectivity filter backbone occur precisely near the S1 binding site.
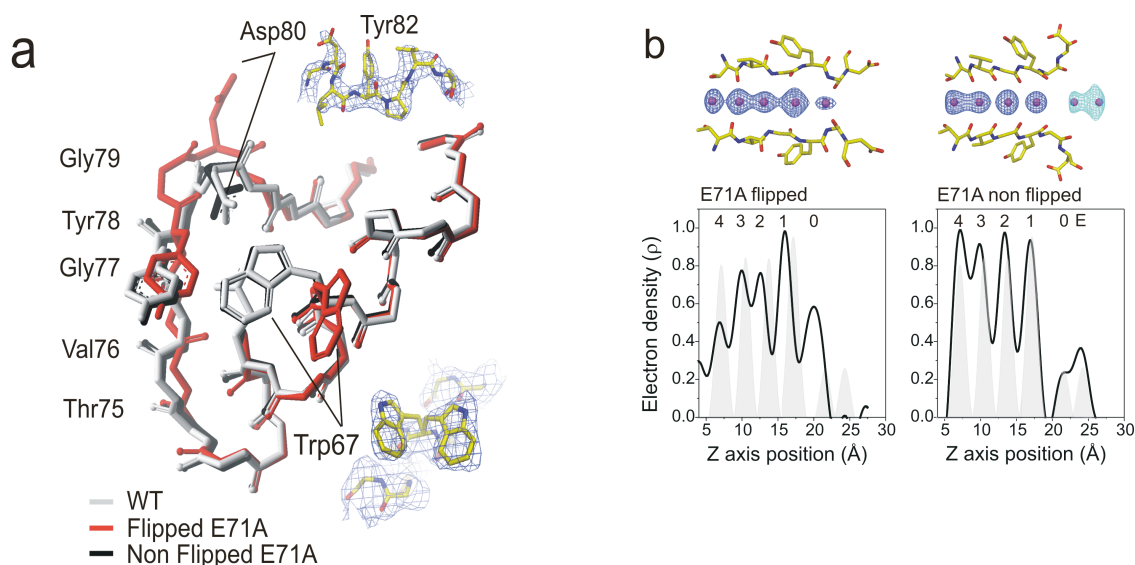
Figure 14 E71A crystal structures comparison. a) Single-subunit line representation of the P-loop of the flipped (red) and non-flipped (black) E71A structures overlapped onto the WT structure (1K4C, in grey) highlights the conformational rearrangements in the backbone of the selectivity filter (residues 75-79). Insets show the side-chain conformational changes in Asp80 and Trp67 as fitted to the 2σ contour of the simulated annealing omit map. The omit maps were calculated for residues 79-84 and 67 respectively, atoms within 3.5 Å from selected residues were also omitted in the calculation. It should be noted that the density attributed to the alternate rotamer of the Trp67 side chain in the flipped X-ray structure is clearly distinct from the density from that of the lipid observed near this position in the WT X-ray structure. b) One-dimensional electron density profiles for the two crystal conformations of the E71A mutant (flipped and non-flipped). Top, Fo-Fc omit maps of K$^+$ ions in the selectivity filter shown relative to the protein model. The electron density maps are shown as a 6σ contour for the flipped E71A conformer and as 7σ (blue) and 4σ (cyan) contours for the non-flipped E71A conformer. Different contour levels were chosen for visual clarity purpose. Bottom: The One-dimensional electron density profile along the central symmetry (Z) axis is shown using the ion in the cavity as Z=0, the grey-shaded peaks represent the profile for the wild-type channel (1K4C at 2.0 Å).

2.4.4 Functional consequences of Fab binding

Examination of the interacting surface between the channel and the antibody reveals the presence of a well-defined salt bridge between residues Asp32 in the B chain of the Fab and Arg64 at the N-terminal end of the pore helix (Fig. 15a, top). This raises issues about the influence of Fab antibody on the conformations observed in the crystal structures of KcsA. It might be recalled that besides E71A, R64A is the only position along the pore helix that generates major increases in the steady-state P_o, having an influence in both open and closed times (Fig. 10c and d). We addressed this issue by recording macroscopic KcsA currents of the reconstituted WT-KcsA/Fab complex after fast pH jumps. As shown in Figure 15a (bottom, red trace) the presence of the antibody substantially reduces inactivation, and stabilizes the channel in its conductive state. Because the structures of WT KcsA with (Zhou et al., 2001b) and without (Doyle et al., 1998) antibody are essentially the same, this result suggests that although the TM2 gate remains closed in the X-ray structure, the Fab-stabilized conformation of the selectivity filter might be a conductive or pre-conductive state.

Macroscopic currents of the reconstituted E71A/Fab complex (Fig. 15b, bottom, red trace), showed no effect on the non-inactivating current, suggesting that the antibody does not exert secondary gating effects. Interestingly, examination of the flipped E71A:Fab interface reveals that the reorientation and stabilization of Asp80 is likely the result of an electrostatic interaction with position Arg93 in the Fab (Fig 15b, top). We interpret this finding to suggest that during gating, residue Asp80 populates a wide range of conformations, both in the WT channel and in the E71A mutant. The presence of the antibody helps stabilize one particular conformation of the filter. So, although it is clear

that Asp80 could move up to ~8 Å, so that it interacts with Arg93 in the Fab, the antibody itself is probably trapping the filter in this "extreme" conformation.
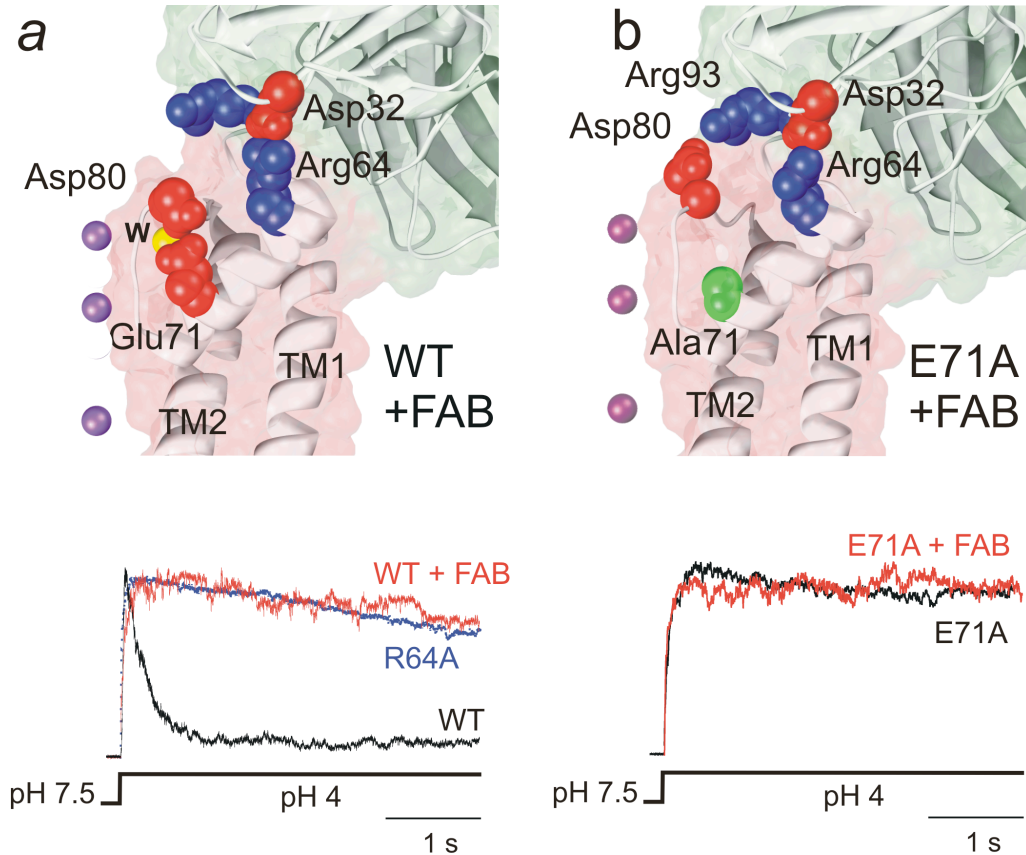
Figure 15 Influence of the Fab fragment binding on KcsA gating. a) Effect of Fab binding on WT KcsA. Bottom, macroscopic K^+ currents after a rapid pH jump (from 7.5 to 4) were obtained from proteoliposomes containing reconstituted KcsA or the KcsA-Fab complex (traces normalized to peak amplitude). The top panel shows the ion pairing between Arg64 in KcsA and Asp32 (CPK representation) in Fab as a possible basis for stabilization of the selectivity filter in the conductive conformation. b) Fab effects on the E71A mutant. Bottom, macroscopic K^+ currents after a rapid pH jump (as in part a). Top, the increased flexibility of Asp80 in the absence of Glu71 places its carboxyl moiety within ion pair range with residue Arg93 in the Fab, leading to a conformational trap of the Asp80-flipped conformation.

2.5 DISCUSSION AND CONCLUSIONS

2.5.1 A mechanistic interpretation of KcsA gating

The finding of a time-dependent inactivation process forces a reinterpretation of KcsA gating as we understand it. It has long been assumed that the low P_o and long closed times were a consequence of the inefficiency in the coupling between proton binding and gate opening, reflecting the limited rates of the transition between closed and open states. The present results reveal that in fact, proton activation is likely to be very efficient, and that the dominant opening gating transition in KcsA under steady state conditions is not the closed-open equilibrium, but the partial recovery from a previously unrecognized C-type inactivated state. This finding also appears to settle the KcsA gating paradox, as it is clear that opening of the intracellular gate is not the only determinant of steady state open probability in KcsA.

On the basis of the present set of results shown in this chapter, we propose that the conductive conformation of the filter, represented by the WT structure (Zhou et al., 2001b), is intrinsically unstable due to the destabilizing interactions between Asp80-Glu71 and Asp80-Trp67 (Fig. 16a, left). Therefore, eliminating the carboxyl-carboxylate interaction between Asp80 and Glu71 (Fig. 16a, right) increases the flexibility of the side chain of Asp80, weakening its (disruptive) hydrogen bonding interactions with Trp67, which is thereby able to undergo a reorientation between two rotamers with similar energies.

The current data can be framed into an explicit mechanistic model of KcsA gating that correlates specific structural snapshots with a sequence of kinetically defined events (Fig. 16b). This model allows for a direct correlation with the key features of KcsA

macroscopic and single channel activity. Hence, the stimulus-dependent gate (TM2) is predicted to be determinant in the duration of individual open channel bursts from transitions among closed states and the open state ($C_1 \leftrightarrow C_2 \leftrightarrow O$). However, the rapid intra-burst behaviour is mostly defined by the $O \leftrightarrow I_1$ equilibrium, while the long closures arise from transitions to the long-lived inactivated state I_2. Removal of the Glu71/Asp80 interaction in the E71A mutant prevents the transition to I_2, unmasking the gating events of the $O \leftrightarrow I_1$ equilibrium at steady state.

The functional state of the flipped E71A structure is not clear at this time. Electrophysiological data demonstrates that the E71A mutant spends most of its time in the conductive conformation. Moreover, the large backbone rearrangements observed in the flipped E71A structure together with the observed changes in ion position and occupancy suggest that the conductive state of the selectivity filter may be supported by a wide range of conformations. It is tempting to suggest that the flipped E71A structure represents a conductive conformation.

While more work will be required to fully characterize all the functional states of the channel, the present results make it clear that the selectivity filter can undergo much larger conformational excursions than previously expected. The present X-ray structures gives us a hint of the range of possible selectivity filter conformations associated with transitions between closed, open and inactivated states.
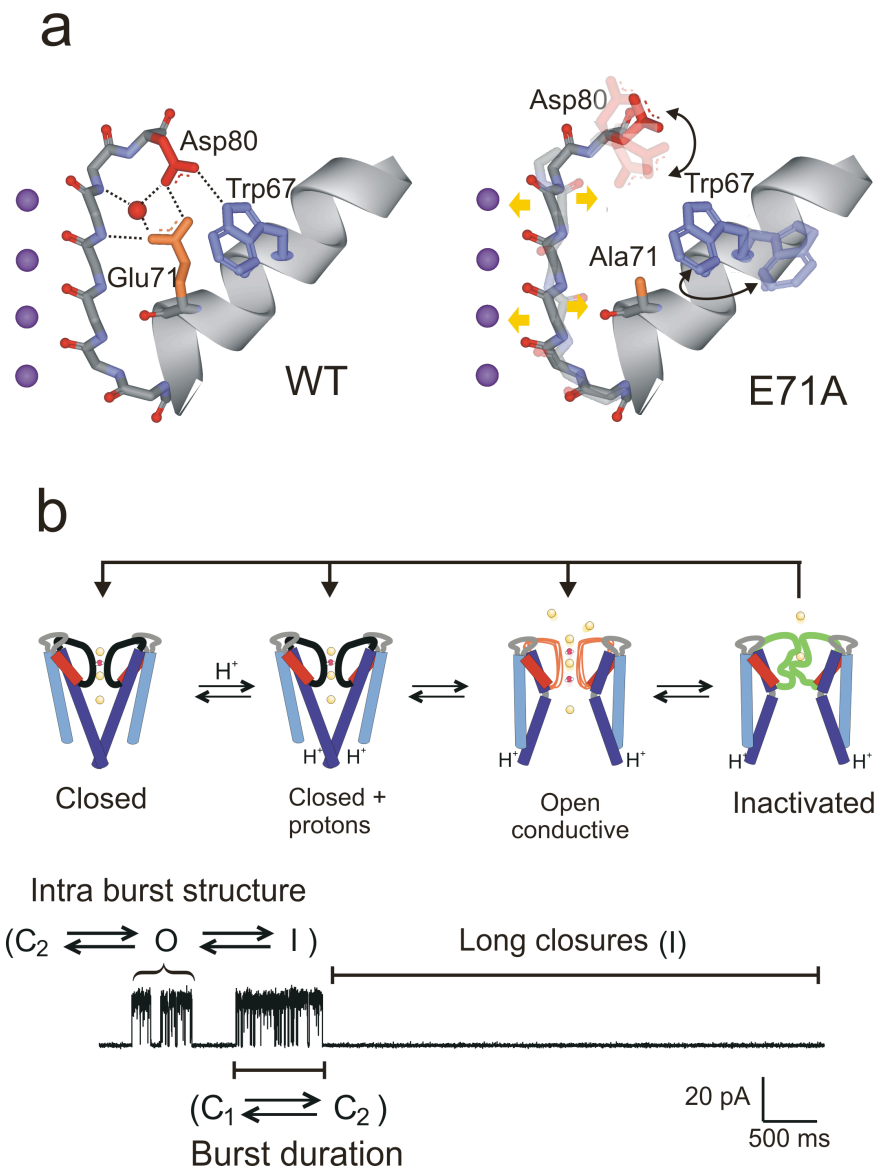
Figure 16 A mechanistic interpretation of KcsA gating. A) Possible mechanism of action of the E71A mutation in stabilizing the open state. A single subunit P-loop is shown with positions Trp67, Glu71 and Asp80 in stick representation. In the WT channel (left), the interaction between Asp80-Trp67 destabilizes the conductive conformation of the filter and promotes inactivation. Eliminating the Asp80/Glu71 carboxyl-carboxylate (E71A, right) disrupts the hydrogen bonding network between the signature sequence (GYGD) and the pore helix, causing an increase in Asp80 dynamics, and perturbing the Asp80-Trp67 interaction. This sharply decreases entry into the inactivated state, stabilizing the open state. b) Top, cartoon representation of the structural conformation associated to each kinetic state. Bottom, correlation of specific kinetic transitions with KcsA single channel behavior. Because stationary gating is dominated by the deep inactivated state, single channel openings occur mainly from rare returns from the inactivated state as a result of conformational changes in the selectivity filter while the lower gate remain open.

Table 1 Data collection and refinement statistics (molecular replacement)

	E71A_non-flipped	E71A_Flipped
Data collection		
Space group	I4	I4
Cell dimensions		
a, c (Å)	155.98, 75.96	155.16, 75.72
α, β, γ (°)		
Resolution (Å)	50.0 – 2.5	50.0 – 2.5
R_{sym} or R_{merge} (%)	6.75 (45.3)	6.90 (57.1)
$I / \sigma I$	41.4 (1.9)	27.2 (2.4)
Completeness (%)	89.2 (48.6)	96.4 (91.9)
Redundancy	6.5	3.9
Refinement		
Resolution (Å)		
No. reflections	27,186	25,067
R_{work} / R_{free} (%)	24.3 / 25.6	24.2 / 26.3
No. atoms		
Protein	4,065	4,070
Ligand/ion	17	17
Water	37	43
B-factors	(Ask for input)	
Protein	83.39	64.23
Ligand/ion	102.53	85.79
Water	72.55	62.60
R.m.s. deviations		
Bond lengths (Å)	0.008	0.007
Bond angles (°)	1.390	1.381

* Each data set was collected from a single crystal frozen in liquid nitrogen.
*Highest-resolution shell is shown in parentheses.

CHAPTER 3: Voltage-dependent gating at the KcsA selectivity filter

3.1 ABSTRACT

In this chapter, we show that the prokaryotic K^+ channel KcsA, although lacking a "standard" voltage sensing domain, displays voltage-dependent gating that leads to an increase in steady-state open probability of almost two orders of magnitude between ±150 mV. Here, we show that voltage-dependent gating in KcsA is associated with the movement of ~ 0.7 equivalent electronic charges. This charge movement produces an increase in the rate of entry into a long-lived inactivated state and appears to be independent of the proton activation mechanism. Charge neutralization at position Glu71 renders the channel essentially voltage independent by preventing entry into the inactivated state. A mechanism for voltage-dependent gating at the selectivity filter is proposed based on the reorientation of the carboxylic moiety of Glu71 and its influence in the conformational dynamics of the selectivity filter.

3.2 INTRODUCTION

Voltage dependent gating is at the core of bioelectric phenomena in intra and inter-cellular communication (Hille, 2001). In voltage-dependent channels, a voltage-sensing domain is linked to the pore domain gate and capable of transducing the energy provided by the transmembrane electric field into domain motion. This rearrangement couple to downstream conformational changes associated with the opening and closing of ion channels (Armstrong, 2003; Bezanilla, 2000; Yellen, 2002), or as shown recently, with the enzymatic activity of nearby soluble domains (Murata et al., 2005). However, any voltage-sensing mechanism requires the movement of charges or reorientation of dipoles in the protein within the voltage field, as originally predicted by Hodgkin and Huxley

(Hodgkin and Huxley, 1952). More than 50 years later, the search continues to define the structural and mechanistic basis of voltage sensing in ion channels and other membrane proteins. In *bona fide* voltage-dependent (Kv) channels, the 4th transmembrane helix (S4) of most voltage sensors is characterized by having a positive charge (Arg/Lys) every three residues. The four consecutive charged positions towards the extracellular face of the channel are responsible for most of the charge movement (Aggarwal and MacKinnon, 1996; Seoh et al., 1996). Recent crystallographic (Jiang et al., 2003) and spectroscopic (Cuello et al., 2004) analysis of KvAP, a prokaryotic voltage-dependent potassium channel, and Kv 1.2 (Long et al., 2005a; Long et al., 2005b), a mammalian Shaker homolog, point to a general architecture of the channel and its gating charge topology. However, the nature and extent of its voltage-dependent conformational rearrangements remain a matter of strong controversy (Ahern and Horn, 2004; Bezanilla, 2005; Cohen et al., 2003).

Although KcsA has become a structural archetype for the pore domain of voltage-dependent channels (Doyle et al., 1998), its structure does not contain an obvious voltage-sensing domain. Interestingly, earlier single channel studies of reconstituted KcsA have shown that, its steady-state gating behaviour is influenced by transmembrane voltage (Cuello et al., 1998; Heginbotham et al., 1999). The relative simplicity of this extremely well-characterized structure and its lack of a "classical" voltage-sensing domain provide a unique opportunity to understanding what is most likely a novel voltage-sensing mechanism for K^+ selective channels.

3.3 EXPERIMENTAL METHODS

3.3.1 Mutagenesis and channel biochemistry

Mutagenesis and channel biochemistry were carried out as discussed in charter 2 (section 2.3.2).

3.3.2 Liposome patch-clamp

Liposome patch-clamp was carried out as discussed in charter 2 (section 2.3.3).

3.4 RESULTS

3.4.1 The voltage dependence of KcsA

The influence of voltage on KcsA gating is best revealed in multi-channel patches (Fig 17a). Under symmetric conditions (200 mM K^+, pH 4.0) and with KcsA oriented with its cytoplasmic end exposed to the bath solution (Fig.17a, left panel), the nominal open probability (NP_o) increase 50 times when comparing steady-state activity between ± 150 mV (Fig.17a, right panel). Figure 17b illustrates this explicitly from all-point histograms obtained for a series of voltages. Multi-Gaussian fits to these histograms were used to obtain the areas of the multiple open levels relative to the closed state and estimate the NP_o at each voltage. Figure 17c shows the resulting voltage-dependence of KcsA activity. The data was fitted to a Boltzmann relation of the form: $NPo = NPo^{max}/[1 + \exp(Fz\delta(V-V_{1/2})/RT)]$, where NPo^{max} is the maximal apparent open probability, $z\delta$ the equivalent charge and $V_{1/2}$ the half point of activation. KcsA data were best fit with $NPo^{max}=0.12$, $z\delta=0.72$ and $V_{1/2}=22$ mV. For comparison purposes, the voltage dependence of the macroscopic conductance in the Shaker K^+ channel (associated with the movement of 3 equivalent charges) is shown by a dashed gray line (Aggarwal and MacKinnon, 1996; Schoppa et al., 1992; Seoh et al., 1996).
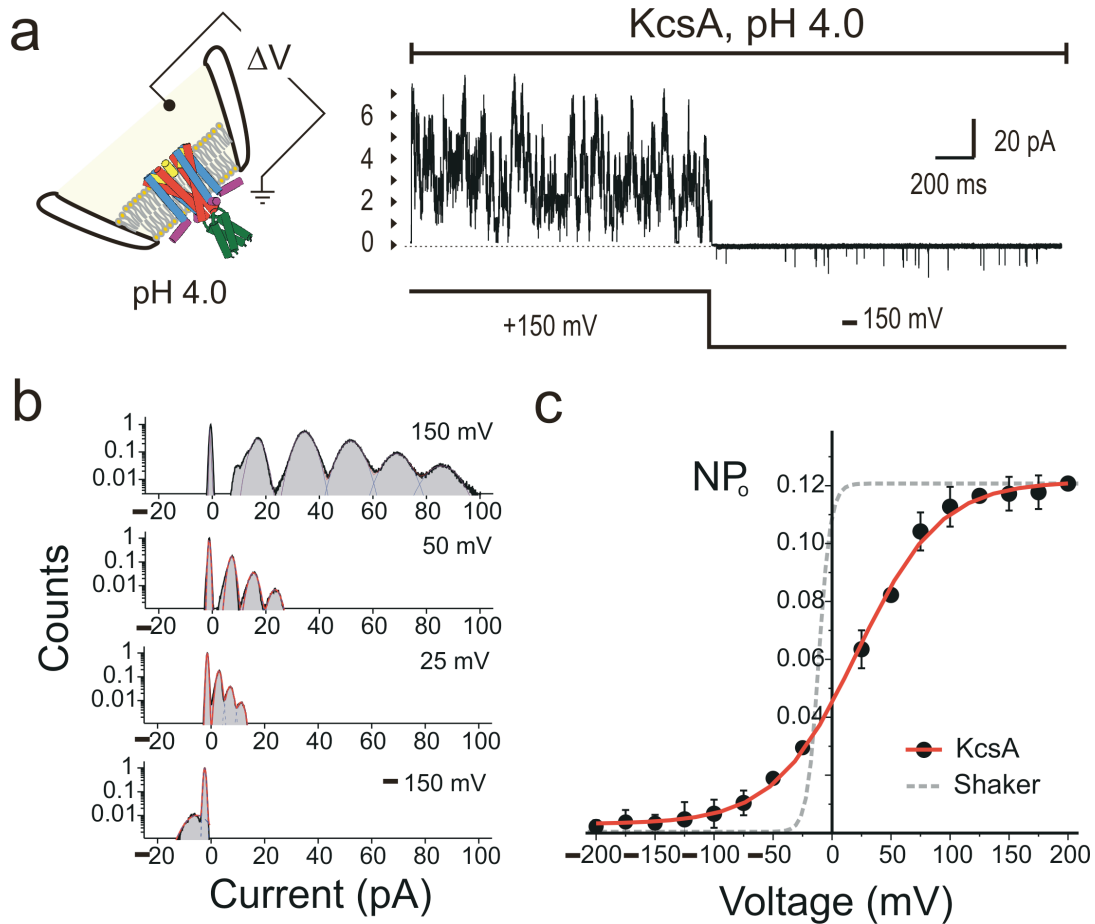
Figure 17 KcsA gating is modulated by transmembrane voltage. a) Steady-state multi-channel patch-clamp record of asolectin-reconstituted KcsA (at least 6 channels are active in the patch). The orientation of KcsA and polarity of the system is shown in the diagram at left. Experiments were performed under symmetric conditions (200 mM K$^+$), pH 4.0. The lower line represents the point at which transmembrane voltage changes from +150 to -150 mV. b) All-points amplitude histogram of a multi-channel patch at a series of voltages. Individual fits to a sum of Gaussians were use to determine the relative area per peak and the NPo value at each voltage. c) Voltage-dependence of open probability. At extreme potentials, the channel is over 50 times more active when depolarized. Data are shown as the mean ± the standard deviation, the continuous curve is the best fit by a Boltzmann function ($V_{1/2}$ = 22 mV, $z\delta$ = 0.72). WT Shaker voltage-dependence is shown as a comparison.

Macroscopic currents measured at different voltages after a pH jump, revealed

that inactivation is more complete and develops with much faster kinetics at negative

potentials (Fig. 18a). Indeed, the voltage-dependence of the inactivation time constant τ_I

(Fig. 18b) essentially match that of the open probability (Fig. 17c). Thus, the increase in

stationary open probability by transmembrane voltage depolarizations can be explained

as a voltage-driven relief of steady state inactivation.
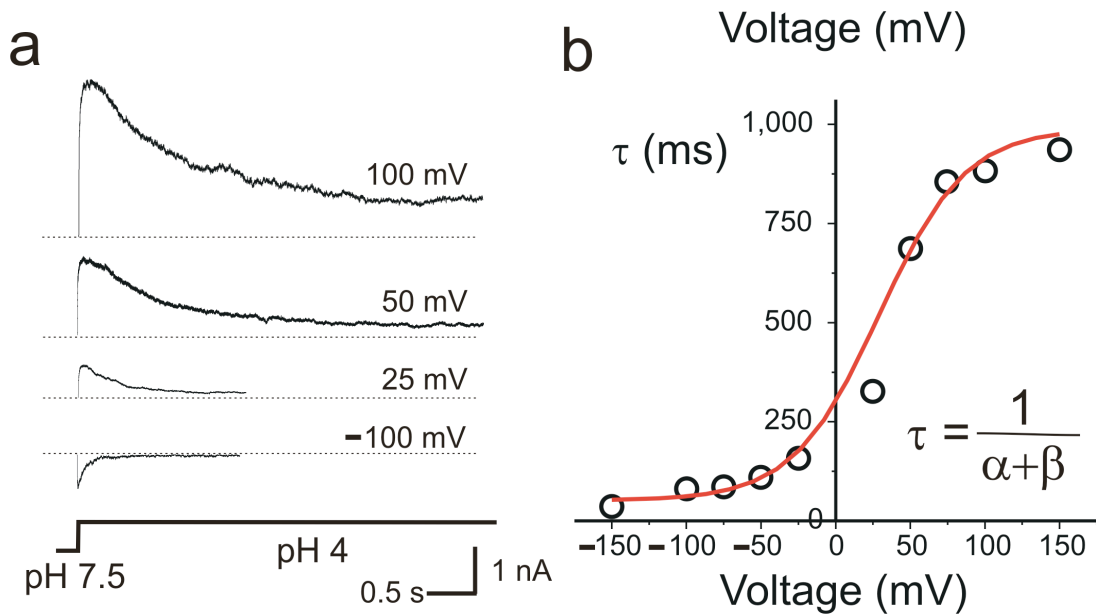
Figure 18 Voltage dependent of KcsA macroscopic current. a) Macroscopic KcsA currents (> 200 channels in the patch) elicited by a fast pH jump (pH 7.5 ➔ pH 4.0) and recorded at various transmembrane potentials. Upon activation, KcsA slowly inactivates to a low steady-state current value. b) Voltage-dependence of the inactivation time constant τ_I. Inactivation decay time constants were fitted to a single exponential function and their voltage dependence to the equation $\tau_I=1/(\alpha+\beta)$ where α is voltage independent and β is of the form $\beta=\beta_0 exp(\pm z\delta V/kT)$.

We next investigate the possible relation between proton activation and voltage gating by looking at the influence of intracellular pH on KcsA voltage dependent gating (Fig. 19). Although the overall data dispersion increases as the maximal open probability decreases (at less acidic pHs), the apparent gating charge estimated from Boltzmann fits does not seem change in the 3-5 pH range (Fig. 19 a, b). A shift in the mid-point of activation for the different pH conditions is in line with the expected changes in surface membrane potential as proton concentration increases (McLaughlin, 1989). These data suggest that activation by protons (associated with the movement of the inner helix bundle TM2), appears to be independent of the inactivation relief by the transmembrane potential, and implies that the voltage and pH sensors in KcsA are likely to be distinct physical entities.

To address the possibility that the permeant ions themselves might be acting as the "gating charge", we determined the value of the equivalent charge (z_{eq}) and mid-point of activation of KcsA under a variety of ionic conditions. Thus, we found very little change in overall voltage dependent for KcsA at low symmetric K^+ (20 mM), under asymmetric K^+ concentrations (20 mM/200 mM, inside/outside), with Rb^+ as charge carrier, and in the presence of high concentrations of Ca^{2+} or Mg^{2+} (Table 2). These data suggest that KcsA voltage dependence is unlikely to result as a consequence of permeant ion rearrangement in the pore or due to voltage-dependent block by divalent cations (which does produce block at high voltages but does not change z_{eq}).
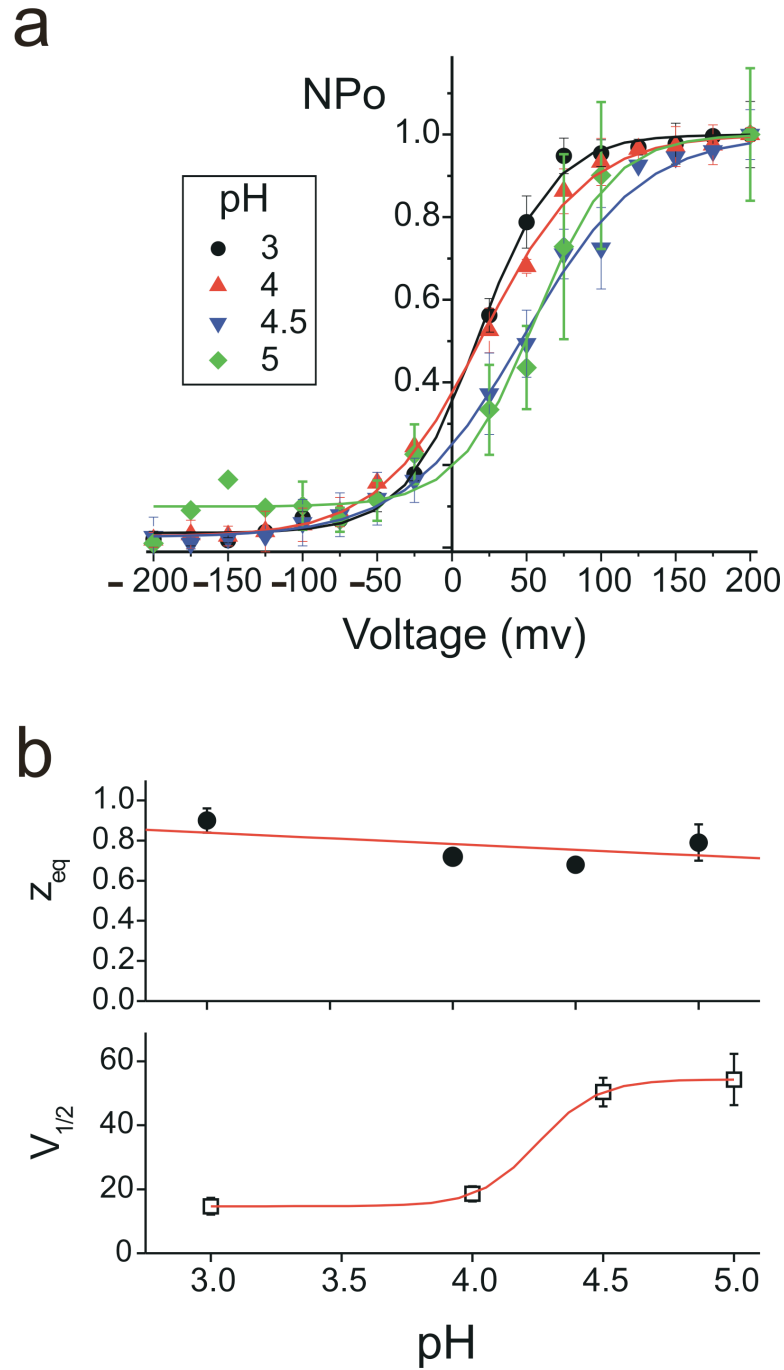
Figure 19 Voltage gating is independent from proton-dependent gating. a) Voltage-dependence of open probability obtained at different pH values. Individual plots were fitted to Boltzmann functions as in Figure 1. b) pH-dependence of the equivalent charge (zδ) and activation mid-points (V$_{1/2}$) as derived from the Boltzmann function fits. Data are shown as mean ± the standard deviation.

Table 2

KcsA voltage dependence under different ion conditions

Ion concentration Intracellular/Extracellular (mM)	Equivalent Charge[1] (Zeq)	Mid-point of Activation[1] (mV)
Symmetric High K^+ (200/200)	0.78 ± 0.03	18.5 ± 2.36
Symmetric Low K^+ (20/20)	0.89	-5.4
Asymmetric K^+ (20/200)	0.99 ± 0.11	-50.9 ± 12.7
Symmetric Rb^+ (200/200)	0.83 ± 0.09	-0.8 ± 0.11
Symmetric Mg^{++} (10/10)	0.73 ± 0.07	22.1 ± 2.3

[1] Except for the low K^+ experiments, data shown as mean $\pm$ SD

3.4.2 Locating the gating charge

What, then, is the identity of the "voltage-sensor" in KcsA? Assuming that voltage modulation derives from the movement of discrete charges across the TM voltage field, neutralization of these charges should drastically decrease KcsA response to transmembrane potentials. A survey of the proposed full-length KcsA reveals a large density of charges at the –N and –C terminal ends, as well as in the extracellular vestibule of the channel (red and blue spheres, Fig. 20a). Most of these charges are predicted to be accessible to the aqueous media (Cortes et al., 2001), outside the influence of the voltage field. This was confirmed by experiments showing that the voltage dependence of KcsA gating is unaffected by deleting either the N-terminal or C-terminal segments of the channel (containing a total of 18 charges, Fig. 20b). Interestingly, deletion of the C-terminus seems to increase the susceptibility of the channel to block at large positive potentials, a phenomenon we have not investigated further.

The remaining 11 charged residues in the channel core were individually mutated to cysteine, and their voltage gating evaluated as above (Fig. 20c). In this survey, z_{eq} remained unchanged for most of the mutants, although large shifts in the mid-point of the Boltzmann distribution (Fig. 20c, bottom) were typically associated with mutations that affected pH dependence (Cuello, L unpublished data). We found that voltage dependence is essentially eliminated by neutralization of a single residue, Glu71, adjacent to the selectivity filter signature sequence. In the high-resolution KcsA structure (Zhou et al., 2001b), this residue is engaged with Asp80 in a strong carboxyl-carboxylate pair, and as shown in the second chapter is one of the key determinants of open state stability and inactivation in KcsA (Cordero-Morales et al., 2006b). Attempts to recover voltage-

dependent gating by covalent modification with MTSES (which adds a negative charge

to the E71C mutant) were unsuccessful, perhaps due to the limited solvent accessibility at

that position.
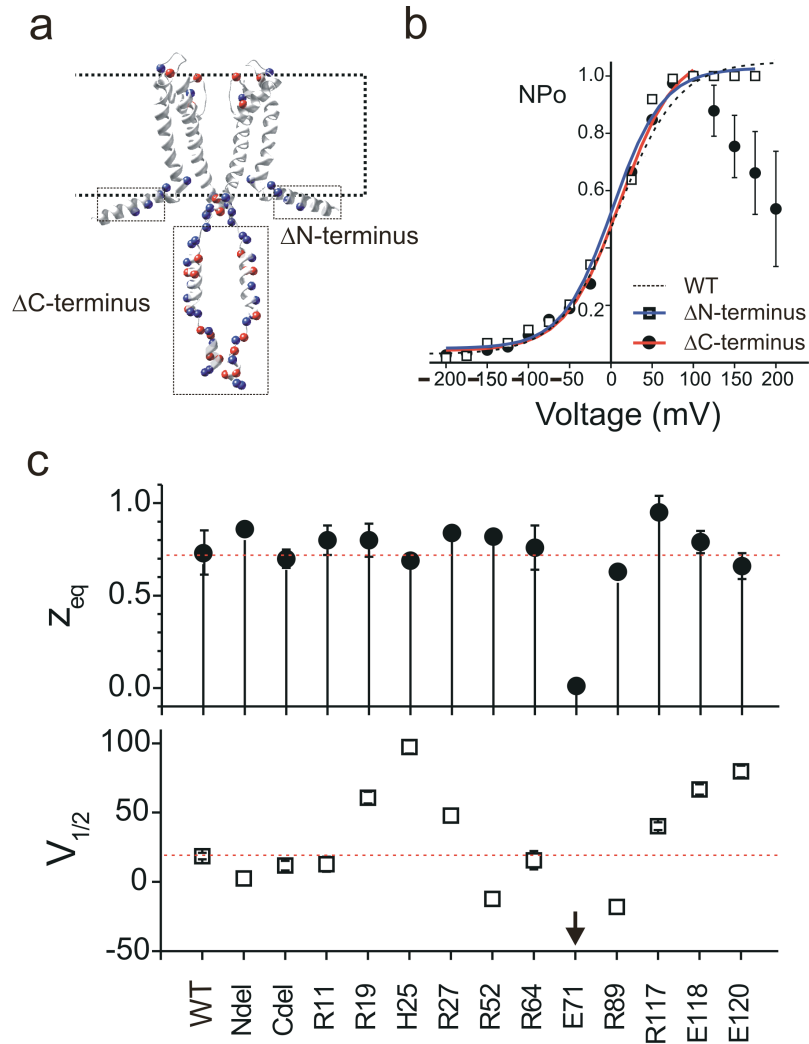
Figure 20 The voltage sensor in KcsA is located at the selectivity filter. a) Distribution of charged residues in the full-length KcsA structure. Negatively and positively charged residues are represented by red and blue spheres, respectively. Broken-line boxes show the extent of deletions in the ΔCterm and ΔNterm constructs. b) Voltage-dependence of open probability for ΔCterm (●) and ΔNterm (□) truncations, as compared to the wild-type channel (broken line). c) Cysteine-scan neutralization of charges in the core (transmembrane) regions of KcsA. Equivalent charge (zδ, top) and activation mid-points ($V_{1/2}$, bottom) for each individual neutralization mutant as derived from Boltzmann function fits. Arrows point to residue Glu71, the only charge neutralization that reduces voltage dependence to a large extent. All data are shown as mean ± the standard deviation.

An analysis of the E71C voltage-dependent gating (Fig. 21) demonstrates that neutralization of Glu71 essentially eliminates gating differences at extreme potentials (Fig. 21a), although it is worth noting that the asymmetries in open channel noise (conduction at negative voltages is much noisier than at positive voltages) remain unaffected by Glu71 neutralizations (Fig. 21 a, b). As it has been suggested previously, (Heginbotham et al., 1999) this behaviour might be the consequence of rapid, unresolved transitions that take place once KcsA opens and could be associated with the direction of current flow. Figure 21c shows the apparent probability vs. voltage curve for the E71C mutant in comparison with the WT channel. Although the Boltzmann fit to the data suggest that the gating charge has been dramatically reduced and the mid-point of the transition shifted to extreme negative potentials ($V_{1/2} \sim$ -400 mV and z_{eq} = 0.052), it is clear that at pH 4.0 E71C is essentially fully open over a wide range of voltages. We found identical results when Glu71 was mutated to alanine.
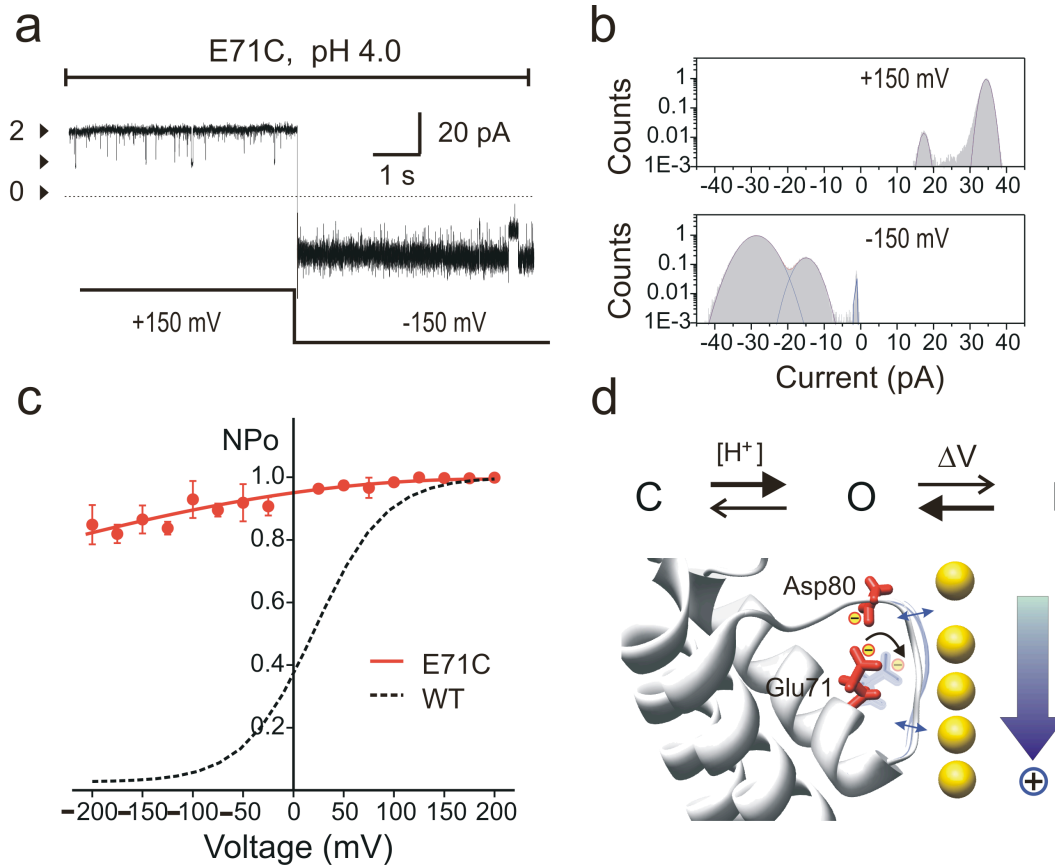
Figure 21 Neutralizing Glu71 sharply reduces the voltage-dependence. a) Steady-state multi-channel (2 channels) patch-clamp record of the asolectin-reconstituted E71C mutant. The lower line represents the point at which transmembrane voltage changes from +150 to -150 mV. b) All-points amplitude histogram from record in a. Individual fits to a sum of Gaussians were use to determine the relative area per peak and the NPo value at each voltage. c) Voltage-dependence of open probability. The continuous line is an approximate fit to a Boltzmann function with $V_{1/2} \sim -400$ mV and $z\delta = 0.052$, data are shown as mean ± the standard deviation. d) A proposed model of the voltage-dependence in KcsA gating. Reorientation of the Glu71 side chain within the voltage field affects its interaction with Asp80 and may promote the destabilization of the inactivated state at positive potentials.

3.5 DISCUSSION AND CONCLUSION

Glu71 has been the subject of theoretical (Berneche and Roux, 2000; Berneche and Roux, 2002; Guidoni et al., 1999; Ranatunga et al., 2001) and experimental (Choi and Heginbotham, 2004) analysis, since its side chain is the only electrically charged group embedded at the core of the selectivity filter. Although there is some consensus regarding the nature of the carboxyl-carboxylate interaction and the sharing of a proton between the two carboxylates (Berneche and Roux, 2000; Berneche and Roux, 2002; Ranatunga et al., 2001), the present findings lead to the conclusion that Glu71 must be a least partially ionized and that the proton is likely to be on Asp80.

How does voltage influence the conformation of the selectivity filter? In chapter 2, we have shown functional and structural evidence to suggest that the interaction between Glu71 and Asp80 might destabilize the conductive conformation of the selectivity filter, facilitating entry into a long-lived non-conducting conformation that bears many similarities with the C-type inactivated state of eukaryotic voltage-dependent potassium channels (Cordero-Morales et al., 2006b). Given the orientation of KcsA in the membrane and direction of the electric field, we propose a mechanistic explanation for the effects of voltage fields on KcsA gating. After imposing a large depolarization, the carboxylic group of Glu71 will tend to reorient towards the intracellular end of the channel (Fig. 21d). This movement would presumably disrupt the Glu71-Asp80 carboxyl-carboxylate pair (which requires the extended conformation of the Glu71 side chain), affecting the conformation of the selectivity filter as shown in chapter 2 (Cordero-Morales et al., 2006b) and thus, either prevent entry into or facilitate exit from the inactivated state.

Based on the present set of results and on the data in the chapter 2, a self-consistent view of KcsA gating is starting to emerge. Channel activation is solely dependent on proton binding somewhere in the intracellular side of the channel. At low pH, proton binding promotes opening of the TM2 inner bundle initiating ion flow through the selectivity filter. However, the conducting conformation of the selectivity filter is meta-stable and undergoes a spontaneous transition into a long-lived non-conducting conformation. Thus, under stationary conditions, gating is dominated by these transitions at the selectivity filter, as the TM2 bundle remains fully open and the observed single channel events correspond to transitions between the inactivated and open state. Since transitions to and from the inactivated state depend on the carboxyl-carboxylate interaction between Glu71 and Asp80, this equilibrium is highly dependent on the orientation of the Glu71 side chain which can reorient according to the direction of the transmembrane voltage field, thus providing an explanation for the voltage-dependent gating events in KcsA. These phenomena might play a physiological role in establishing and modulating potassium fluxes in prokaryotes under steady-state conditions.

CHAPTER 4: Molecular driving forces determining potassium channel slow

inactivation

4.1 ABSTRACT

Potassium channels undergo a time dependent slow inactivation process that plays a key role in modulating cellular excitability. In this chapter, we show that in the prokaryotic proton-gated potassium channel KcsA, the number and strength of hydrogen bonds interactions between residues in the selectivity filter and its adjacent pore helix determine the rate and extent of C-type inactivation. Upon channel activation, the interaction between residues at positions Glu71 and Asp80, promotes a filter constriction parallel to the permeation pathway, which affects K^+ binding sites and presumably abrogates ion conduction. Coupling between these two positions results in a quantitative correlation between their interaction strength and the stability of the inactivated state. Engineering of these interactions in the eukaryotic voltage-dependent potassium channel Kv1.2 suggests a similar mechanistic principle for other K^+ channels. These events provide a plausible physical framework to understand C-type inactivation in K^+ channels.

4.2 INTRODUCTION

In potassium channels, C-type inactivation is an effective mechanism to control the duration of the conductive state through structural rearrangements along the permeation pathway (Hoshi et al., 1991; Yellen, 1998). This inactivation process has been correlated to conformational changes around the selectivity filter and the extracellular regions of the channel (Kiss et al., 1999; Liu et al., 1996; Yellen et al., 1994), it is inhibited by high extracellular K^+ and the blocker Tetraethylammonium (TEA) (Choi et al., 1991; Lopez-Barneo et al., 1993), and can be modulated by permeant ions like Rb^+, which have long

residence time in the selectivity filter (Demo and Yellen, 1992), decreasing the rate of inactivation (Choi et al., 1991). However, the molecular mechanism and conformational changes associated with C-type inactivation remain unresolved, mostly due to a limited understanding of the molecular forces that drive the selectivity filter to its inactivated conformation and lack of structural information.

Several pieces of evidence support the critical role of a network of interactions behind the selectivity filter on channel gating for a number of K^+ channels (Kurata and Fedida, 2006; Seebohm et al., 2003). A point mutation in Kv2.1 (D378E), equivalent to Asp80 in KcsA, affects the single channel behavior by the destabilization of the open state (Chapman et al., 2006). Moreover, mutations in the selectivity filter and pore helix of *Shaker,* hERG, and inward rectifiers also have large effects on gating properties (Ficker et al., 1998; Lu et al., 2001; Yifrach and MacKinnon, 2002). In addition, recent data point (Chapter 2) to a mechanistic equivalence between inactivation in a prokaryotic channel KcsA (from *Streptomyces lividans)* and C-type inactivation in eukaryotic voltage-dependent K^+ channels (Cordero-Morales et al., 2006b; Gao et al., 2005). In KcsA, the selectivity filter is stabilized by a hydrogen bond network, which includes interactions between the carboxylate groups of Glu71/Asp80 (Fig. 21d), Trp67/Asp80 and a buried water bound to the backbone amide nitrogen of Gly79/Leu81 (Zhou et al., 2001b). Disrupting these interactions exerts a major influence on the inactivation process of KcsA as shown in chapter 2 and 3 (Cordero-Morales et al., 2006a; Cordero-Morales et al., 2006b). The Glu71/Asp80 carboxyl-carboxylate interaction is present in other bacterial channels, however its role is less understood (Kuo et al., 2003), and similar

electrostatic interactions exist in eukaryotic inward rectifiers (Yang et al., 1997a), but is not typically found in eukaryotic voltage-gated K^+ channels.

We suggested in chapter 2 that the conductive conformation of the selectivity filter is intrinsically unstable due to interactions between residues in the external vestibule and pore helix (Cordero-Morales et al., 2006b). In this model, the movement of TM2 (the inner helix bundle) during gating allows the selectivity filter to fluctuate between conductive and non-conductive conformations before collapsing into the more stable inactivated state. Thus, to understand the molecular basis of C-type inactivation we need to identify and characterize the driving forces responsible for the transition between conductive and deep inactivated conformations of the K^+ channel selectivity filter. In this chapter, we address two fundamental questions regarding C-type inactivation: the nature of the microscopic forces that drives the transitions from the conductive to non-conductive state of the selectivity filter, and the putative structural rearrangements leading to inactivation. To this end, we have systematically analyzed the role of the interaction between positions Glu71 and Asp80 in KcsA using functional, spectroscopical, structural and computational approaches, and extended our findings to Kv1.2, a voltage-gated K^+ channel from rat brain.

4.3 EXPERIMENTAL METHODS

4.3.1 Mutagenesis and channel biochemistry

Mutagenesis and channel biochemistry were carried out as discussed in chapter 2 (section 2.3.2) with the exception of KcsA E71H mutant. Several changes to the conventional expression and purification protocol were used to preserve the oligomeric properties of this mutant (Fig. 22). Induction was carried out with 0.5 mM IPTG in the presence of 10% glycerol, 10 mM Ba^{2+} at 27°C for 6 h. Membranes containing E71H channel were solubilized for 3 hours at 4°C in 200 mM KCl, 50 mM Tris, 10% glycerol, 10 mM DDM pH 8 and then incubated for 3 h at 4°C with Co^{2+}-based metal-chelate chromatography resin.
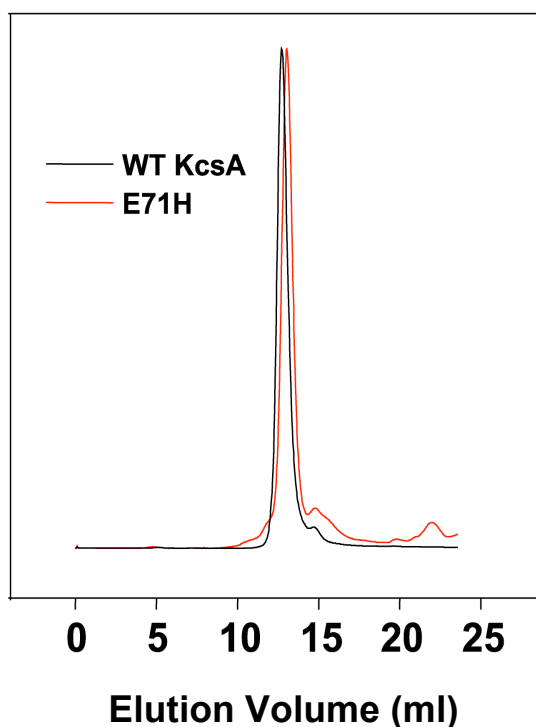
Figure 22 Hydrodynamic properties of E71H mutant. Gel filtration chromatogram superposition of WT and E71H. Overall, E71H retain WT KcsA oligomeric properties.

4.3.2 Liposome patch-clamp

Liposome patch-clamp was carried out as discussed in charter 2 (section 2.3.3), with the exception of E71H, which was reconstituted in 1:25 protein:lipid ratio for macroscopic currents.

4.3.3 Two-electrode voltage-clamp

cRNA from rat Kv1.2 (rKv1.2, accession number: X16003, GI:1235594) was prepared with the mMESSAGE mMACHINE T7 kit (Ambion Inc., Austin, TX) following linearization of plasmid cDNA. Defolliculated stage IV and V *Xenopus* oocytes were injected with 5 ng WT or mutant rKv1.2 cRNA and cultured in ND96 supplemented with 50 µg/ml gentamycin and 1% penicillin/streptomycin at 16°C. Whole-cell currents were measured 48 hours post-injection using a Geneclamp 500 amplifier (Axon Instruments, Inc.). Data were sampled at 5 kHz and recorded using Clampex software (Axon Instruments, Inc.). Leak and capacitance was subtracted online using a P/4 protocol. Bath solution was (in mM) 96 NaCl, 4 KCl, 1 $MgCl_2$, 0.3 $CaCl_2$, 10 HEPES (pH 7.6).

4.3.4 EPR spectroscopy

EPR spectroscopy was carried out as discussed in charter 2 (section 2.3.4).

4.3.5 X-ray crystallography

KcsA (pQE32 vector) mutant E71S in the presence/absence of 5 mM TBA, and E71T were crystallized (in collaboration with Vishwanath Jogini from Eduardo Perozo's laboratory) in the presence of an antibody Fab fragment following published protocols (Zhou et al., 2001b). Beam-like crystals of KcsA-Fab complex appeared after one week in a sitting drop containing 23–26% PEG400 (v/v), 50 mM magnesium acetate, 50 mM sodium acetate (pH 4.8-5.4) at 19°C. Crystals diffracted to Bragg spacing of 2.05 Å for

E71S with TBA, 2.2 Å for E71T and 2.3 Å for E71S without TBA. Data were

collected at the GM/CA-23-ID beamline at the Advanced Photon Source and processed

with HKL2000 (Otwinowski and Minor, 1997). Glu71 mutant structures were solved by

molecular replacement using the WT KcsA-Fab complex structure (PDB entry 1K4C) as

search model. All the structures are solved using Fab and KcsA without the selectivity

filter as the initial model for molecular replacement. Refinement of the structures was

carried out through multiple cycles of manual rebuilding using the program O (Jones et

al., 1991) and refinement using CNS (Brunger et al., 1998). Data collection and

refinement statistics are given in Table 3. E71S (TBA) PDB ID: 2P7T.

4.3.6 Molecular dynamics

All molecular dynamics carried out in this work were done in collaboration with a

post-doctoral fellow (Vishwanath Jogini) in Eduardo Perozo's laboratory and Benoit

Roux. The simulation system was represented by an atomic model of KcsA (PDB ID:

1K4C) channel embedded in dipalmitoylphosphatidylcholine (DPPC) surrounded by an

aqueous solution of 150 mM KCl. The microscopic system was composed of KcsA

tetramer of 404 amino acids (6284 atoms), 112 DPPC molecules, 6384 water molecules,

3 K^+ ions in the pore (S_0-S_2-S_4 positions in the selectivity filter). To make the entire

system electrically neutral, 6 K^+ and 21 Cl^- were added in the bulk solution to mimic 150

mM KCl. All the calculations were performed using c29a2 or c32a2 of the biomolecular

simulation program CHARMM (Brooks et al., 1983). The simulation methodology has

been described previously (Berneche and Roux, 2000).

Different Glu71 mutants are generated *in silico* and carefully equilibrated before

production run. For the umbrella sampling PMF calculations, a total of 180 independent

E71A simulations of 2 ns with a biasing harmonic potential centered on RMSD of the filter (varying successively from 0 to 2 every 0.1 Å) and $71C_\alpha$ - $Asp80C_\alpha$ (varying successively from 8.5 to 12.5 every 0.5 Å) were generated with a force constant of 40 kcal mol^{-1}Å^{-2} and 10 kcal mol^{-1}Å^{-2}, respectively. All the biased simulations were unbiased using the weighted histogram analysis method (WHAM) (Kumar et al., 1992) to calculate the full PMF. First, MD simulations were performed in the presence of an artificial biasing potential on RMSD of the filter to obtain the entire conformational space traversed by the filter at given C_α-C_α distance. Next, the bias introduced by this potential is removed to obtain the unbiased free energy surface of the system.

4.4 RESULTS

4.4.1 Functional role of the Glu71/Asp80 interaction

To understand the nature of the interaction between Glu71/Asp80 (Fig. 23a) and its role in C-type inactivation, we have systematically analyzed the functional effects of a series of side-chain substitutions at position 71 at the KcsA pore helix (Fig. 23b). Of the 15 single point mutations introduced 9 (Gly, Ala, Ser, Cys, Thr, Val, Gln, His and Ile) were suitable for electrophysiological analysis. Trp and Pro were not used in this study to avoid the impact that these residues might cause on folding and assembly. Arg and Lys substitutions severely compromised channel folding and expression. Figure 23b shows that most of the mutations yield functional channels that exhibit low levels of inactivation (Gly, Cys, Val, Gln and Ile) or display only partial inactivation (Ser and Thr), as quantified by the ratio between steady-state and the macroscopic peak currents. However, substitution to histidine not only enhances the rate but also the extent of inactivation,

following pH-mediated activation (Fig. 23b, c), presumably by establishing a stronger

ionic interaction with Asp80.
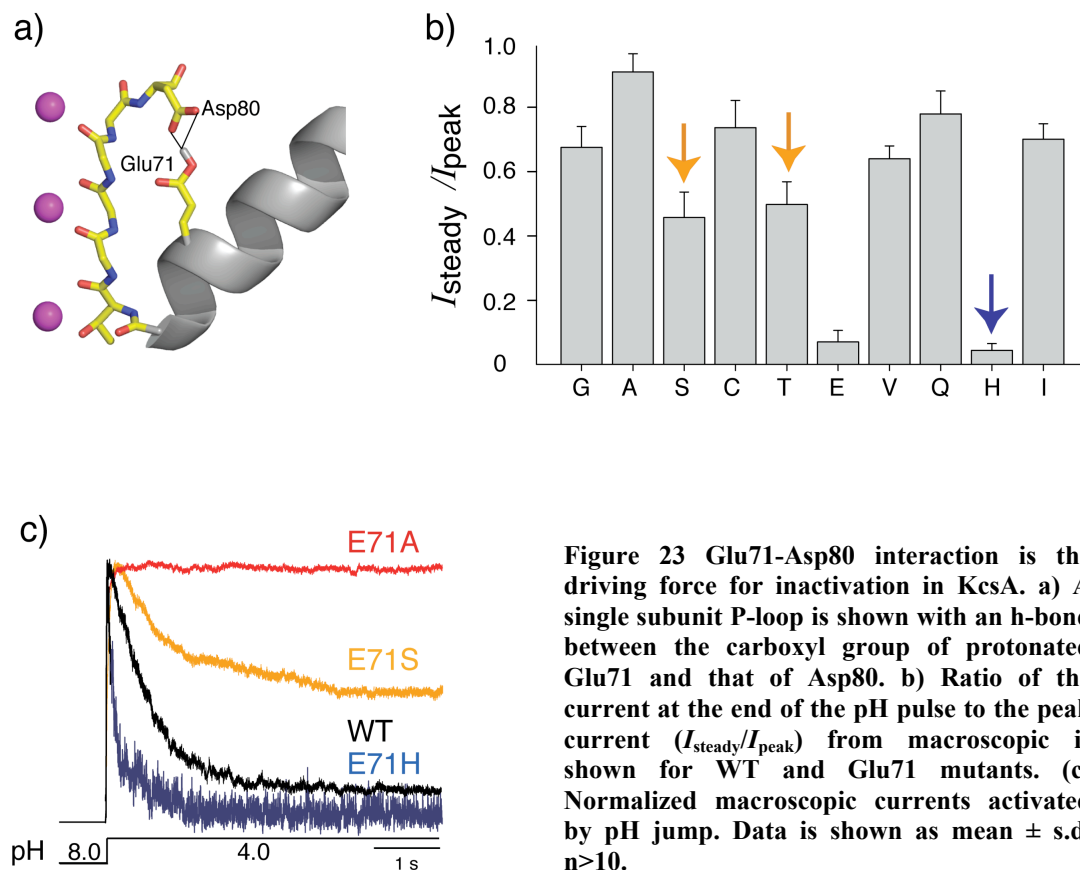
Figure 23 Glu71-Asp80 interaction is the driving force for inactivation in KcsA. a) A single subunit P-loop is shown with an h-bond between the carboxyl group of protonated Glu71 and that of Asp80. b) Ratio of the current at the end of the pH pulse to the peak current (I_{steady}/I_{peak}) from macroscopic is shown for WT and Glu71 mutants. (c) Normalized macroscopic currents activated by pH jump. Data is shown as mean ± s.d. n>10.

Macroscopic current behavior is fully recapitulated at the single channel level (Fig. 24a). At steady state, single channel recordings of E71H and WT channels are dominated by very long silent periods ($\tau > 10$ s) interrupted by bursts of activity. E71S displays shorter non-conductive periods ($\tau \sim 1\text{-}2$ s), while E71A is characterized by long open times with brief sojourns to non-conductive conformations. As expected, we also found an inverse relationship between the rate of inactivation and the open dwell times of different mutants (Fig. 24b). Mutations that remove inactivation (i.e. E71A) show long mean open times (~ 100 ms), whereas the deeply inactivated E71H mutant opens with very brief spikes (mean open times < 2 ms). In addition, the slowest closed time constant (Fig. 24b, red arrow) is directly proportional to the rate of inactivation. These results suggest that the functional effect of these mutations is a consequence of the chemical property of the side-chain at position 71, and have a dramatic influence on the stability of the conductive conformation of KcsA.

To evaluate the contribution of the selectivity filter and the inner helical bundle gate to the steady-state gating of these mutants, we followed the conformation of TM2 by EPR spectroscopy (Fig. 24c). We generated mutants E71H and E71S into a KcsA background containing mutation G116C. This cysteine provides a spin labelling site to report the pH-dependent conformational changes in TM2 (Cordero-Morales et al., 2006b; Perozo et al., 1998; Perozo et al., 1999). Comparison of the CW-EPR spectra line shape of spin-labelled G116C, E71A/G116C, E71S/G116C and E71H/G116C mutants at pH 7.0 and 4.0 revealed that the magnitude of the opening at the lower gate (estimated from the dipolar spectral amplitude ratio) is essentially identical. Thus, the dramatic differences in steady state nominal open probability among these mutants are not due to

changes in the inner bundle gate behavior, rather solely determined by the conformational changes at the selectivity filter.
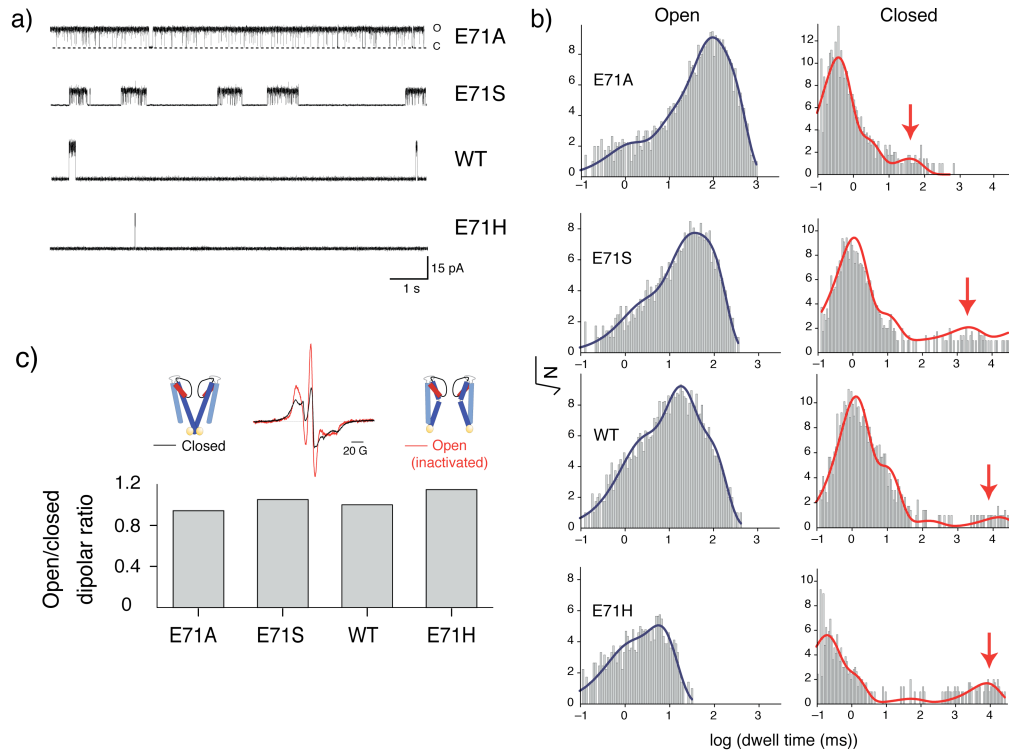
Figure 24 Inverse relationship between the rate of inactivation and the open dwell times. a) Representative singles channels traces of WT and Glu71 mutants obtained at pH 4 and +150 mV in symmetric 200 mM KCl solutions. The long closed time periods characteristic of WT KcsA inactivation (absent in E71A) are present in E71H and to less extent in E71S single channel records. b) Dwell time distribution from records in (a). Red arrow points to the dominant slowest closed time constant. c) Opening of the intracellular gate monitored by CW-EPR from spin labels attached at residue G116C in WT-type and in mutants that abolish (E71A/G116C-SL) or recover (E71S,H/G116C-SL) inactivation. Top, representative CW-EPR spectra of G116C-SL obtained from reconstituted channels at pH 7 (black) or pH 4 (red). Bottom, the extent of intracellular gate opening derived from the amplitude ratio of spectra (dipolar ratio Ω, square).

As a histidine residue could render a positive charge at position 71, we expect E71H to restore the critical interaction between position 71 and 80 necessary for the selectivity filter to inactivate (Cordero-Morales et al., 2006b). To test the interaction between imidazolium-carboxylate moieties (His71/Asp80), we analyzed the voltage modulation of KcsA gating (Fig. 25) (Cordero-Morales et al., 2006a). pH-jump experiments show that, contrary to WT KcsA, the rate and extent of inactivation in E71H are enhanced at depolarizing and decrease at hyperpolarizing potentials (Fig. 25a, b). This inversion in the voltage-dependence of inactivation would be expected if the transmembrane voltage field promotes a reorientation of the positive imidazolium group so that at inside positive potentials, it moves towards the Asp80 carboxylate, strengthening the His71-Asp80 interaction (Fig. 25c). The opposite voltage would thus weaken the interaction, as confirmed experimentally.

Inset in Figure 25a compares the absolute macroscopic currents of reconstituted E71H and WT. Ion current density for the E71H mutant was much lower than the WT even though the quantity of reconstituted protein was four times larger. Additionally, when reconstituted at equal protein:lipid ratio, the EPR spectra of WT/G116C and E71H/G116C showed similar amplitudes, suggesting that there is no difference in the amount of reconstituted channels (Fig. 26). These results imply that the large majority of E71H channels are already pre-inactivated (Baukrowitz and Yellen, 1995; Panyi and Deutsch, 2006) or they inactivate faster during the activation process (Smith et al., 1996).
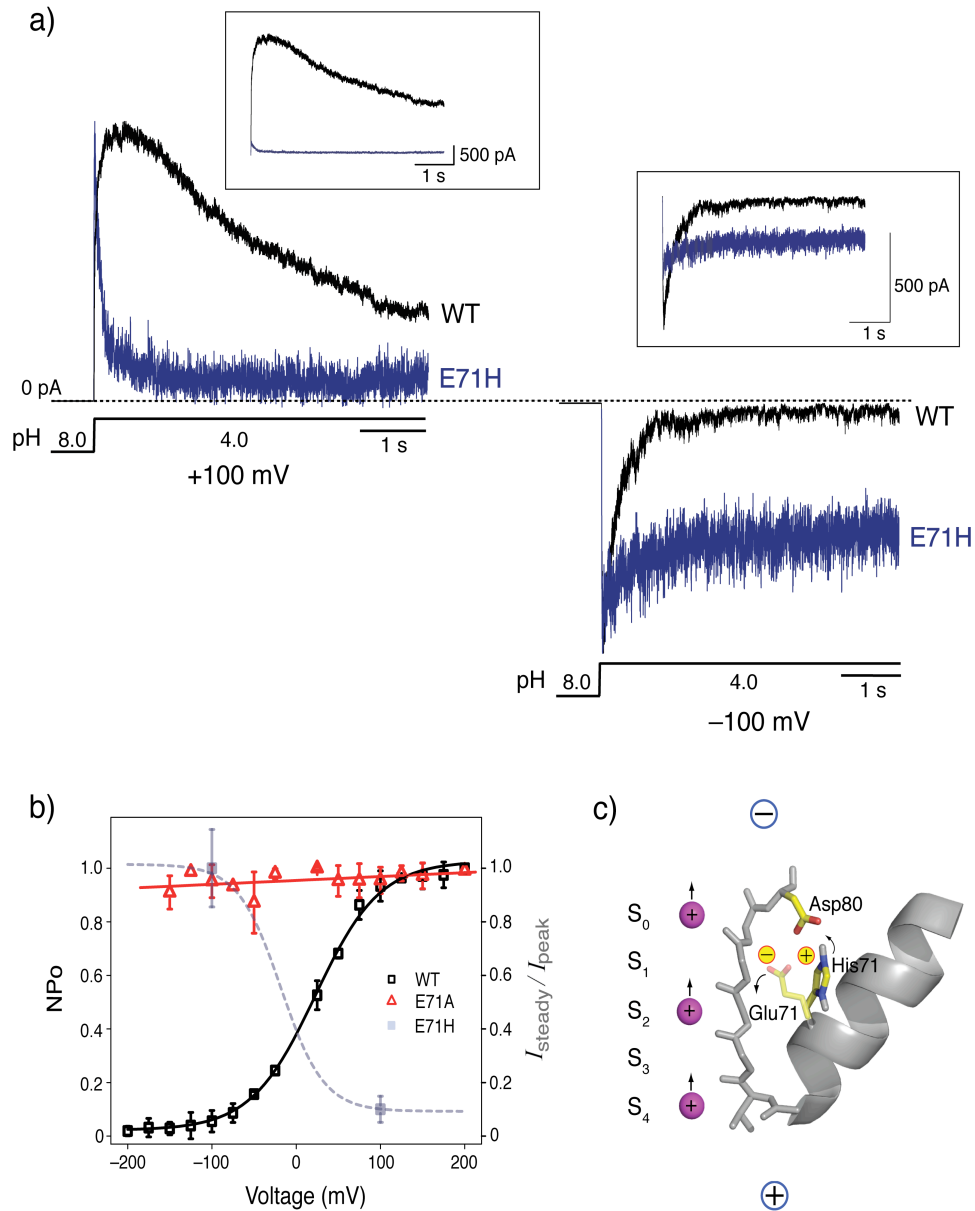
Figure 25 Histidine at position 71 inverts the voltage-dependence of inactivation. a Normalized currents in E71H show faster time constant of inactivation at depolarizing potential (+100 mV = 97 ± 29 ms) and slower at hyperpolarizing potential (-100 mV = 121 ± 469 ms) when compared to WT (+100 mV = 1733 ± 550; - 100 mV = 354 ± 59 ms). Inset shows a comparison of the absolute macroscopic currents between E71H and WT. **b** Steady state NPo vs. voltage curves were fitted to a Boltzmann function with $V_{1/2}$ = 22 mV, $z\delta$ = 0.72 (WT). E71A is fit to a linear regression with slope of > 0.001. A pseudo Boltzmann fit based on the two observations in E71H macroscopic shows the inversion of the voltage dependence. Two data points are included due to the very low channel activity of E71H. **c** Model of voltage dependent modulation at the KcsA filter. Data is shown as mean ± s.d. n>10.
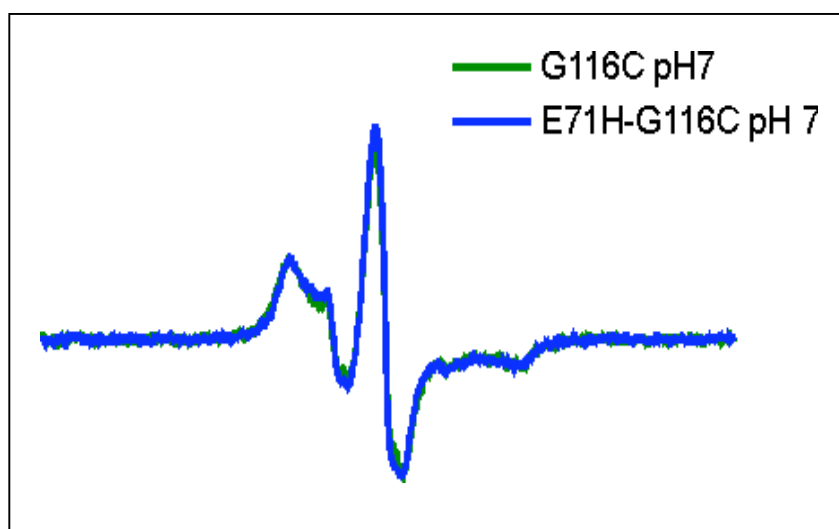
Figure 26 CW-EPR signal for G116C (WT) and E71H-G116C at pH 7.

4.4.2 Structural analysis of KcsA inactivation mutants

In collaboration with Vishwanath Jogini, we pursued a systematic structural analysis of KcsA mutants. Because of their varied open probabilities, mutants E71S and E71H represent ideal candidates for the structural investigation of the molecular interactions responsible for C-type inactivation. An initial puzzle was the mechanism by which E71S influences P_o in KcsA. This side chain is not long enough to establish a direct interaction with the Asp80 carboxylate and thus, should behave like E71A (a similar rational is true for E71T). Preliminary molecular dynamics simulation of E71S suggested that a water molecule might bridge the interaction between this side chain and Asp80.

To test this hypothesis, the crystal structures of the E71S with TBA (Fig. 27), PDB ID: 2P7T.), E71S and E71T without TBA (Fig. 28a, b) were solved at 2.05 Å, 2.3 Å and 2.2 Å resolutions, respectively. As expected, the distance between the carboxylate group of Asp80 and hydroxyl group of Ser71 is 5.2 Å, too far to support any direct interaction. But as predicted from MD simulations, we find a crystallographic water connecting these residues through a well-defined set of hydrogen bonds, as illustrated by the F_o-F_c omit map in Figure 27 (inset). This relay water would account for the interaction (albeit weaker) between the pore helix and external vestibule rendering an intermediate inactivated phenotype (Fig. 23c). An interesting observation from the MD simulation is the occupancy of this water molecule. In a 4 ns simulation, water is present in between Asp80 and E71S 2/3rd of the time (data not shown), a fact that correlates well with the strength of this interaction. Further, the B-factor for this water in the crystal structure is 40 Å^2, about twice that of the well-ordered water (20 Å^2) behind the filter.

These two findings suggest that the water molecule is disordered, and this can account

for the intermediate phenotype of E71S.
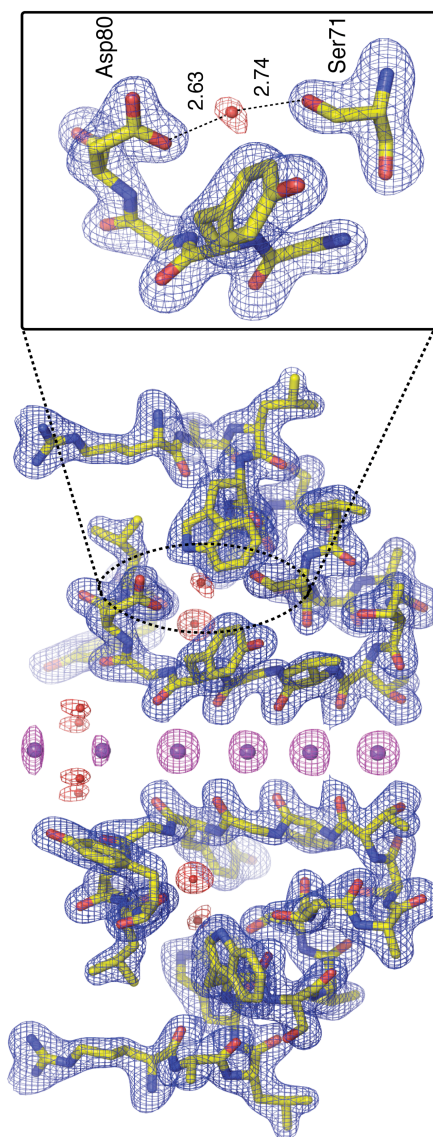
Figure 27 Structural basis of inactivation in E71S. Crystal structure of E71S with TBA at 2.05 Å. F_o-F_c omit map of the filter corresponding to residues 64-82 from two diagonally symmetric subunits. The polypeptide chain is in stick representation and the blue mesh corresponds to the F_o-F_c electron density map at $\sigma = 3.0$. Ions and water are represented as spheres with $\sigma = 5.0$ for the ions (magenta mesh); two outermost ions are at $\sigma = 2.5$) and $\sigma = 3.0$ for the water molecules (red mesh). Inset, single subunit representation of the H-bond interaction between E71S and Asp80 mediated through a crystallographic water.

Table 3. Data collection and refinement statistics. E71S (TBA) PDB ID: 2P7T.

	KcsA E71S+TBA
Data collection	
Space group	I4
Cell dimensions	
a, b, c (Å)	156.34, 156.34, 76.0
α, β, γ (°)	90.0, 90.0, 90.0
Resolution (Å)	50.0-2.05
R_{merge} or R_{sym} (%)[a,b]	5.0 (26.9)
I / σI	33.5 (4.5)
Completeness (%)[a]	99.5 (97.8)
Redundancy	4.4 (4.1)
Refinement	
Resolution (Å)	50.0-2.05
No. reflections	50,887
R_{work} / R_{free} (%)[c]	21.9/23.4
No. atoms	
Protein	4,071
Ion	6
Lipid	41
Water	155
B-factors	
Protein	55.94
Ion	35.70
Water	50.33
R.m.s deviations	
Bond lengths (Å)[d]	0.006
Bond angles (°)[d]	1.285

[a]Values in parentheses are for the highest-resolution shell (2.15 Å – 2.05 Å).
[b] $R_{symm} = \Sigma \,|\, I - <I>| \,/\, \Sigma <I>$
[c]$R = \Sigma | Fo - Fc| \,/\, \Sigma$ Fo, 10% of the data that were excluded in the refinement were used in the R_{free} calculation.
[d]RMSD of bond is the root-mean-square deviation of bond angle and length
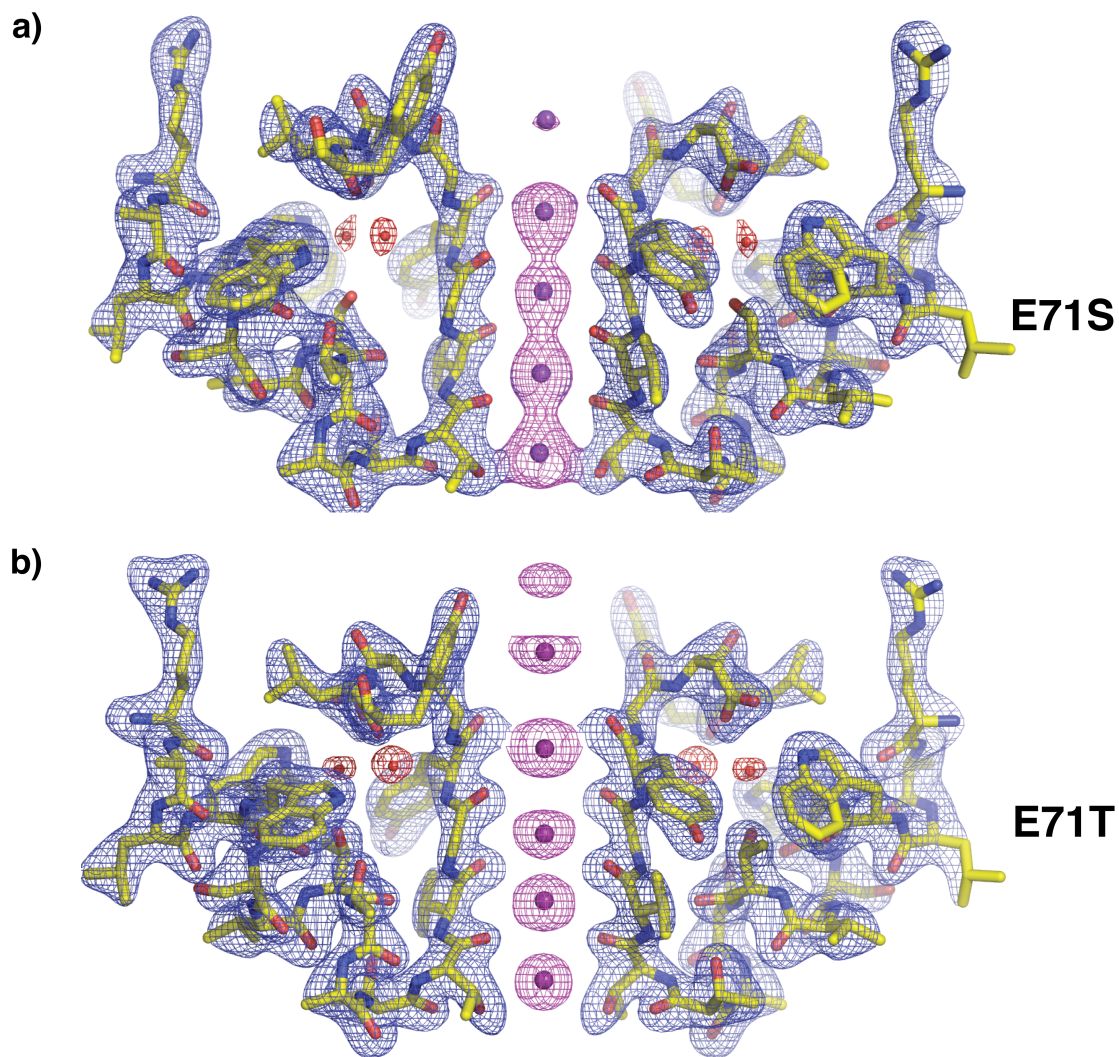
Figure 28 Crystal structure of a) E71S (2.3 Å) and b) E71T (2.2 Å) mutants without TBA. Electron density map of the selectivity filter from residue 64-82 from two diagonally symmetric subunits are shown. The polypeptide chain is in a stick representation and all the mesh corresponds to the Fo-Fc omit map. $\sigma = 3.0$ for the protein (blue mesh), $\sigma = 3.0$ for the ions (magenta mesh) and $\sigma = 1.5$ for the water (red mesh).

The interaction between His71 and Asp80 seems to be strong enough to promote a deep inactivated state (Fig. 23c and 25a). As a result, E71H represents a promising target for the structural determination of the inactivated state of the selectivity filter. Though vigorously pursued, we have been unsuccessful in our attempts to determine the crystal structure of E71H mutant, mostly due to its altered interaction with the Fab fragment, which is required to achieve high resolution structure (Fig. 29). Alternatively, we used MD simulations to characterize the role of E71H in the transition to the C-type inactivated form of the filter.

In silico mutation of WT KcsA to E71H$^+$ and subsequent equilibration of the system (Fig. 30) show that the selectivity filter becomes unstable (RMSD = 1.5 Å) shortly after constraints are released, affecting K$^+$ binding sites. Analysis of the 1 ns E71H MD trajectory leads to three important conclusions. First, the presence of oppositely charged residues in a low dielectric cavity results in instantaneous formation of a salt bridge between His71 and Asp80 (Fig. 30). Second, compared to the E71A simulation, the C$_\alpha$-C$_\alpha$ distance between His71 and Asp80 is reduced by 1-2 Å (Fig. 31) as a result of the strong interaction between these two residues. This in turn leads to a considerable deformation of the selectivity filter and pinching at the S$_1$ site. Third, unlike equivalent simulations in WT and E71A, ions move from their initial S$_0$-S$_2$-S$_4$ configuration to a new, S$_1$-S$_4$ arrangement with S$_0$ leaving the binding site (Fig. 30, upper right panel). These results establish that the nature of the hydrogen-bond network at the selectivity filter, dominated by 71-80 interaction and the charged state at position 71 determine both the stability of the conductive conformation and its entry into the non-conductive C-type inactivated state.
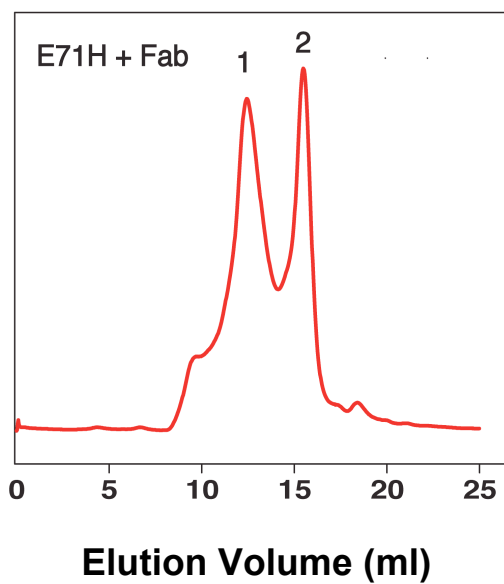
Figure 29 E71H fails to form a stable complex with the Fab fragment (a single monodisperse peak) . We have pursued the crystal structure determination of the E71H mutant vigorously but unsuccessfully. Nonetheless, as binding of the Fab to KcsA requires interaction with the extracellular loop and pore helix, this unexpected result points to the possibility that the three-dimensional conformation of this epitope is significantly changed for this particular mutant in a state-dependent way (Liu et al., 1996). Channel fraction (1) and Fab fragment fraction (2).
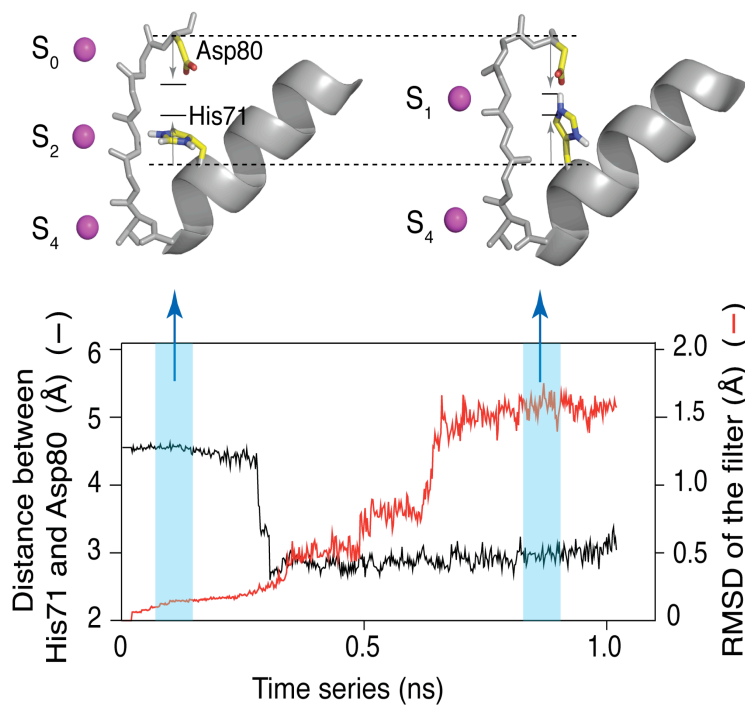
Figure 30 Structural basis of inactivation in E71H. Time series of the distance between E71H and Asp80, and RMSD of the filter. After releasing the constraints, the minimum distance between His71 and Asp80 is sharply reduced (black), followed by distortion of the filter (red). Simulation was stopped at 1 ns after filter became distorted. Initial configuration of the channel has the His71 rotamer away from Asp80 (upper left panel). About 300 ps into the simulation (constrains released) an ion pair interaction is formed between His71 and Asp80 (upper right panel).
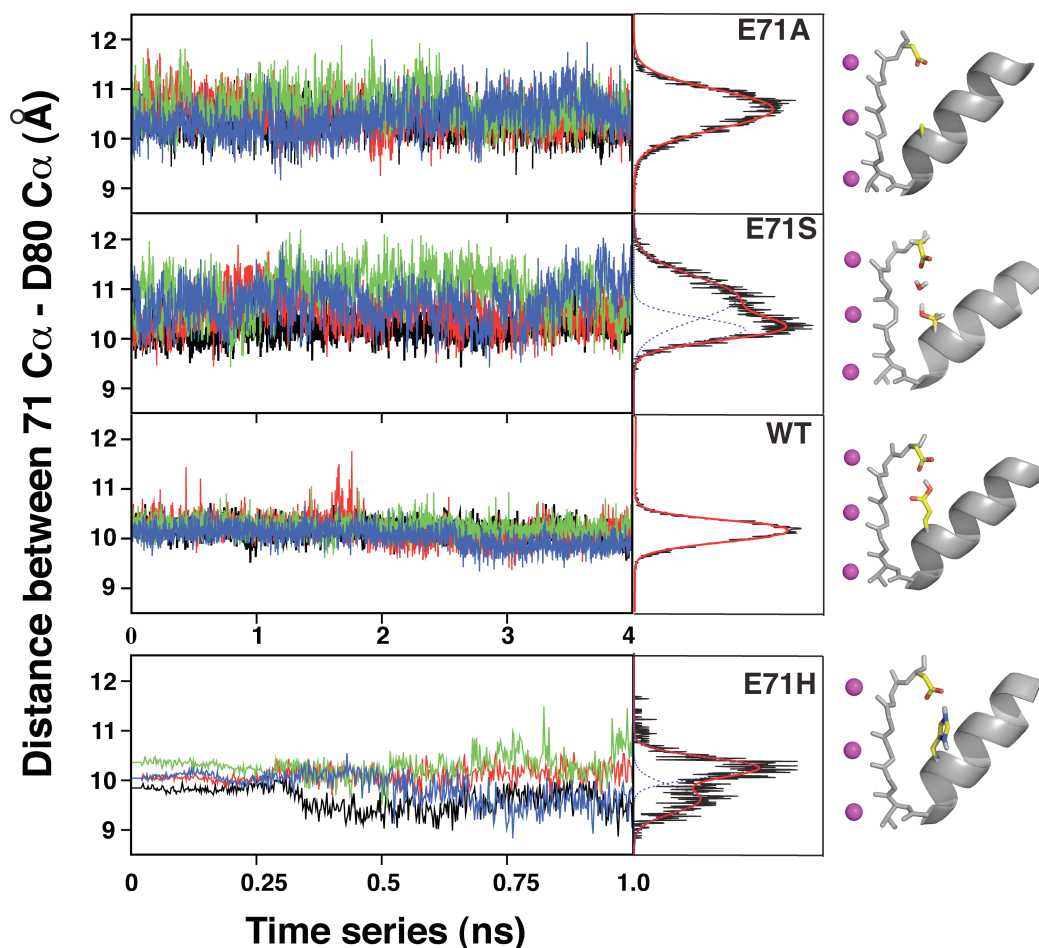
Figure 31 Time series of 71C$_\alpha$-Asp80 C$_\alpha$ distance extracted from MD simulations of E71A, E71S, WT and E71H. Different Glu71 mutants are generated *insilico* and equilibrated carefully before production run with ions in S$_0$-S$_2$-S$_4$ configuration in the selectivity filter as shown in the right panel. Each color represents a monomer. Middle panel, frequency distribution of the 71 C$_\alpha$-Asp80 C$_\alpha$ distance evaluated from MD trajectories where red line represents Gaussian fits. Distances used for extraction of individual PMF profile of different mutants (Fig. 33b) are obtained from Gaussian fits and crystal structures. WT and E71A crystal structures show C$_\alpha$ - C$_\alpha$ distance of 9.9 Å and 10.0 to 12.5 Å respectively, whereas from MD we obtained 10.0 Å and 10.6 Å. E71S and E71H distance frequency distribution can be fit to two Gaussians with highest amplitude at 10.2;10.8 and 9.6;10.1 respectively. From above, qualitatively we choose C$_\alpha$-C$_\alpha$ distances of 11.0, 10.4, 9.9 and 9.6 Å for E71A, E71S, WT and E71H respectively.

4.4.3 The driving forces of C-type inactivation

The present set of mutants affords us the opportunity to probe the structural and energetic aspects of the selectivity filter interactions responsible for C-type inactivation in KcsA. MD simulations were carried out on WT, E71A, E71S and E71H to test the stability, conformational dynamics of the selectivity filter and the role of different side chain pairings to Asp80. What then determines the rate and extent of C-type inactivation in this group of mutants?

At first, we found a very strong correlation between NPo and the strength of interaction in the X71-Asp80 pair (Fig. 32), where X71 stands for any of the tested side chains. We assign interaction strength as the number of hydrogen bonds (plus an electrostatic component in the case of E71H) associated to residues Trp67, X71 and Asp80 in each case (Fig. 32, upper panel; number within brackets). Interaction strength, in turn, directly correlates with the X71-Asp80 C_α-C_α equilibrium distance in each mutant (from crystallography and MD simulations).

For instance, the C_α-C_α distance in the two crystals structure forms of the non-inactivating E71A mutant ranges between 10 to 12.5 Å and fluctuates near 11 Å in MD simulations. From the MD trajectories, the increasingly inactivating E71S, WT and E71H mutants showed C_α-C_α distance distributions centered around 10.4 Å, 9.9 Å and 9.6 Å, respectively (Fig. 31). As a consequence of these results, we propose that the open conductive state of E71S, WT and E71H becomes increasingly unstable in response to the H-bond network between positions in the pore helix (residue 71) and the external vestibule of the pore (residue 80). Interactions between these two sites promote a

compression of the selectivity filter parallel to the permeation pathway, which

energetically biases it towards the inactivated conformation.
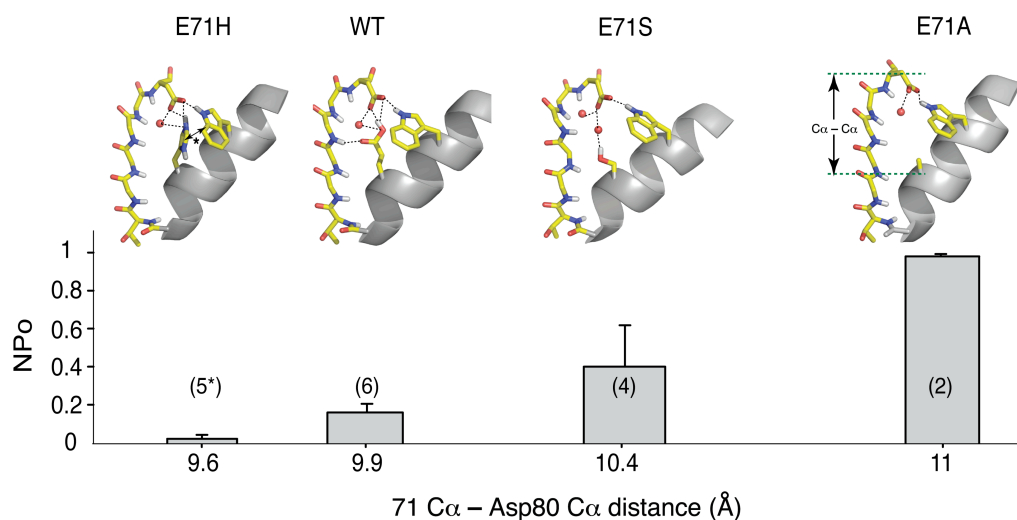
Figure 32 Relation between the open-channel probability (evaluated from Gaussian fits of all point time histogram) and equilibrium $71C_\alpha$-$Asp80C_\alpha$ distance extracted from MD simulations and crystal structures. Within parenthesis is the number of H-bond interactions involving residues 67, 71 and 80. (*) represents extra cation-π (protonated E71H and Trp67) and ionic (protonated E71H and Asp80) interaction in E71H apart from H-bond network. Data is shown as mean ± s.d. n>10.

The structural and energetic aspects of the molecular interactions responsible for C-type inactivation in KcsA were probed through additional MD simulations, as a way to test the stability and conformational dynamics of the selectivity filter. To evaluate this possibility we calculated, using umbrella sampling simulations (Torrie and Valleau, 1977), the free energy surface or potential of mean force (PMF) corresponding to the filter conformation as a function of the backbone distance (C_α-C_α) between positions 71 and 80.

The free energy landscape shown in Figure 33a, is a two-dimensional PMF carried along two reaction coordinates, RMSD of the filter and C_α-C_α distance. The L-shaped surface clearly shows two minima, one at 0.6 Å RMSD corresponding to a normal selectivity filter, favored at longer C_α-C_α distances, and a second one at ~0.9 Å RMSD at smaller C_α-C_α distances, putatively associated with a non-conductive conformation of the selectivity filter. This is best revealed by looking at sections (Fig. 33b) of the PMF extracted for average distances corresponding to WT (9.9 Å) and the mutants affecting inactivation (E71A = 11 Å, E71S = 10.4 Å, and E71H = 9.6 Å). When the PMF energies are normalized to the 0.6 Å RMSD conducting filter minima, the relative position of the second minima ($\Delta\Delta G$) correlates well with the stabilization of the inactivated state according to the sequence E71A<E71S<WT<E71H (Fig. 33b, c). This suggests that constriction of the selectivity filter ($71C_\alpha$-Asp80C_α) parallel to the permeation pathway increase the stability of a distorted filter (pinching at the S_1 site and increase in the diameter at S_2-S_3 binding site).

This interpretation is strongly supported by the presence of a linear correlation between the $\Delta\Delta G$ (Fig. 33c) for the conductive, putatively inactivated conformation of

the selectivity filter (calculated from Fig. 33b) and the log of the ratio of probability

between the open and non-conductive states of the channel (measured from single

channel records), shown in Figure 32. This result further demonstrates that the entry into

the C-type inactivated state is energetically favorable and principally driven by the

strength of the interaction between the pore helix and the external vestibule in KcsA.

Interestingly, the distorted filter obtained from the PMF calculations resemble previously

reported non-conductive filter structures (Lenaeus et al., 2005; Zhou et al., 2001b) (Fig.

33b, right bottom panel and Fig. 34).
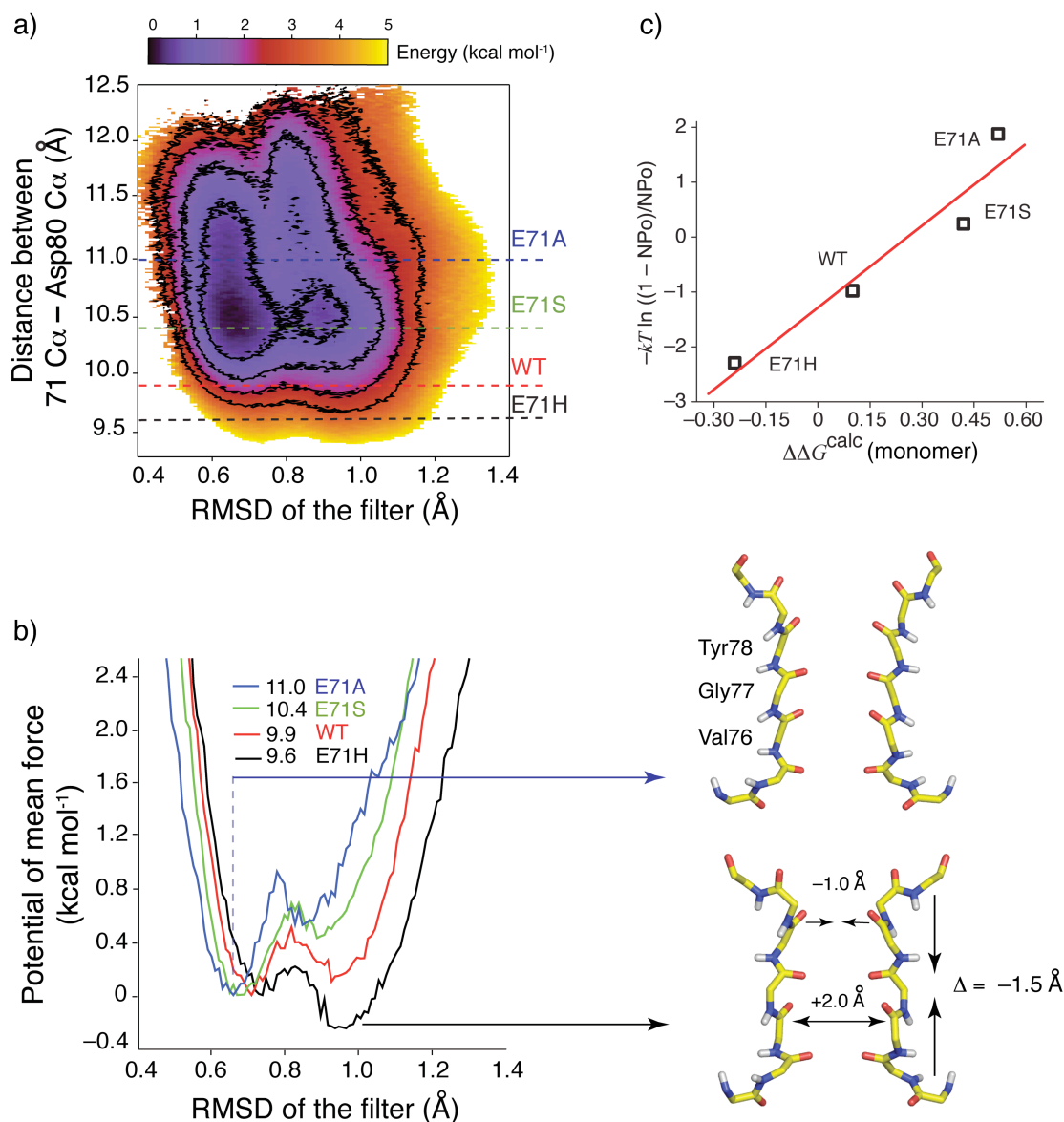
Figure 33 Correlation between the extent of inactivation and the energetics of selectivity filter distortion. a) 2D-PMF with RMSD of the filter and distance between $71C_\alpha$-Asp80C_α as the reaction coordinates. Each contour level corresponds to energy of 0.75 kcal mol^{-1}. b) 1D-PMF extracted from 2D-PMF using Boltzmann averaging of energy at C_α-C_α distances of 9.6±0.25 (E71H-like), 9.9±0.25 (WT-like), 10.4±0.25 (E71S-like) and 11.0±0.25 (E71A-like). Right panel, structures of the filter extracted from the simulation with RMSD = 0.6 Å and $71C_\alpha$-Asp80C_α = 11.0 Å, similar to the putative conductive conformation (top), and with RMSD = 1.1 Å and $71C_\alpha$-$80C_\alpha$ = 9.6 Å, a putative non-conductive conformation (bottom). c) Correlation between the calculated $\Delta\Delta G$ between putative conductive and inactivated filter structures for four different side-chain substitutions at position 71 and the experimentally-determined ratio between conductive and non-conductive probabilities. The straight line corresponds to a linear fit ($y = 4.9*x - 1.2$) with $R^2 = 0.92$.
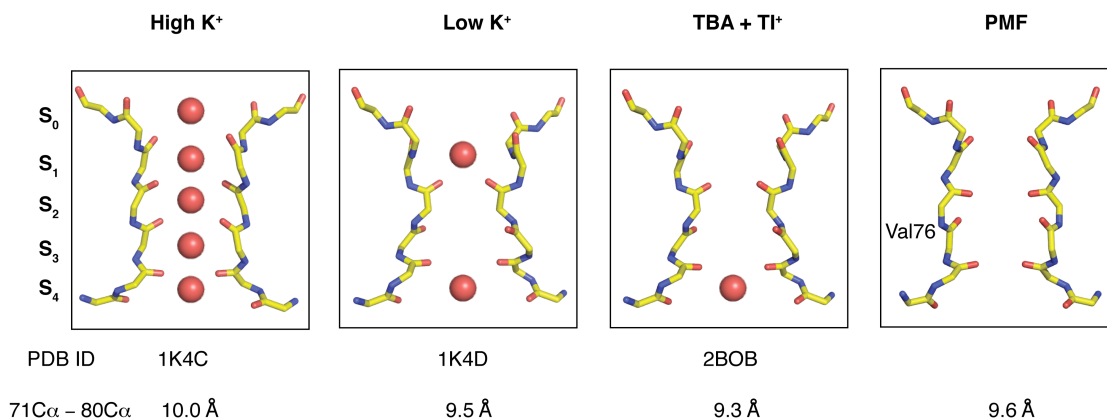
Figure 34 Comparison of the non-conductive state of KcsA selectivity filter obtained from crystal structures and PMF calculations (Zhou et al., 2001b). Stick representation (backbone) of residues 74-80 from diagonally symmetric subunit. For reference, the left most panel represents the high K^+ crystal structure with a putatively conductive filter configuration. In the right most panel, the filter structure obtained from PMF calculations resemble with the low K^+ and TBA+Tl$^+$ crystal structures predicted to be non-conductive. In these three non-conductive structures, i) Val76 carbonyl is flipped out with respect to the pore axis, hence increasing the diameter of the filter. This structural change had been correlated to C-type inactivation in previously observed MD simulations (Berneche and Roux, 2005); ii) a constriction at the S_1 binding site; iii) distance between Glu71 C_α - Asp80 C_α are shorter when compared to the conductive state of the filter.

4.4.4 Engineering hydrogen-bond network in Kv potassium channels

The extent to which a system of H-bond interactions serves as the basis to understand C-type inactivation in K^+ channels was tested in Kv1.2, a voltage-gated K^+ channel from rat brain that belongs to the *Shaker* K^+ channel family (Stuhmer et al., 1989). In the absence of the *β*-subunit, Kv1.2 shows little or no C-type inactivation. Eukaryotic Kv channels have a conserved valine in the equivalent position to Glu71 in KcsA, unable to engage in a direct interaction with the Asp80 equivalent, whereas glutamate in that position might interact with Asp379 (Fig. 35, inset). Normalized macroscopic currents show that in Kv1.2, substitution of V370E accelerated and enhanced the inactivation process, similar, though not as complete as in KcsA (Fig. 35 and Table 4). Additionally, the serine substitution also promoted inactivation but to a lesser extent. No currents were observed for homotetramers of V370H, but co-expression of WT and V370H renders functional channels with faster inactivation than WT Kv1.2 (not shown), implying that a histidine residue at position 370 also promotes inactivation by a similar mechanism to that in KcsA. These results suggest that the inactivation at the selectivity filter of Kv channels can also be regulated by the hydrogen-bond network between the pore helix and residues in the external vestibule adjacent to the selectivity filter.
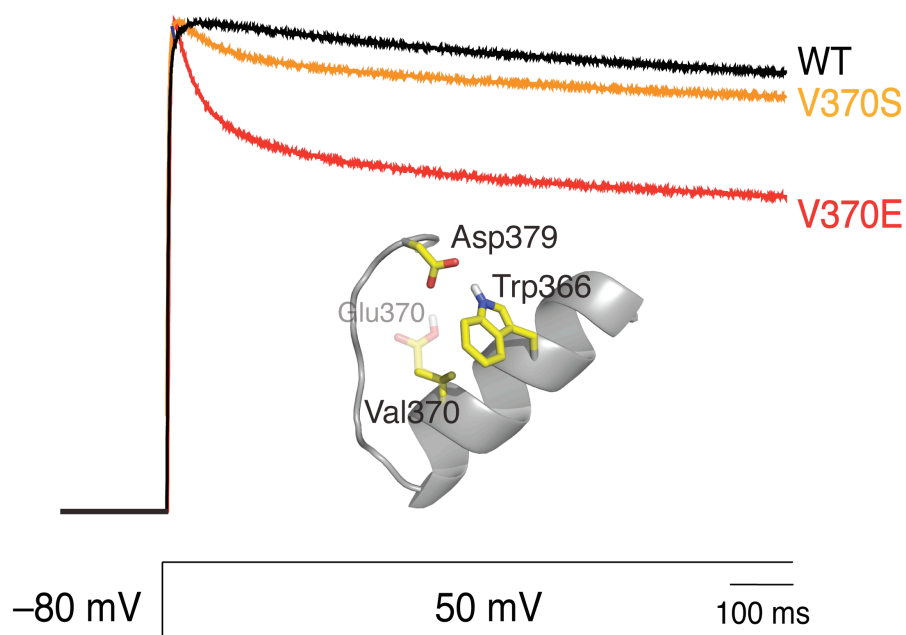
Figure 35 Mutations at position 370 enhance C-type inactivation in Kv1.2. Normalized currents of mutants V370S and V370E elicited by depolarizing voltage step from a holding potential of -80 mV to +50 mV. The inactivation rate of WT Kv1.2 speeds-up considerably with the single amino acid substitution V370E and V370S. Inset shows a single subunit P-loop with the interaction of Val370 (V370E transparent) and that of Asp379 in stick representation.

Table 4 Kv1.2 (WT and mutants) time constant of inactivation.

	τ_1 (ms)	τ_2 (ms)
WT	--------	1002 ± 213
V370S	93 ± 17	1600 ± 738
V370E	40.1 ± 2.8	487.6 ± 42

4.5 DISCUSSION AND CONCLUSION

In response to prolonged stimulus, potassium channels typically become non-conductive through a process known as slow or C-type inactivation. This has been associated with a distortion in the selectivity filter (Liu et al., 1996) and it is mechanistically distinct from N-type inactivation, which occurs intracellularly and involves a blocking particle within the permeation pathway (Hoshi et al., 1991). C-type inactivation plays a critical role in establishing and controlling firing patterns in neurons (Bean, 2007) as well as in determining the length and frequency of the cardiac action potential (Smith et al., 1996; Spector et al., 1996). The molecular events leading to the loss of ion conduction at the selectivity filter are yet to be fully understood but it is clear that a combination of functional, with static and dynamic structural information will be essential for this task. The present set of results in this chapter provides a mechanistic explanation of the driving forces and a plausible molecular mechanism of the transition between the conducting and non-conductive states of the selectivity filter in K^+ channels.

There is compelling evidence suggesting that the selectivity filter plays a critical role in gating by acting as a second gate in a variety of K^+ channels (Berneche and Roux, 2005; Blunck et al., 2006; Bruening-Wright et al., 2002; Claydon et al., 2003; Cordero-Morales et al., 2006b; Sun et al., 1996). Early data on the effect of permeant ions on gating (Demo and Yellen, 1992; Spruce et al., 1989; Swenson and Armstrong, 1981) suggested that the selectivity filter might be involved in both permeation and gating functions. Ions with longer occupancy in the selectivity filter (Rb^+, Cs^+, NH_4^+) tend to slow-down entry into the inactivated state through a "foot in the door mechanism" in which the resident ion stabilizes the conductive conformation (Demo and Yellen, 1992;

Swenson and Armstrong, 1981). Furthermore, there is a clear correlation between the occurrence of sub-conductance levels with altered selectivity and mutations in the selectivity filter (Chapman et al., 1997; Zheng and Sigworth, 1997). Mutations at the selectivity filter (Lu et al., 2001) or surrounding structure (Alagem et al., 2003; Chapman et al., 2006; Proks et al., 2001; Sun et al., 1996), showed dramatic effects on rapid gating transitions, while others revealed a large influence in the kinetics and extent of C-type inactivation. Moreover, increasing K^+ concentration or binding of the blocker TEA in the extracellular region leads to dramatic decrease of C-type inactivation (Baukrowitz and Yellen, 1995; Choi et al., 1991; Lopez-Barneo et al., 1993). These results suggest, quite convincingly, that the selectivity filter and its associated support structures (pore helix, turret loop) play a key role in the gating process, both at slow (C-type inactivation) and fast (single channel flicker) timescales.

Several lines of evidence point to a mechanistic equivalence between KcsA inactivation and C-type inactivation in eukaryotic voltage-dependent K^+ channels. Mutation of Tyr82 (functionally equivalent to Thr449 in *Shaker* and to Ser631 in hERG), and mutation of Glu71 (functionally equivalent to Val438 in *Shaker* and to Ser620 in hERG) affect the rate and extent of inactivation (Ficker et al., 1998; Lopez-Barneo et al., 1993; Yifrach and MacKinnon, 2002). Additionally, the rate of C-type inactivation similarly depends on extracellular K^+ as its eukaryotic counterparts (Cordero-Morales et al., 2006b). Given the high degree of sequence conservation in the K^+ channel selectivity filter, it can be expected that these channels would display a common mechanism of C-type inactivation.

We have shown that conformational changes at the selectivity filter of KcsA exert a critical role in the inactivation gating process, particularly those involving interactions between residues Trp67 and Glu71 at the pore helix and Asp80 at the end of the signature sequence in the mouth of the pore. Disrupting the interaction between residues Glu71 and Asp80 relieves C-type inactivation in KcsA, and mutation E71A essentially abolishes it, boosting steady state open probability. Using CW-EPR spectroscopic measurements and fluorescence lifetime spectroscopy in combination with pore mutants of wildly different open probabilities (Blunck et al., 2006; Cordero-Morales et al., 2006b), we previously showed that once the intracellular gate formed by the TM2 helices is maximally activated, it plays a minimal role in stationary gating. Based on these results, we proposed a model in which selectivity filter is intrinsically unstable and movement of the TM2 gate allows the selectivity filter to undergo a rearrangement that leads to a more stable inactivated state.

Previous work by Liu and collaborators (Liu et al., 1996), have suggested that C-type inactivation involves a local rearrangement and constriction of the outer mouth of *Shaker* K$^+$ channel. Our results show agreement with this finding as observed by pinching of the S$_1$ site in KcsA under MD simulations. However, we propose that this conformational change in the outer mouth is a consequence of a preceding event, driven by the network of interactions between the pore helix and the external vestibule, as determined by electrophysiological measurements and MD simulations. This set of interactions promotes a constriction of the selectivity filter parallel to the permeation pathway, leading to a distorted filter (Fig. 33b). This configuration is reminiscent of previously determined WT KcsA structures at low potassium concentration (Zhou et al.,

2001b), in the presence of intracellular blocker (Lenaeus et al., 2005) (Fig. 34), and M96V mutant (Lockless et al., 2007). It should be considered that these crystal structures and our present computational model (biased to a closed-inactivated conformation) were obtained with the channel inner gate (TM2) in its closed conformation. Still, the presence of a closed-inactivated state at the functional level in *Shaker* (Baukrowitz and Yellen, 1995; Claydon et al., 2007; Panyi and Deutsch, 2006) supports the structural basis of an inactivated state even when the lower gate in closed. Given the stability of the inactivated conformation of the filter induced by the His71-Asp80 interaction in E71H, this mutant remains a viable candidate for the structure of a closed-inactivated form of the filter.

The present mechanistic interpretation of our results is summarized in Figure 36. The stability of the selectivity filter is modulated by the presence of a series of interactions pictured as "molecular springs". Weakening a key spring in the network (E71A mutant, bottom panel), stabilizes the conductive state of the filter. Increasing the strength of the spring (E71H mutation, top panel) stabilizes the non-conductive state by causing a decrease in the $71C_\alpha$-$Asp80C_\alpha$ distance, pinching at the S_1 site and widening of the S_2-S_3 binding sites. Indeed, we find that the differences in the rate of inactivation between KcsA WT and mutants are driven by the strength of the interaction involving residues in the pore helix and external vestibule, according to the sequence E71A<E71S<WT<E71H (Fig. 32). We suggest that this overall mechanism might represent the actual events that occur during the transition from the conductive to non-conductive state of the WT KcsA selectivity filter.
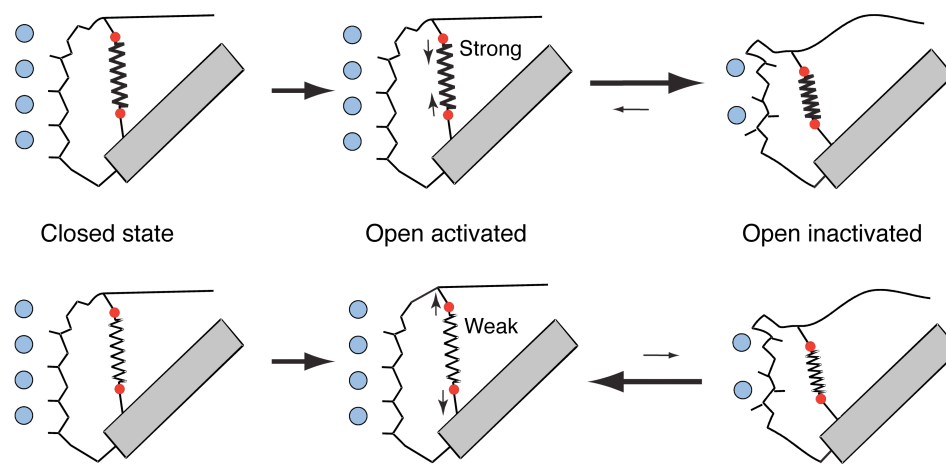
Figure 36 Structural rearrangements during C-type inactivation at the filter. Cartoon representation of molecular events during KcsA gating.

However, in relation to KcsA, Kv channels present a more complex situation. Even though the Glu71-Asp80 molecular spring corresponding to KcsA is absent, other interactions might play equivalent roles during the C-type inactivation process (Fig. 37). Nevertheless, as shown above, C-type inactivation in Kv channels can be enhanced by the addition of a KcsA-equivalent molecular spring. Taken together, the present results in KcsA and Kv1.2 provide a plausible framework to understand the molecular mechanism for C-type inactivation in K^+ channels.
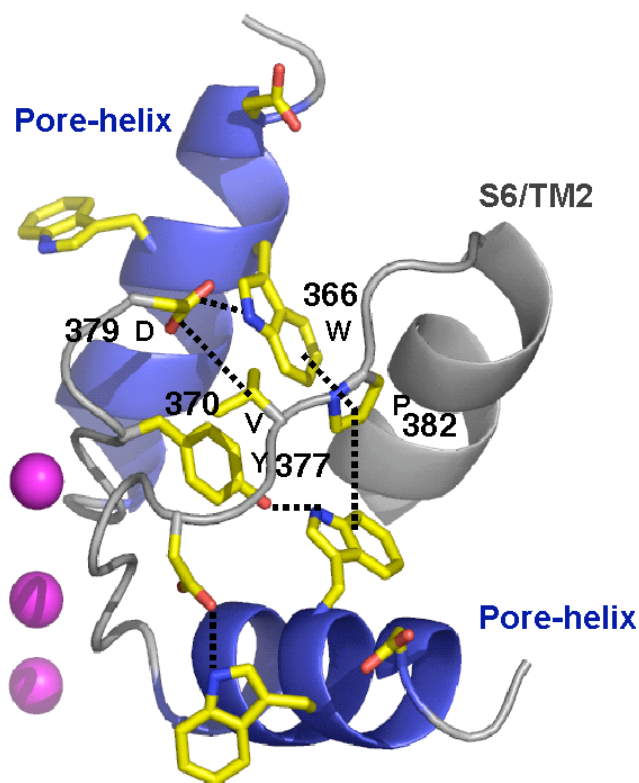
Figure 37 Schematic representation of putative interactions in Kv1.2 pore (Long et al., 2005a). In Kv channels several residues are involved in both intra- and inter-subunit contacts that can transfer the conformational wave from the activation gate to the inactivation gate. Network of interactions involving pore helix and external vestibule are as follows (Residues within the bracket corresponds to KcsA): i) H-bond between Asp379 (Asp80) and Trp366 (Trp67), ii) and between Tyr377 (Tyr78) and Trp366 (Trp67), iii) aromatic cuff involving Trp366 (Trp67), Trp367 (Trp68) and Pro382 (Pro83). All these interactions are likely to influence the conformation of the residues Asp379-Pro382 (Asp80-Pro83), which in turn can trigger the deformation of the selectivity filter. Although the nature of the interactions between pore helix and external vestibule in Kv1.2 are less understood in other Kv channels, these interactions have been shown to play a pivotal role in the gating process (Chapman et al., 2001)

CHAPTER 5: A multipoint hydrogen bond network driving potassium channel

C-type inactivation

5.1 ABSTRACT

C-type inactivation in K^+ channels is a molecular mechanism that locks the selectivity filter in a non-conductive state. The prokaryotic proton-gated potassium channel KcsA undergoes a time dependent inactivation process, which is modulated by transmembrane voltage but not by pH. The interaction between Glu71 and Asp80 is one of the key driving forces that promote filter instability through a compression of the selectivity filter parallel to the permeation pathway, which energetically biases it towards the inactivated conformation (Cordero-Morales et al., 2007). Here, we show that the interactions involving residues Trp67, Tyr78 and Asp80, conserved in most potassium channels, constitutes another critical interaction between the selectivity filter and its adjacent pore helix which determines the rate and extent of C-type inactivation. Analyzing equivalent interaction in the eukaryotic voltage-gated K^+ channel Shaker and Kv1.2 suggests the presence of a common gating mechanism. The present results provide evidence that the hydrogen bond network and Van der Waals interaction at the selectivity filter serves as the basis for C-type inactivation in the K^+ channel family.

5.2 INTRODUCTION

Potassium channels are membrane proteins that play an essential role in cell excitability and whose pore-domain provides the structural components required for permeation, selectivity and gating. The slow inactivation process in K^+ channels is a well-known and effective process to abrogate ion conduction through structural rearrangements at the selectivity filter and the extracellular entrance (Cha and Bezanilla,

1997; Cordero-Morales et al., 2006b; Cordero-Morales et al., 2007; Hoshi et al., 1990; Liu et al., 2002; Liu et al., 1996; Loots and Isacoff, 1998; Yellen et al., 1994). The structure of the selectivity filter is greatly conserved among the K^+ channel family (Long et al., 2005a; Nishida et al., 2007; Zhou et al., 2001b), yet the presence of a common gating mechanism is not clear.

A key structural component of the filter of K^+ channels is the presence of a conserved ring of aromatic residues involved in intra- and inter-subunits contact. For instance, in KcsA and Kv1.2 crystal structures, a tyrosine from the signature sequence, TVGYGD, is engaged in a hydrogen bond with the tryptophan side chain on the pore helix from the adjacent subunit. This hydrogen bonding pattern has been suggested to stabilize the structure of the selectivity filter (Doyle et al., 1998; Long et al., 2005a; Zhou et al., 2001b). Additionally, the hydrogen bond interaction between the tryptophan on the pore helix and aspartate in the extracellular loop (Fig. 38a, see below) is highly conserved and the strongest interaction at the selectivity filter of K^+ channels suggested from molecular dynamics simulations (Peng et al., 2007; Shealy et al., 2003).

Interestingly, overlapping the structures of the conductive and non-conductive states of KcsA selectivity filter shows that aromatic residues in the P-loop undergo considerable conformational changes (Lockless et al., 2007; Valiyaveetil et al., 2006a; Zhou et al., 2001b), suggesting that these residues play an important role during gating. Furthermore, NMR studies on KcsA reveal considerable conformational difference in the backbone angle of Tyr78 between the conducting (pH 4) and non-conducting (pH 7) state (Baker et al., 2007), and in the presence or absence of gating modifier, Kaliotoxin (Lange et al., 2006).

Similarly, numerous studies support the role of a network of hydrogen bond interactions behind the selectivity filter during channel gating in a number of K^+ channels (Kurata and Fedida, 2006; Seebohm et al., 2003). A point mutation in Kv2.1 (D378E, from the GYGD), affects the single channel behavior by the destabilization of the open state (Chapman et al., 2006). Moreover, mutations in the selectivity filter and pore helix of Shaker, hERG, and inward rectifiers also have large effects on gating properties (Alagem et al., 2003; Ficker et al., 1998; Yifrach and MacKinnon, 2002).

In Shaker K^+ channel, substitution of the tryptophan residue to phenylalanine at the pore helix (W434F) has been the center of attention for more than a decade. Because of its ability to completely abolish K^+ currents without affecting the intracellular gate it has been used as a convenient tool to measure gating currents (Perozo et al., 1993). The block of K^+ current was later explained by Yang and collaborators (1997) using tandem tetrameric constructs of Shaker (Yang et al., 1997b). They were able to show that with one or two subunits mutated, W434F produces measurable K^+ currents with a time dependent inactivation process modulated by permeant ion like Rb^+, external K^+ and TEA (tetraethylammonium), concluding that the W434F homotetramer results in a constitutively C-type inactivated channel. In addition to the W434F substitution, mutations at Tyr445 (to either proline or alanine) and Asp447 (to asparagine) also blocked ion conduction, and only allowed gating current measurements, suggesting that these residues are critical in the pore gating of the Shaker K^+ channel (Heginbotham et al., 1994; Hurst et al., 1996).

Similar to C-type inactivated channel, Na^+ currents pass through W434F channels in the absence of K^+ suggesting that the permeation pathway is not completely occluded,

but there might be small rearrangement at the selectivity filter that might allow Na^+ permeation (Starkus et al., 1997). However, the molecular mechanism and the conformational changes by which Shaker W434F mutant lock the selectivity filter in the inactivated state remains unresolved.

Previously, we have shown that KcsA E71A (non-inactivating mutant) crystal structure undergoes large structural excursions at the P-loop and provide a glimpse of the range of conformations available to this region of the channel during gating (Cordero-Morales et al., 2006b, chapter 2). Furthermore, we have also shown that the hydrogen-bond network at the selectivity filter (Glu71-Asp80) is the driving force that promotes instability through a compression of the selectivity filter parallel to the permeation pathway, which energetically biases it towards the inactivated conformation (Cordero-Morales et al., 2007, chapter 4).

In this paper, as a continuation of our studies of gating at the selectivity filter, we studied the functional role of conserved tryptophan residue in the pore helix of KcsA (Trp67), Shaker (Trp434) and Kv1.2 (Trp366), in an attempt to establish the role of these residues in C-type inactivation. Here, we report that the Trp67 and Asp80 interaction in KcsA constitutes another critical hydrogen bond interaction between the selectivity filter and its adjacent pore helix which determines the rate and extent of C-type inactivation. Additionally, substitution of different aromatic residues at position 67 suggest that the inactivation process in the mutants could involve a putative interaction between residue at position 67 and Tyr78, which forms the first binding site of the selectivity filter, possibly leading to the stabilization of an intermediate inactivation state (Chakrapani et al., 2007b). KcsA results can be extended to Shaker and Kv1.2, thus establishing the network

of hydrogen bond interactions and Van der Waals at the selectivity filter as the driving force promoting C-type inactivation in the K^+ channel family.

5.3 EXPERIMENTAL METHODS

5.3.1 Mutagenesis and channel biochemistry

Mutagenesis and channel biochemistry were carried out as discussed in charter 2 (section 2.3.2)

5.3.2 Liposome patch-clamp

Liposome patch-clamp was carried out as discussed in charter 2 (section 2.3.3).

5.3.3 Two-electrode voltage-clamp

Two-electrode voltage-clamp was carried out as discussed in charter 4 (section 4.3.3). We used the Shaker Δ4-46 channel in the following called ShIR, lacking the fast N-type inactivation (Hoshi et al., 1990).

5.3.4 Kinetic analysis. Single channel recordings (±150 mV) were analyzed using QUB software. The closed-open transitions within the records were detected using segmental-*k*-means (SKM) algorithm or the half-amplitude threshold criterion. The numbers of closed and open states were determined by sequentially adding a state and then evaluating the model based on log-likelihood criterion. A best fit model for the mutant was described by two closed and one open state. Simulations of the macroscopic currents were done using the Mac module within the QUB suite.

5.3.5 Molecular dynamics. Molecular dynamics was performed as previously described (Cordero-Morales et al., 2007, chapter 4). Briefly, the simulation system was represented by an atomic model of KcsA (PDB ID: 1K4C) channel embedded in dipalmitoylphosphatidylcholine (DPPC) surrounded by an aqueous solution of 150 mM

KCl. The microscopic system was composed of KcsA tetramer of 404 amino acids (6284 atoms), 112 DPPC molecules, 6384 water molecules, 3 K^+ ions in the pore (S_0-S_2-S_4 positions in the selectivity filter). To make the entire system electrically neutral, 6 K^+ and 21 Cl^- were added in the bulk solution to mimic 150 mM KCl. All the calculations were performed using c29a2 or c32a2 of the biomolecular simulation program CHARMM (Brooks et al., 1983). The simulation methodology has been described previously (Berneche and Roux, 2000). W67F and W67Y mutants are generated *in silico* and carefully equilibrated before production run.

5.4 RESULTS

Functional role of the 67-Asp80 interaction

To identify new regions of KcsA that modulate the inactivation process at the selectivity filter, we focused our attention on the interaction between Trp67 and Asp80, a partnership conserved in most potassium channels. Macroscopic currents elicited by pH jump experiments under depolarizing conditions (+150 mV) reveal that disruption of the 67-80 interaction by a Phe67 substitution produces non-inactivating macroscopic currents (similar to E71A, Fig. 38b). However, substitution to tyrosine enhanced the rate and extent of inactivation, presumably by reestablishing the 67-80 interaction (Fig. 38a, b, d). Macroscopic current behavior was fully recapitulated at the steady state single channel level (Fig. 38c, d), the long closed-time periods characteristic of WT KcsA inactivation ($\tau_c > 10$ s) were absent in the W67F mutant (similar to E71A, with mean open time of ~ 100 ms). On the other hand, W67Y substitution recovers WT KcsA properties with long closed-time periods and short mean open times (Fig. 38c). Tryptophan substitution was fully selective to K^+ against Na^+ under bi-ionic conditions (Fig. 38d). As shown

previously, we found that the non-inactivating KcsA mutants are more selective to K^+ than the WT or inactivating mutants (determined by the shift in the apparent reversal potential) (Cordero-Morales et al., 2006b, chapter 2). These results suggest that Trp67 and Asp80 constitute another critical hydrogen bond interaction between the selectivity filter and its adjacent pore helix which modulate the rate and extent of C-type inactivation in KcsA.
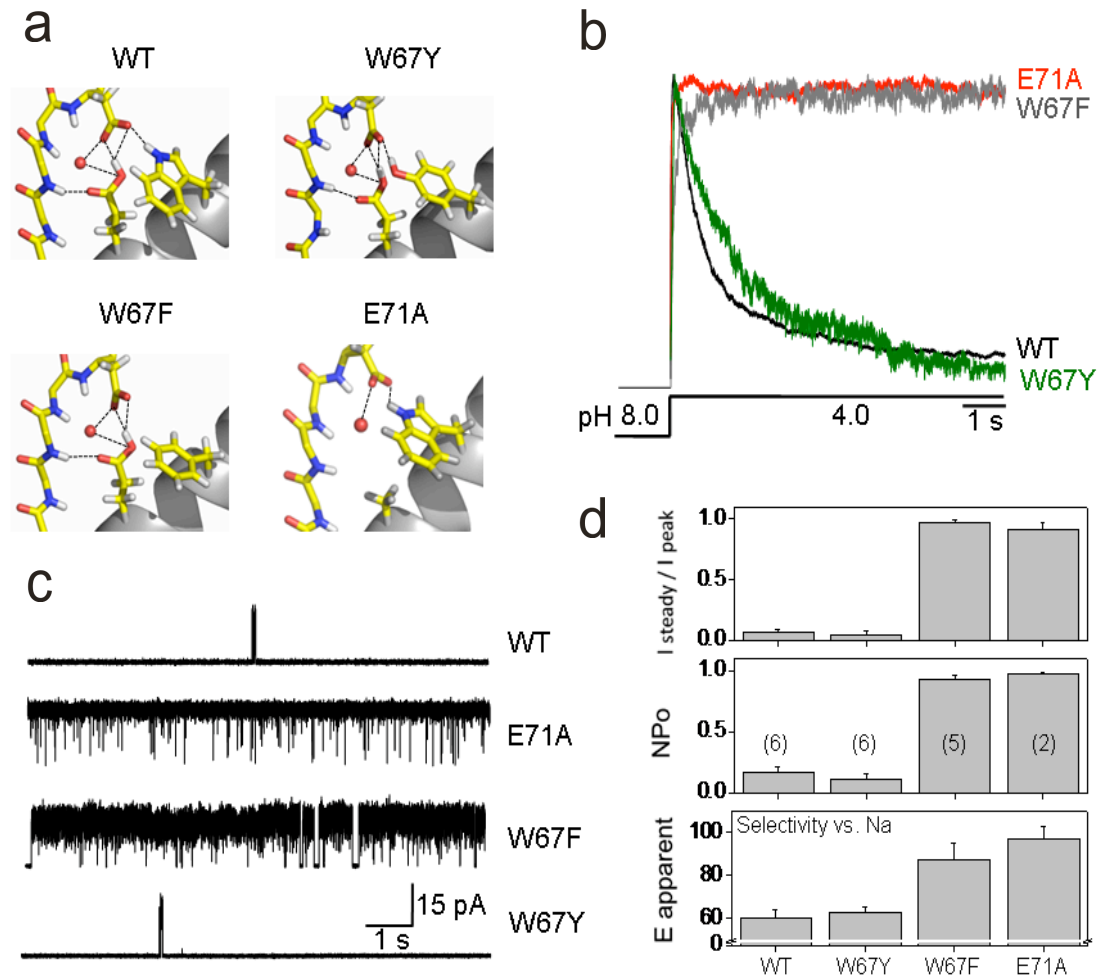
Figure 38 The Glu71-Asp80 and Trp67-Asp80 hydrogen-bond interactions between the pore helix and external vestibule are the driving force for C-type inactivation in the selectivity filter of KcsA. a) Single subunit P-loops (WT and mutants) with the hydrogen-bond network. b) Normalized macroscopic currents activated by pH jump (from 8 to 4) show the complete elimination of the time-dependent inactivation process in W67F at depolarizing potentials in symmetric 200 mM KCl. Moreover, the rate and extent of inactivation is recovered by a tyrosine substitution at position 67, presumably by reestablishing the 67 and Asp80 interaction through a hydrogen-bond. c) Representative single-channel traces from WT channel Glu71 and Trp67 mutants obtained at pH 4 and +150 mV in symmetric 200 mM KCl. The long closed-time periods characteristic of WT KcsA inactivation are absent in W67F, but still present in single channel recordings of W67Y. d) Ratio of the current at the end of the pH pulse to the peak current (I_{steady}/I_{peak}), from macroscopic current traces is shown for WT and mutants. Nominal open probability evaluated from Gaussian fits of all-points histograms. Selectivity vs. Na$^+$ estimated from single-channel I-V ramps under bi-ionic conditions. $E_{apparent}$ is the potential at which K$^+$ currents can be resolved. Data shown are means ± s.d. $n > 10$.

Substituting a Phenylalanine at position Trp67 enhances the rate and extent of inactivation at hyperpolarizing potentials. Normalized macroscopic currents of W67F mutant at -150 mV show faster time constant of inactivation than WT KcsA (Fig. 39a, right panel). Ion current density for W67F (Fig. 39a, inset) was much lower than WT at hyperpolarizing potentials, even when the amount of current was the same at +150 mV, suggesting that the large amount of channels at -150 mV are pre-inactivated (Baukrowitz and Yellen, 1995; Chakrapani et al., 2007a; Panyi and Deutsch, 2006) or they inactivated faster than the activation process (Smith et al., 1996). As expected, steady state single channel recordings of W67F at hyperpolarizing potentials are dominated by very long silent periods interrupted by burst of activity, also characteristic of WT and inactivating mutants (Fig. 39b, bottom). To evaluate the contribution of W67F to the voltage dependence of inactivation, we obtained the nominal open probability (NPo) from single channel records at several voltages (Fig. 39c). In spite of the changes in gating of W67F, we found marginal differences in the voltage dependence between W67F ($z = 1$) and WT KcsA ($z = 0.7$), given that the gating charge is still present in this mutant (Fig. 39d, Glu71 (Cordero-Morales et al., 2006a)).

How does W67F influence the conformation of the selectivity filter? At depolarizing potential, the carboxylic group of Glu71 tends to orient towards the intracellular end of the channel (Fig. 39d) which would weaken the Glu71-Asp80 interaction (critical for inactivation) and thereby increase the flexibility of Asp80. Yet this flexibility would be restricted by a second interaction between Trp67-Asp80 in WT. However, in the absence of this hydrogen bond (W67F), the flexibility of Asp80 increases much more dramatically, therefore decreasing the strength of Glu71-Asp80

interaction as experimentally observed (Fig. 39a, +150 mV). Hyperpolarizing voltages should align and favor Glu71-Asp80 interaction, thus increasing inactivation as shown in Figure 39a (-150 mV). These results show that KcsA inactivation is also modulated by the 67-Asp80 interaction, however, these results could not rule out the possibility of Phe67 affecting or modulating inactivation through another region of the selectivity filter.
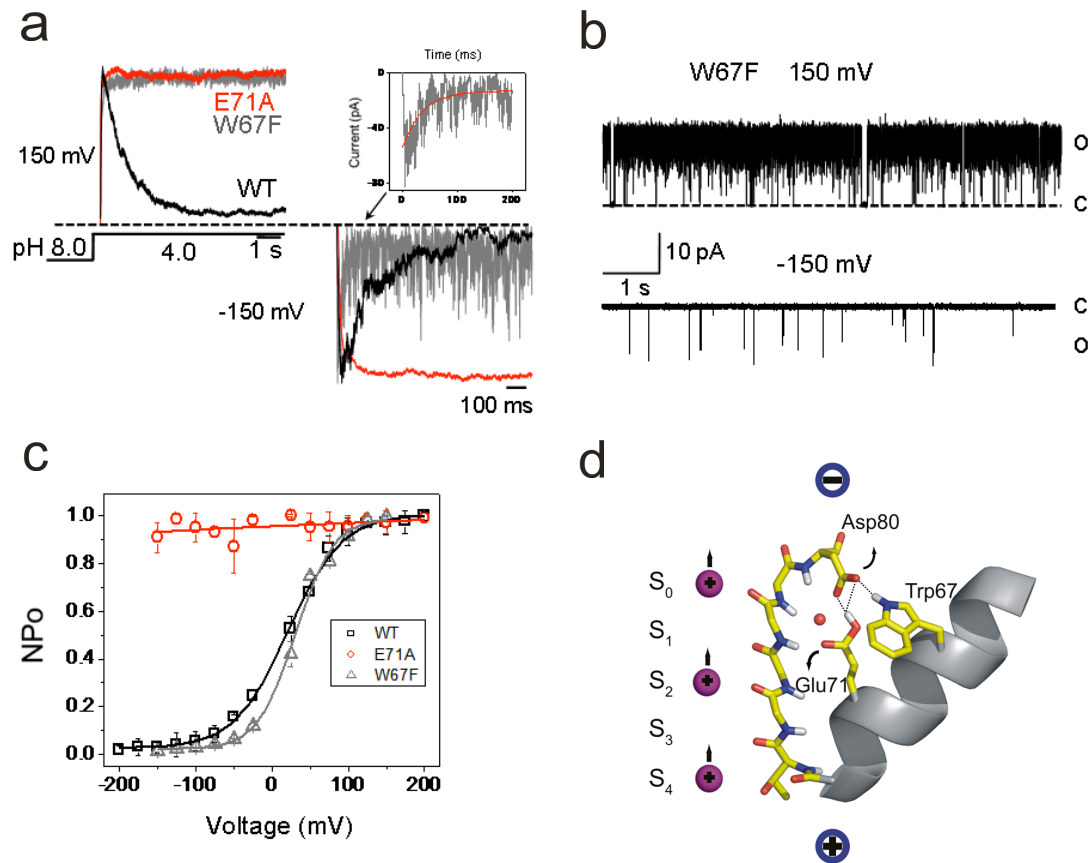
Figure 39 Phenylalanine at position 67 enhances the rate and extent of inactivation at hyperpolarizing potentials. a) Normalized macroscopic currents in the W67F mutant show a faster inactivation time constant at hyperpolarizing potentials (-150 mV, 30.71 ± 17.38 ms), and a slower time constant at depolarizing potentials compared to WT currents (-150 mV, 500 ± 220 ms; +150 mV, 1300 ± 789 ms). Inset, shows a higher resolution detail of W67F macroscopic current (Top). b) Representative single channel traces from W67F obtained at pH 4 and ± 150 mV, under symmetric 200 mM KCl. The long closed-time periods characteristic of inactivation are present at hyperpolarizing potentials but absent at depolarizing ones. Thus single-channel recapitulates the macroscopic current behavior. c) Steady state NPo vs. voltage curves were fitted to a Boltzmann function with $V_{1/2}$ = 22 mV, zδ = 0.72 (WT, black), $V_{1/2}$ = 30 mV, zδ = 1.0 (W67F, gray). E71A (red) is fit to a linear regression with slope of > 0.001. Data shown are means ± s.d. *n* > 10. d) Model of voltage-dependent modulation at the selectivity filter.

In order to study the effect of W67F in similar conditions to those used for Kv channels, we measured its macroscopic current behavior by pH jump experiments, elicited under asymmetric conditions (200 mM K^+ intracellular / 5 mM K^+ + 195 mM glycine extracellular; $E_{rev} \sim$ -85 mV). Figure 40a shows that inactivation is absent at potentials more depolarizing than +50 mV, but is present at hyperpolarizing ones with increasing rate. W67F substitution shows faster time constant of inactivation (measured by fitting a single exponential to the decay phase; Fig. 40a, red curve) than WT KcsA at any given potential (Fig. 40b, c). The enhanced inactivation process of KcsA by W67F substitution, resemble the results of the permanently C-type inactivated mutant W434F in Shaker, but with a lesser extent in KcsA (Perozo et al., 1993; Yang et al., 1997b).

The position Trp67 near the C-terminal end of the pore helix, in KcsA, is highly conserved throughout the eukaryotic K^+ channel family. On the other hand, in the prokaryotic K^+ channel family there is invariably a tryptophan or a tyrosine, suggesting that amino acids with the capability of establishing hydrogen bond are required at this position. To test the hypothesis that disrupting Trp67-Asp80 interaction allows Asp80 to be more flexible producing non-inactivated macroscopic currents at depolarizing potential (Fig. 38b), we analyzed the functional effect of the tyrosine substitution at position Trp67 under symmetrical conditions (200 mM K^+) recorded at several membrane potential. Representative macroscopic current traces show that mutation W67Y restores C-type inactivation in KcsA (Fig. 41a). This mutant recovered the inactivation phenotype (although slightly faster than WT KcsA, Fig. 41b, c) presumably by reestablishing a stronger 67 and Asp80 interaction through a hydrogen bond (Fig. 38a), therefore the flexibility of Asp80 will decrease and promote inactivation through a

filter constriction parallel to the permeation pathway (Glu71-Asp80)(Cordero-Morales et al., 2007).
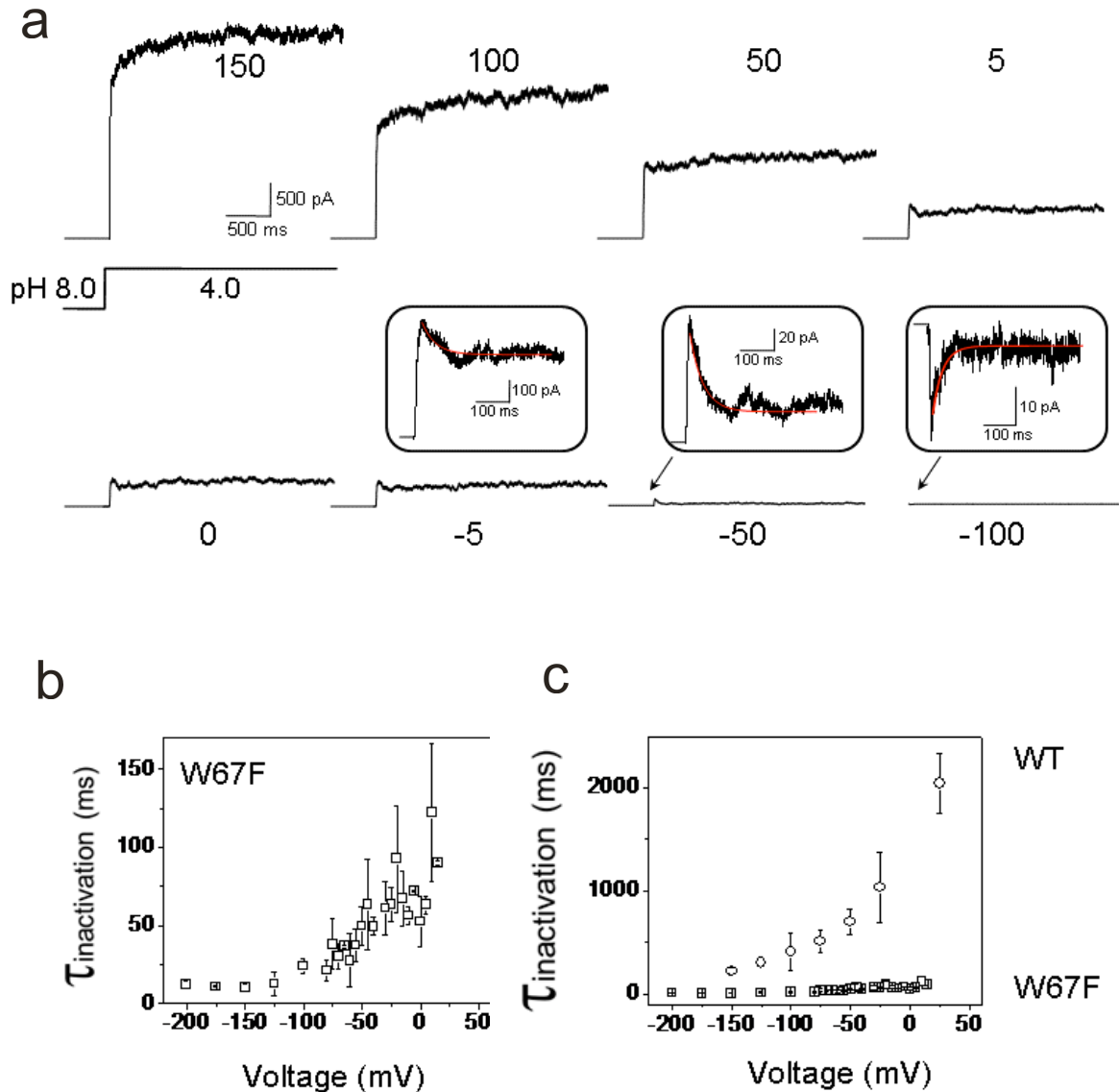
Figure 40 Comparison of the time constant of inactivation for WT KcsA and W67F mutant. a) Macroscopic currents elicited in response to pH jump under asymmetric solutions (200 mM K$^+$ intracellular / 5 mM K$^+$ extracellular + 195 mM glycine) recorded at various membrane potentials. At potentials lower than 50 mV (more hyperpolarizing) macroscopic currents reveal the presence of an inactivation process with rising rates of inactivation. b) Time constant of inactivation of W67F, measured by fitting a single exponential to the decay phase of the macroscopic, was plotted as a function of voltage. c) Comparison of the time constant of inactivation shows that W67F (Square) inactivates much faster at every potential in asymmetric conditions than WT KcsA (Circle). Data shown are means ± s.d. $n > 10$.
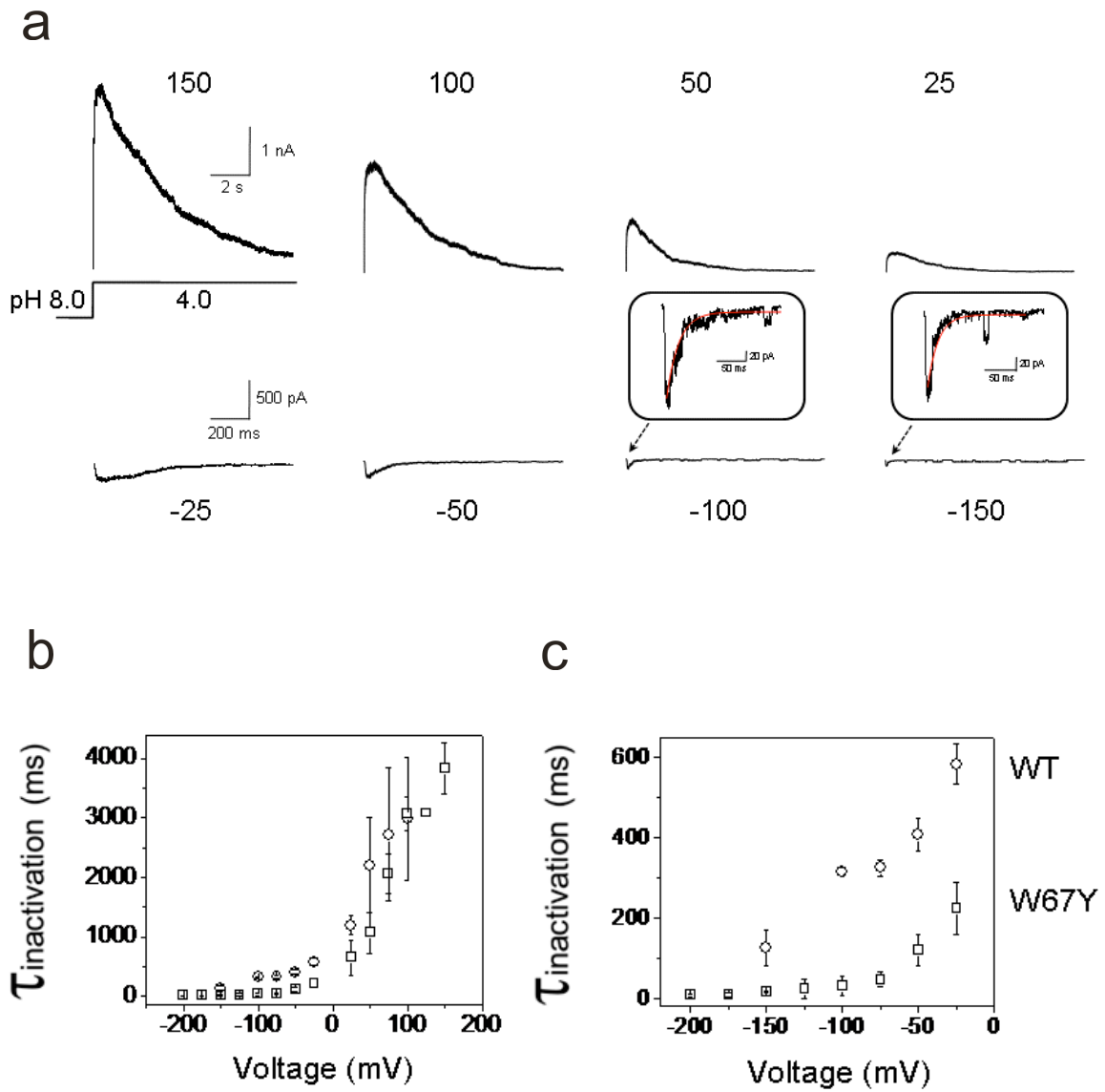
Figure 41 Mutation W67Y restores C-type inactivation in KcsA. This mutant recovered the inactivation phenotype presumably by reestablishing the 67 and Asp80 interaction through a hydrogen bond. a) Macroscopic currents elicited in response to pH jump under symmetric solutions (200 mM K$^+$) recorded at various membrane potentials. b) Time constant of inactivation of W67Y, measured by fitting a single exponential to the decay phase of the macroscopic, was plotted as a function of voltage. c) Comparison of the time constant of inactivation shows that W67Y (Square) inactivates slightly faster at every potential than WT KcsA (Circle). Data shown are means ± s.d. $n > 10$.

Structural basis of inactivation in W67F mutant

A detailed understanding of the gating mechanism at the selectivity filter can be achieved by high resolution structural snapshots of the filter in different states together with real-time dynamics data. Thus, to understand the molecular basis of C-type inactivation, we had pursued the crystal structure determination of the W67F and W67Y mutants vigorously but were unsuccessful. Nonetheless, as binding of the Fab to KcsA requires interaction with the extracellular loop and pore helix, this unexpected result points to the possibility that the three-dimensional conformation of this epitope is significantly changed for these mutants. In addition, attempts to obtain the crystal structures in the absence of Fab fragments were also unsuccessful, likely due to changes in the extracellular loop of these mutants critical for crystal packing. As an alternative approach, we used molecular dynamics simulations to evaluate the effect of W67F and W67Y mutants on the C-type inactivated state of the filter.

Analysis of 5 ns molecular dynamics trajectory of these mutants led to one important discovery. Following the disruption of the 67-Asp80 hydrogen bond by the Phe67 substitution, there is a decrease in the minimum distance (~ 4.2 Å, average) between heavy atoms on Phe67 at the pore helix and Tyr78 at the selectivity filter suggesting that Phe67 modulates KcsA gating either through disrupting 67-Asp80 interaction or establishing a new interaction 67-Tyr78 (Fig. 42a). Previously, it was well established that repulsive or attractive interactions (Fig. 42b, green shaded area, attractive) between two aromatic groups depend on the distance between the centre of mass of the aromatic planes and their orientation with respect to each other (Hunter, 1993; Hunter et al., 1991). Analyzing the distance between aromatic groups and the

orientation of their planes from 5 ns MD simulations, we found that Phe67-Tyr78 interaction might be repulsive resulting in a reorientation of Tyr78 leading to a faster inactivation (Fig. 40c and 42b). The presence of a bulky indole ring at position Trp67 in WT channel decreases the distance between aromatic planes, and a slight tilt in orientation results in an attractive interaction that might partially stabilize Tyr78 (Fig. 42a, b), not allowing it to undergo conformational changes unlike Phe67, hence lesser inactivation (Fig. 40c).

In the case of tyrosine substitution at residue 67, time series of the minimum distance between Tyr78 and Tyr67 mutant shows longer distance (~ 4.6 Å) than Phe67, presumably re-establishing 67-Asp80 interaction orients Tyr67 away from Tyr78 and closer to Asp80, which in turn promote the C-type inactivation at depolarizing potential (Fig 38b and 41). These results suggest that repulsive (Phe67-Tyr78) interactions between aromatic residues at the pore helix and selectivity filter would enhance the inactivation process in comparison to WT KcsA. These data establish that the nature of the hydrogen bond network (71-Asp80 and 67-Asp80) and interactions involving aromatic residues at the selectivity filter determines its entry into the non-conductive C-type inactivated state.
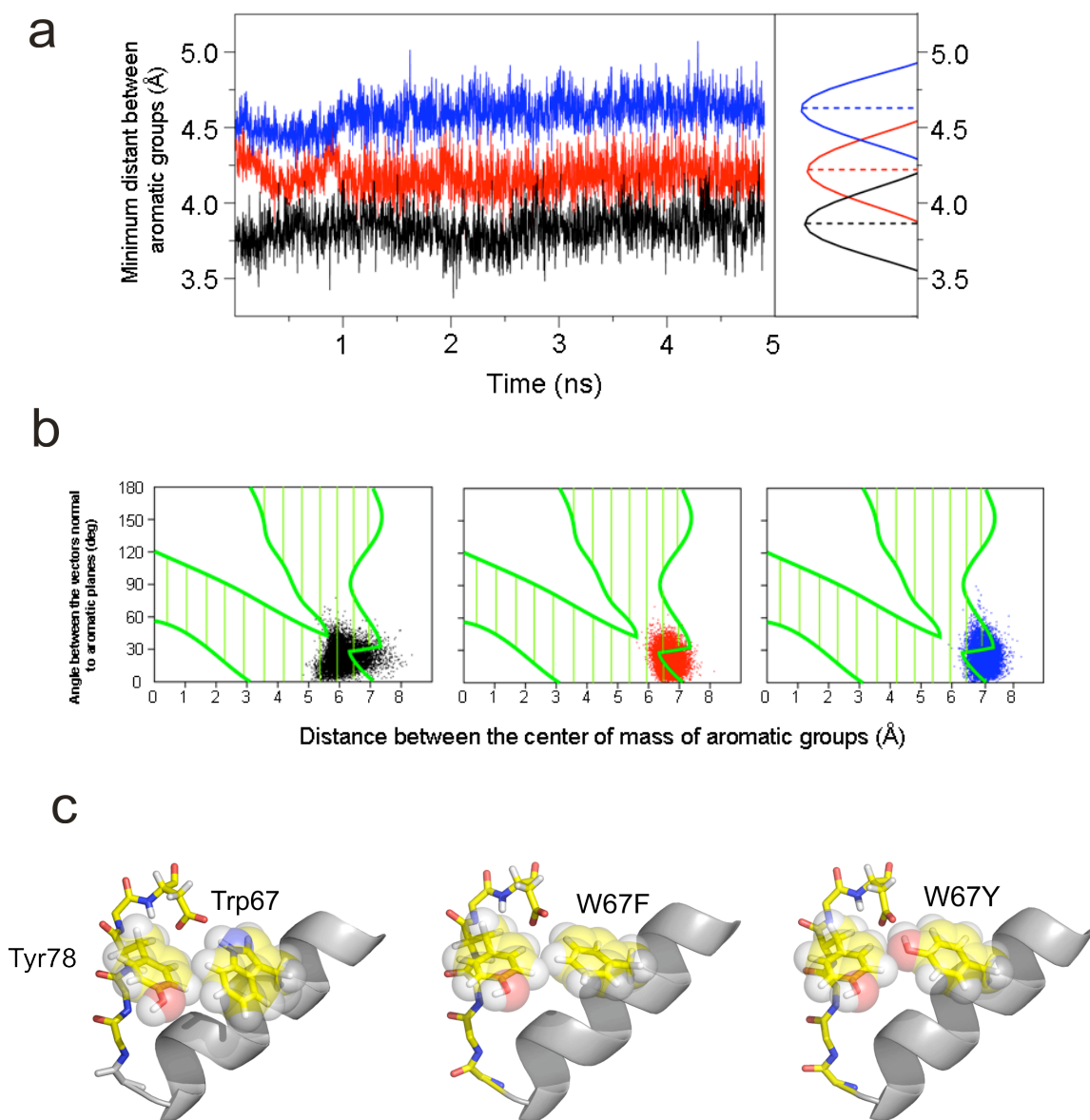
Figure 42 Structural basis of inactivation in W67F mutant. a) Time series of the minimum distance (Å) between Tyr78 and Trp67 (black), Phe67 (red) and Tyr67 (blue) heavy atoms on aromatic group. Decreased distance between Tyr78 and Phe67 suggests that inactivation in Phe67 could also result from the conformational changes in Tyr78 induced by Phe67. b) Scatter plot of the distance between centre of mass of aromatic groups and the orientation angle of the vectors normal to the aromatic planes generated from 5 ns MD trajectory. The green shaded region corresponds to the favourable attractive interaction for given distance and angle. In WT KcsA, W67 and Tyr78 aromtic rings are favourable positioned to have attractive interaction, whereas, W67F and Tyr78 have edge-to-edge unfavourable interaction. Distance beyond 7.5 Å is non-interacting region where in aromatic rings are far away c) Top and side view of the putative interaction involving residues Asp80, Tyr78, Trp67, Phe67 and Tyr67.

The functional effect of W67F in KcsA has been evaluated in the presence of the Glu71-Asp80 interaction, which is absent in the Kv family. To understand the nature of the Trp67-Asp80 interaction, we have taken advantage of the non-inactivated KcsA E71A, a mutant with only two hydrogen bond interaction at the selectivity filter (Fig. 38a). As expected the double mutant does not show inactivation at depolarizing potentials, however at hyperpolarizing potentials, there appears to be a decline in the amplitude of the macroscopic current with no evident time-dependent decay (Fig. 43, left bottom). At the level of single-channels, the depolarization potentials elicit currents with very high open probability similar to those of E71A mutants, while at hyperpolarization potentials the channel openings are interrupted by long closures (to a lesser extent than WT KcsA, Fig. 43, right bottom). Furthermore the single-channel current amplitude at (+/-150 mV) is almost identical which suggests that the decline in the macroscopic current is not due to a decrease in conductance, but must arise from another effect, presumably an inactivation process (Fig. 43, bottom panel). In collaboration with Sudha Chakrapani (Post-Doc at Perozo E, laboratory), we evaluated this possibility by model-based kinetic analysis of steady state single-channel currents at the two extreme potentials. The rate of entry and exit into the two inactivated states reveals that the double mutation greatly stabilizes an intermediate inactivated state at hyperpolarization potential in comparison with depolarizing ones. These rapid transitions into and out of an intermediate closed state (Ii) state underlie the decline in the peak amplitude without a concomitant decay of the macroscopic current (shown in the simulated traces, Fig. 44).

This result could be explained by the putative interaction between Phenylalanine (W67F) and Tyr78 (which forms the first binding site of the selectivity filter, (Fig. 42c),

possibly leading to stabilization of intermediate inactivation state at hyperpolarizing

potentials (Chakrapani et al., 2007b). Likewise, W67F-Tyr78 interaction (in KcsA) could

explain the enhancement of C-type inactivation of Shaker by a Phenylalanine substitution

(W434F) at equivalent position to 67(Yang et al., 1997b).
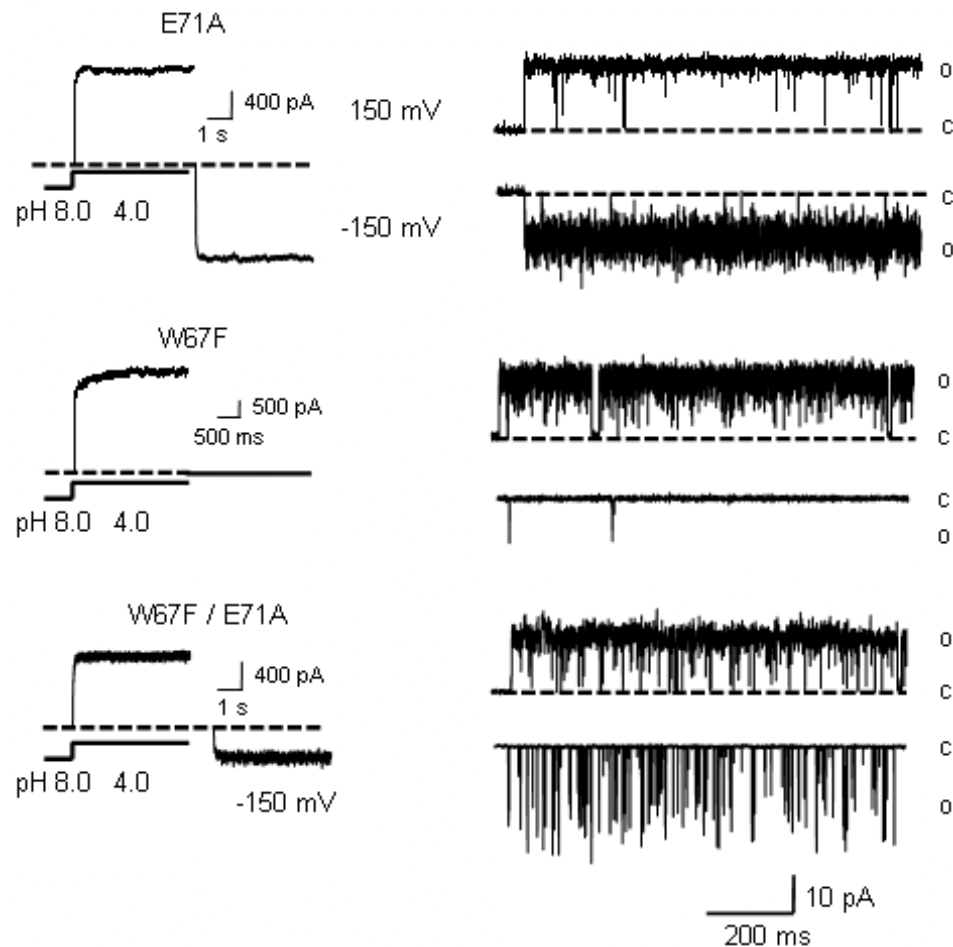
Figure 43 W67F stabilizes the intermediate inactivation state in the non-inactivating E71A mutant. Macroscopic and single-channels behavior are shown for single and double mutants at the selectivity filter (E71A, W67F and W67F/E71A). (Left, bottom) KcsA double mutant shows a decrease in the current amplitude at hyperpolarizing potentials in comparison with depolarizing ones. (Right, bottom) This behavior is reflected at the single channel level as enhanced transitions to an intermediate inactivated state that is clearly absent in the E71A mutant. Single channel conductances at hyperpolarizing potential (-150 mV) were similar between WT KcsA and double mutant.
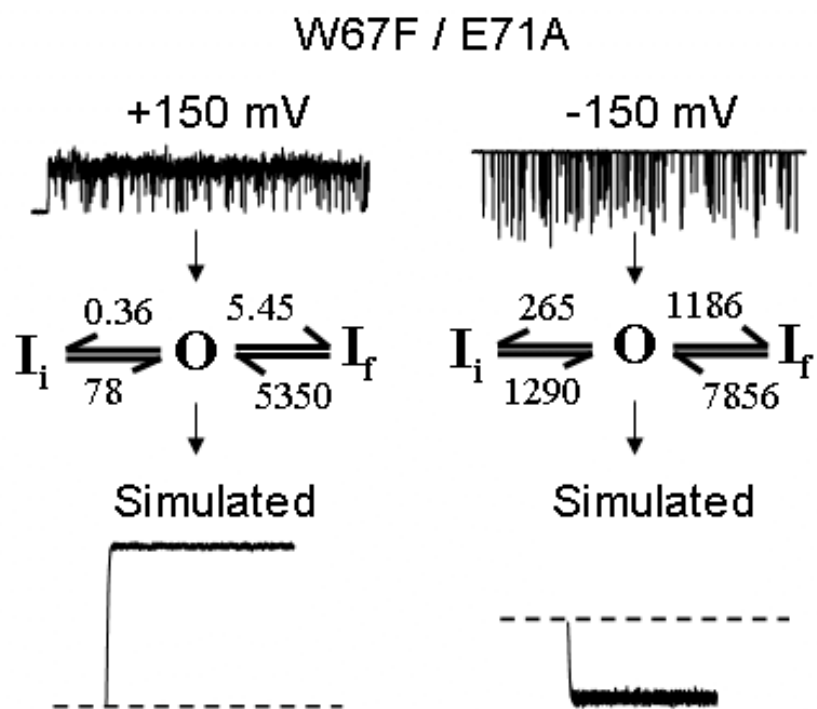
Figure 44 Simulated macroscopic currents from singles channel recordings of W67F/E71A mutant. Single channel recordings (±150 mV) were analyzed using QUB software and the closed-open transitions were detected using segmental-*k*-means (SKM) algorithm and half-amplitude threshold criterion. The numbers of closed and open states were determined by sequentially adding a state and then evaluating the model based on log-likelihood criterion. A best fit model for the mutant was described by two closed and one open state. Macroscopic currents simulated from the model derived under steady state conditions recapitulated the experimental findings from the macroscopic currents (Fig, 43, bottom panel).

Hydrogen-bond interactions at the selectivity filter serve as the basis for inactivation in eukaryotic Kv channels.

The engineering of hydrogen bond interactions between the pore helix and the external vestibule in Kv channels have been suggested to modulate C-type inactivation (Cordero-Morales et al., 2007). Although, one of the critical interactions that determine inactivation in KcsA is absent in Kv channels (Glu71-Asp80), eukaryotic K^+ channels have the conserved equivalent interaction between the pore helix and the external vestibule (Trp67-Asp80 for KcsA, Trp434-Asp447 for Shaker and Trp366-Asp379 for Kv1.2). This hydrogen bond interaction (Trp-Asp) in Kv channels has been determined using molecular dynamics as the strongest interaction at the selectivity filter and suggested to play the same important role in gating (Peng et al., 2007).

Normalized macroscopic currents elicited by a depolarizing voltage step from a holding potential of -80 mV to +60 mV showed that in Shaker, W434Y substitution recovers the ionic current lost in W434F, possibly by re-establishing the 434 and Asp447 interaction through a hydrogen bond and moving away from Tyr445 (Fig. 45). Interestingly, the time constant of inactivation for W434Y is still much faster than WT Shaker, presumably due to a stronger interaction between 434 and Asp447. These results could be explained if the W434F mutant enhances inactivation through the interaction with Tyr445 in the filter signature sequence, but in the case of W434Y this interaction is compromised by an h-bond with Asp447, which in turn recover the ionic current. On the other hand, normalized macroscopic currents showed that in Kv1.2, W366Y mutation almost recovers the WT Kv1.2 behavior (Fig. 46). However, in contrast to Shaker, W366F Kv1.2 shows robust macroscopic current with fast time-constant of inactivation.

Inset in Figure 46, shows a higher resolution detail of W366F macroscopic current.

The present set of results from KcsA, Shaker and Kv1.2 suggest that the hydrogen bond

network at the selectivity filter serve as the basis for C-type inactivation in the K^+

channel family.
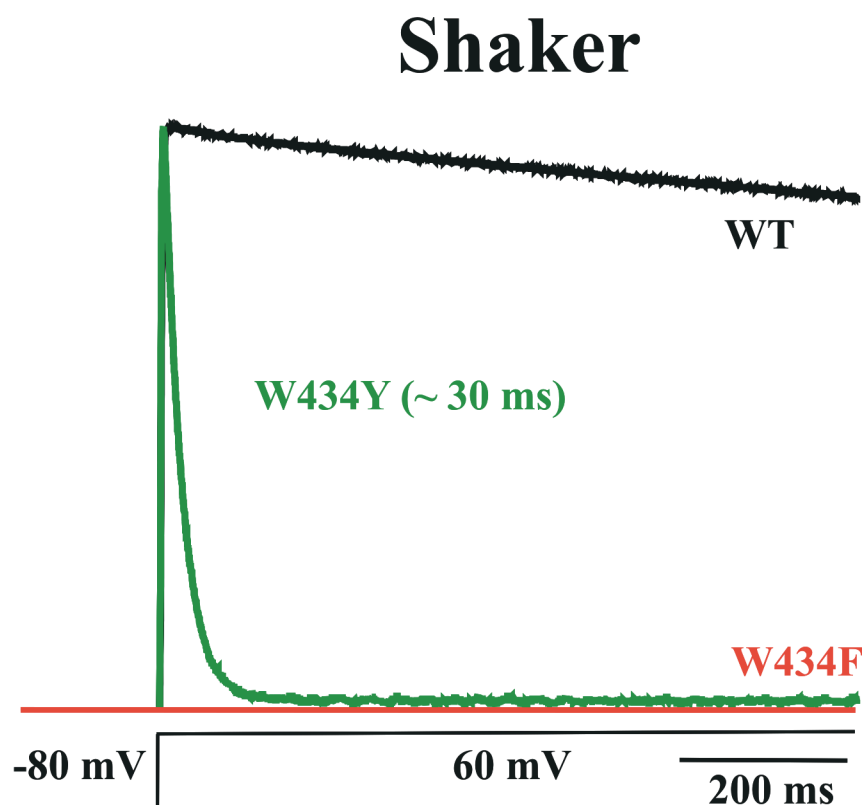
Figure 45 Hydrogen-bond interactions at the selectivity filter serve as the basis for C-type inactivation in Shaker. Normalized macroscopic currents of WT Shaker, W434F and W434Y mutants are shown. W434Y substitution recovers the ionic current lost in W434F, possibly by re-establishing the 434 and Asp447 interaction through a hydrogen bond, conserved in most potassium channels. Interestingly, the time constant of inactivation for W434Y is still much faster than WT Shaker. Currents were elicited by a depolarizing voltage step from a holding potential of -80 mV to +60 mV.
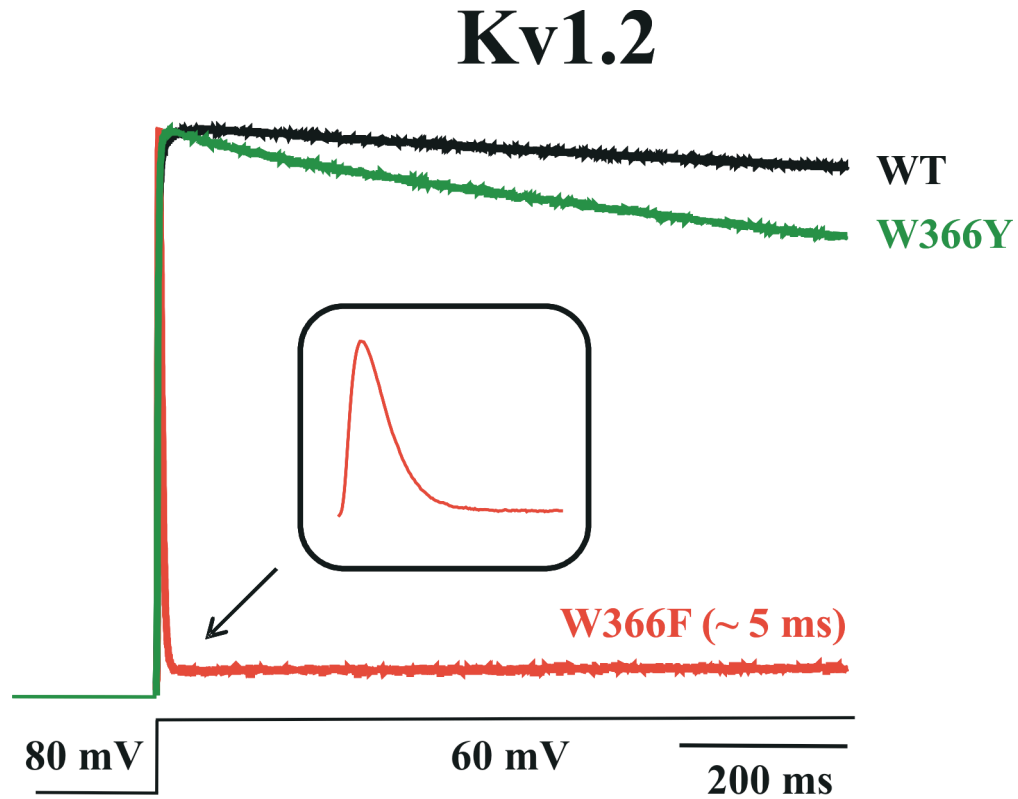
Kv1.2

Figure 46 Hydrogen-bond interactions at the selectivity filter serve as the basis for C-type inactivation in Kv1.2. Normalized macroscopic currents of WT Kv1.2, W366F, and W366Y mutants are shown. W366Y mutation in Kv1.2 almost recovers the WT Kv1.2 behavior. However, in contrast to Shaker, W366F Kv1.2 shows robust macroscopic current with a fast time-constant of inactivation. Inset, shows a higher resolution detail of W366F macroscopic current Currents were elicited by a depolarizing voltage step from a holding potential of -80 mV to +60 mV.

5.5 DISCUSSION AND CONCLUSION

Many ion channels use the inactivation process to regulate ion conduction, which in turn is coupled to several physiological processes. Inactivation mechanism in K^+ channels has been the primary focus of ion channel research. However, the molecular mechanism and conformational changes associated with C-type inactivation are not completely resolved, mostly due to a limited understanding of the molecular forces that drive the selectivity filter to its inactivated conformation and lack of structural information. Previously we have demonstrated a mechanistic equivalence between KcsA inactivation and that of voltage-dependent K^+ channels (Cordero-Morales et al., 2007). In KcsA the rate of inactivation is modulated by the permeant ion (Chakrapani et al., 2007a; Cordero-Morales et al., 2006b), which is a hallmark of C-type inactivation (Lopez-Barneo et al., 1993). This result points to the well-known role of the external K^+ binding site in stabilizing the conductive conformation of the selectivity filter (Baukrowitz and Yellen, 1995).

In addition ample mutagenesis studies in several K^+ channels have been able to point out critical residues that modulate inactivation. As an example, residue Tyr82 in KcsA and the equivalent Thr449 residue in Shaker accelerate C-type inactivation when mutated to alanine (Cordero-Morales et al., 2006b; Lopez-Barneo et al., 1993). Furthermore, mutations of Ser620 in hERG (equivalent to position Glu71 in KcsA) have a large impact on the rate of C-type inactivation (Ficker et al., 1998). Changes in K^+/Na^+ selectivity found in C-type inactivating channels also support the mechanistic equivalence between the potassium channel family (Cordero-Morales et al., 2006b; Kiss et al., 1999; Starkus et al., 1997). These evidences suggest that detailed understanding of

the molecular basis of inactivation in KcsA would provide new insight and make further inroad towards mechanistic interpretation of inactivation process in other eukaryotic channels.

The prokaryotic proton-gated potassium channel KcsA undergoes a time dependent inactivation process, which is modulated by transmembrane voltage but not by pH (Chakrapani et al., 2007a; Chakrapani et al., 2007b; Cordero-Morales et al., 2006a; Cuello et al., 1998; Heginbotham et al., 1999). We have demonstrated previously that the hydrogen bond between residues in the pore helix and external vestibule determine the rate and extent of the C-type inactivation (Cordero-Morales et al., 2007). Glu71 and Asp80 interaction is one of the key driving forces that promote rearrangements at the filter and extracellular entrance which biases it towards the non-conductive conformation. Disrupting this interaction (E71A) relieves C-type inactivation, and thereby increasing the steady state open probability.

Moreover, using CW-EPR spectroscopic measurements and fluorescence lifetime spectroscopy in combination with pore mutants of widely different open probabilities (Blunck et al., 2006; Cordero-Morales et al., 2006b), we previously showed that once the intracellular gate formed by the TM2 helices is maximally open (pH 4), it plays minimal role in stationary gating. Based on these results, we proposed a model in which selectivity filter is intrinsically unstable and movement of the TM2 gate allows the selectivity filter to undergo a rearrangement that leads to a more stable inactivated state.

High resolution KcsA structures suggest that the selectivity filter is also stabilized by the hydrogen bond between Trp67 and Asp80 (Fig. 38a) (Zhou et al., 2001b), an interaction conserved in most potassium channels (Shealy et al., 2003). Furthermore,

aromatic residues at the filter have been suggested to undergo considerable conformational changes (Tyr78 and Trp67) presumably involved in KcsA gating (Baker et al., 2007; Lange et al., 2006; Lockless et al., 2007; Valiyaveetil et al., 2006a). In this work, as a continuation of our studies on the gating at the selectivity filter, we functionally evaluated the conserved aromatic residue in the pore helix of KcsA (W67), Shaker (W434) and Kv1.2 (W366), in an attempt to establish the role of these residues on C-type inactivation.

Substitution of Trp67 to phenylalanine in the pore helix of KcsA has a dual effect modulated by transmembrane voltage. First, at positive potentials Phe67 decreases the rate and extent of inactivation as determined by macroscopic and single channel currents (Fig. 38, 39 and 40). Positive potentials tend to orient the charged Glu71 towards the intracellular end of the channel causing the weakening of several hydrogen bonds (Fig. 39d), moreover the flexibility of Asp80 further increases due to the disruption of the Trp67-Asp80 interaction induced by the Phe67 substitution. These conformational changes will prevent the collapse of the filter, since removing hydrogen bonds between the pore helix and the extracellular vestibule results in a stabilization of the conductive state. Second, negative potentials favor Glu71-Asp80 interaction, subsequently re-establishing the inactivation process (Fig. 39a). However, W67F proceeds with a faster time constant of inactivation when compared to WT KcsA (Fig. 40c).

On the other hand, W67Y substitution restores the C-type inactivation present in WT KcsA (Fig. 41), presumably by reestablishing the 67 and Asp80 interaction (Fig. 38a). Therefore, the flexibility of Asp80 will decrease and promote inactivation through a filter constriction parallel to the permeation pathway (Glu71-Asp80) (Cordero-Morales et

al., 2007). This result also suggests a stronger interaction between position 67 and Asp80, since the time constant of inactivation of W67Y shows slightly faster inactivation when compared to WT KcsA (Fig. 41c).

Our results from molecular dynamics simulations suggest that Phe67 further enhance the inactivation process by modulating ion conduction through a direct interaction with Tyr78, which forms the first binding site of the selectivity filter (Fig. 42). Due to the lack of hydrogen bond with Asp80, the phenylalanine is in close proximity to Tyr78 aromatic group, leading to edge-to-edge orientation, resulting in repulsive interaction. These findings are in excellent agreement with single-channel data of the double mutant E71A-W67F, where even in the absence of any hydrogen- bonding interaction between the pore helix and the external vestibule, the channel shows intermediate inactivation suggesting a mechanism of Phe67 action that extends beyond constriction of the selectivity filter. KcsA results therefore suggests that the modulation of the K^+ binding site in Shaker, through Phe434-Tyr445 interaction, might underlie the molecular mechanism by which W434F mutant locks the selectivity filter in the inactivated state.

Similar to KcsA, C-Type inactivation in Kv channels can be modulated by the hydrogen bond interaction at the selectivity filter (Cordero-Morales et al., 2007). Small differences in this network of interaction might account partially for the large degree of C-type inactivation in the potassium channel family. In Shaker, W434Y mutant recovers the ionic current lost in W434F (Fig. 45), possibly by re-establishing the 434 and Asp447 interaction through a hydrogen bond and avoiding interaction with Tyr445 at the

selectivity filter. As in KcsA, W434Y Shaker shows fast inactivation ($\sim$ 30 ms) probably due to a stronger interaction with Asp447 (Fig. 45).

Likewise, W366Y in Kv1.2 almost recovers the WT Kv1.2 behavior with a modest faster inactivation (Fig. 46). Interestingly, in contrast to Shaker the W366F substitution shows macroscopic current but with very fast inactivation ($\sim$ 5 ms, Fig. 46). This suggests that the interaction between phenylalanine at the pore helix and tyrosine on the filter depends on the ability of the channel to undergo fast inactivation. Kv1.2 shows very slow inactivation compared to Shaker and hence the orientation of tyrosine of TVGYG in Shaker is closer to pore-helix compared to Kv1.2. Similar is true in KcsA where in, double mutant W67F-E71A with non-inactivating mutation E71A showed less inactivation.

The present mechanistic interpretation of our results is summarized in Figure 47. The stability of the K$^+$ channel selectivity filter is modulated by the presence of a series of interactions pictured as "molecular springs". Weakening the springs in the network by mutations (E71A and W67F, bottom panel), stabilizes the conductive state of the filter at positive potentials. However, the non-conductive state is stabilized by reestablishing the hydrogen bond network (E71S and W67Y), which promotes a constriction of the selectivity filter parallel to the permeation pathway. We suggest that this overall mechanism might include the events that occur during the transition from the conductive to non-conductive state of the K$^+$ channel.
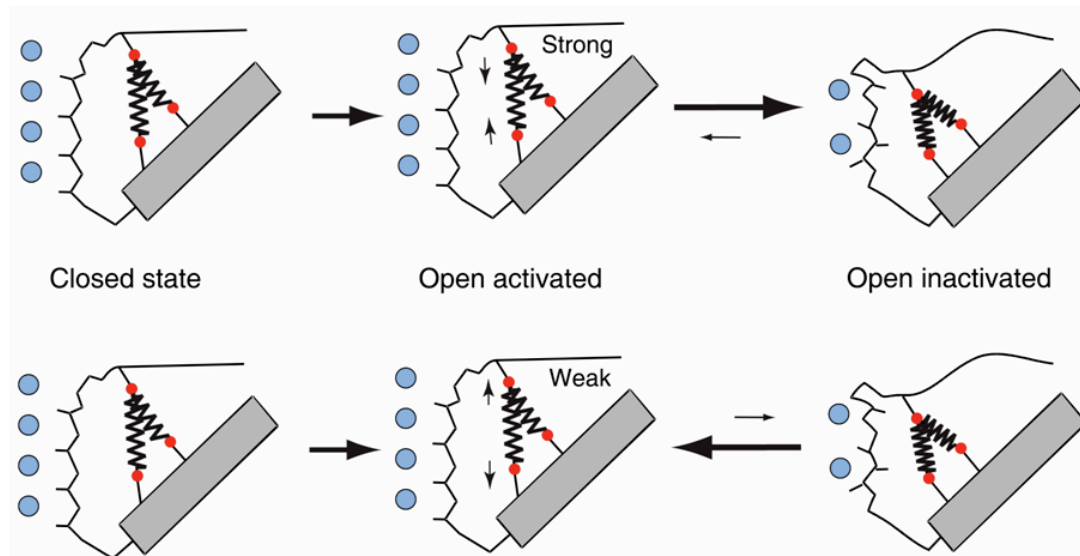
Figure 47 Structural rearrangements during C-type inactivation at the selectivity filter. Shown is a cartoon representation of a mechanistic interpretation of the molecular events during KcsA gating. This model shows the presence of two key interactions (Glu71-Asp80, Trp67-Asp80) which are the main driving force of KcsA inactivation.

CHAPTER 6: Multiple gating modes in KcsA are determined by the selectivity filter dynamics

6.1 ABSTRACT

In this chapter, we show that in KcsA, a proton-activated potassium channel, steady state kinetic transitions are determined solely by the selectivity filter dynamics. Here, we have functionally characterized the effect of a series of side chain substitutions, on position 71, in an attempt to understand the role of the selectivity filter in the gating process. Macroscopic and single channel currents demonstrate that at position 71 both side-chain volume and charge affect the kinetics properties of KcsA. Three distinct groups were determined by their side-chain volume, open probability, single channel flickering behavior and dwell time distribution. Moreover, macroscopic currents from these mutants showed a decreased in the rate of inactivation, similar to the non-inactivating E71A mutant. These results showed that multiple gating regimes in KcsA are determined by the selectivity filter, since we were able to modulate the P_o, mean open and mean closed times by introducing different side-chain at the Glu71 position.

6.2 INTRODUCTION

The role of the selectivity filter on channel gating has been studied for many years. Several pieces of evidence seem to point out the filter as a region with a great influence over the gating behavior, and in fact it has been proposed to function as a "pore gate" (Liu and Joho, 1998; Mienville and Clay, 1996; Proks et al., 2001; Zheng and Sigworth, 1997). There has been a vast amount of work on the effect of certain permeant ions on gating (Demo and Yellen, 1992; LeMasurier et al., 2001; Lopez-Barneo et al., 1993; Shapiro and DeCoursey, 1991; Spruce et al., 1989; Swenson and Armstrong,

1981). Ions with long resident times (like Rb$^+$) tend to stabilize the open state through a "foot in the door" mechanism on the gate. Additionally, ion channels seem to populate sub-conducting conformations on the way to the open state, and these sub-conducting states show altered selectivities (VanDongen, 2004). Moreover, unnatural amino acid mutagenesis targeted to the signature sequence of an inward rectifier K$^+$ channel revealed dramatic consequences upon rapid gating transitions (Lu et al., 2001), again, pointing out the selectivity filter as a contributor to the gating process.

A previous structural work suggested that subtle conformational changes occur in regions flanking the selectivity filter, upon pH activation (Perozo et al., 1999). On the other hand, X-ray crystallography suggested that two different conformations of the selectivity filter could account for the channel flickering and the permeant ion effect on gating (Zhou et al., 2001b). Moreover, kinetic variability and modal gating at the single-channel level, under stationary conditions in WT KcsA gating is characterized by a highly variable and complex kinetic behavior, the origin of which is poorly understood. The overall gating heterogeneity arises from variation in the open probability as well as mean open and mean closed times (Cordero-Morales et al., 2006b, chapter 2). In this chapter, we provide additional evidences suggesting that the fast gating transitions in KcsA channels are determined by the conformational dynamics at the selectivity filter.

6.3 EXPERIMENTAL METHODS

6.3.1 Mutagenesis and channel biochemistry

Mutagenesis and channel biochemistry were carried out as discussed in chapter 2 (section 2.3.2).

6.3.2 Liposome patch-clamp

Liposome patch-clamp was carried out as discussed in chapter 2 (section 2.3.3).

6.3.3 X-ray crystallography

KcsA (pQE32 vector) mutant E71Q/I and Gly were crystallized (in collaboration with Vishwanath Jogini from Eduardo Perozo's laboratory) in the presence of an antibody Fab fragment following published protocols (Zhou et al., 2001b). Beam-like crystals of KcsA-Fab complex appeared after one week in a sitting drop containing 23–26% PEG400 (v/v), 50 mM magnesium acetate, 50 mM sodium acetate (pH 4.8-5.4) at 19°C. Crystals diffracted to Bragg spacing of 2.5 Å for E71Q, 2.2 Å for E71I and 2.5 Å for E71G. Data were collected at the GM/CA-23-ID beam-line at the Advanced Photon Source and processed with HKL2000 (Otwinowski and Minor, 1997). Glu71 mutant structures were solved by molecular replacement using the WT KcsA-Fab complex structure (PDB entry 1K4C) as search model. All the structures were solved using Fab and KcsA without the selectivity filter as the initial model for molecular replacement. Refinement of the structures (Gln, Ile and Gly) are not complete at this point, still multiple cycles of manual rebuilding using the program O (Jones et al., 1991) and refinement using CNS (Brunger et al., 1998) are required.

6.4 RESULTS AND DISCUSSION

6.4.1 Side-chain substitutions at position 71

In an attempt to understand the kinetics properties of KcsA, functional and structural characterization of a series of side chain substitutions were performed, varying charge and side chain volume at position 71. Of the fifteen single point mutations introduced, nine (Gly, Ala, Ser, Cys, Thr, Val, Gln, His and Ile) were suitable for electrophysiological analysis. Trp and Pro were not used in this study to avoid the impact that these residues might cause on folding and assembly. Arg and Lys substitutions severely compromised channel folding and expression. Glu71 mutant's share the same hydrodynamic properties of WT KcsA purified protein, checked by gel-exclusion chromatography in a Superdex 200 column (Fig. 48a). Single channel traces show that at position 71, both, side-chain volume and charge affect KcsA gating properties. Figure 48b shows single channel records of representative Glu71 substitutions obtained under symmetric conditions (200 mM K^+, pH 4.0). Although we found a wide range of kinetic behaviors from these mutants set, none of the substitutions displayed the long closed-times period characteristic of WT KcsA inactivation. Because of this feature, open probabilities were also significantly higher, therefore these mutants constituted an important tool to carry out single channel kinetic analysis, given the fact that the P_o of the WT is so low, making difficult this kind of analysis.

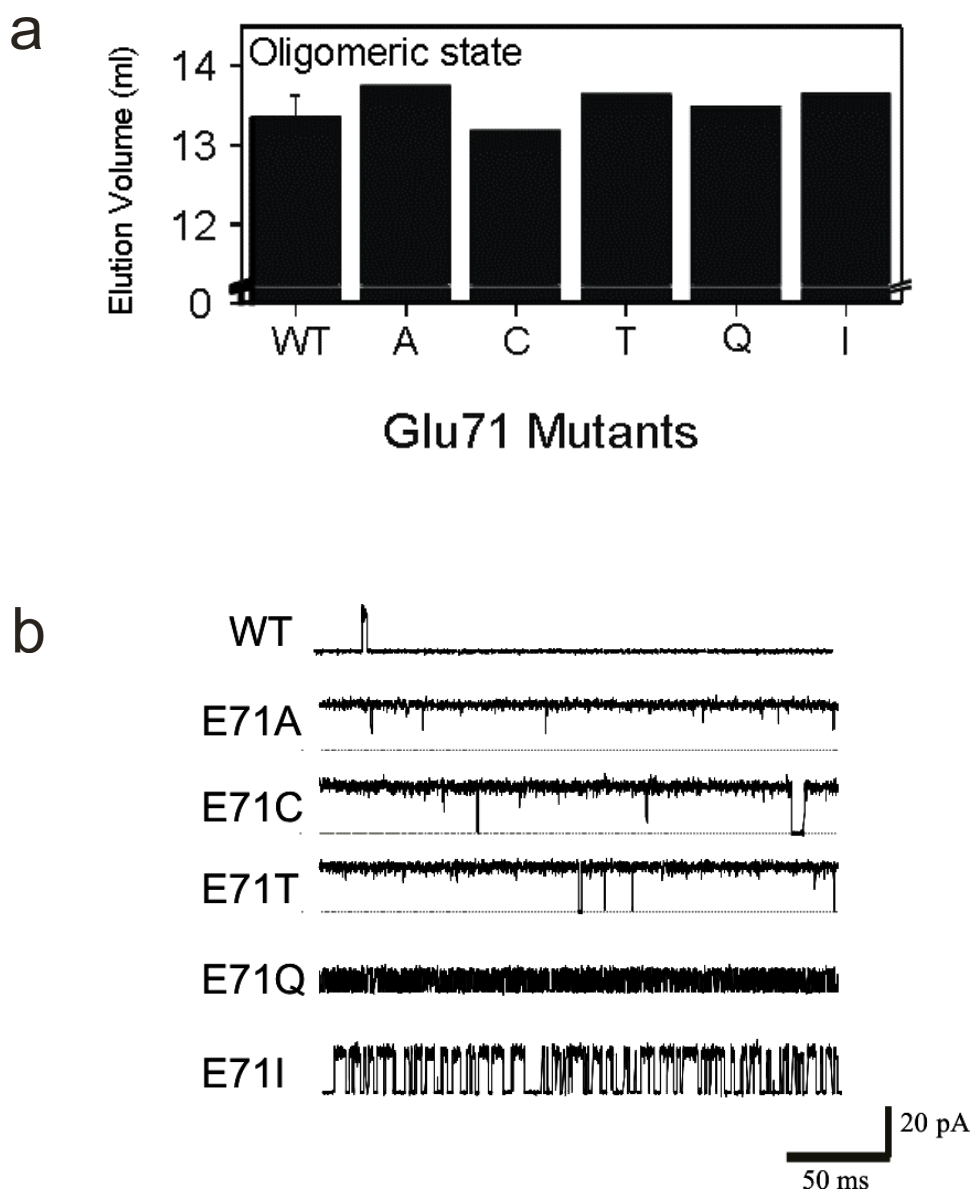**Figure 48 Hydrodynamics properties of Glu71 side-chain substitutions. a) Hydrodynamic properties of the mutants evaluated from gel filtration chromatography elution volume. b) Representative single channel traces for each mutant, at pH 4 and +150 mV in symmetric 200 mM K$^+$. Closed states are represented by horizontal broken lines and openings are upward deflections.**

6.4.2 Fast gating transitions are determined by the conformational dynamics at the selectivity filter.

From single channels analysis, three distinct groups were determined by their flickering behavior and dwell time distribution, the first represented by small side chain volume residues (Ala, Cys and Thr < 120 A^3) with $P_o \approx 0.9$ and mean open times > 70 ms (Fig. 49). The second group with middle side-chain volume is represented only by the WT KcsA (Glu71 $\approx$ 140 A^3) with an apparent $P_o \approx 0.17$ and a mean open time < 30 ms. The last group represented by Gln and Ile (> 140 A^3) substitutions showed a $P_o \approx 0.5$ and a mean open time less than 6 ms. Moreover, all the substitutions had a mean closed time < 7 ms, in contrast to the WT KcsA that had > 500 ms, suggesting that the inactivated state is inhibited in all mutations. In agreement with the single channel analysis, macroscopic currents from Glu71 substitutions (Fig. 50) showed a decrease in the rate of inactivation, similar to the non-inactivating E71A mutant, supporting that the deep inactivated state is reduced in all the mutations.
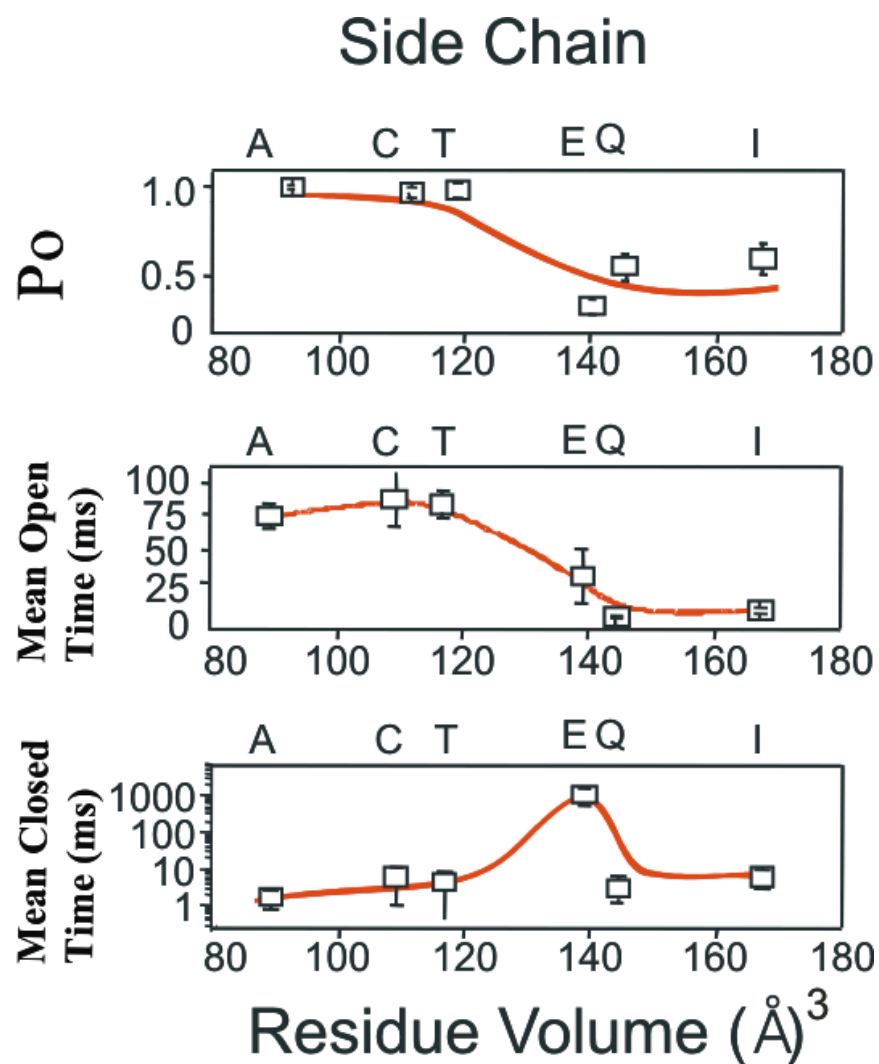
Figure 49 Different side-chain volume and charge substitutions at position Glu71 affect gating at the selectivity filter. (Top) Open probability for each mutant evaluated from Gaussian fits of all-points-histograms of single channel traces. (Middle and bottom) Mean open and closed times obtained from idealization of single channel traces.

E71A
E71C
E71T
E71Q
E71I

1 s

WT

pH 7.5

4
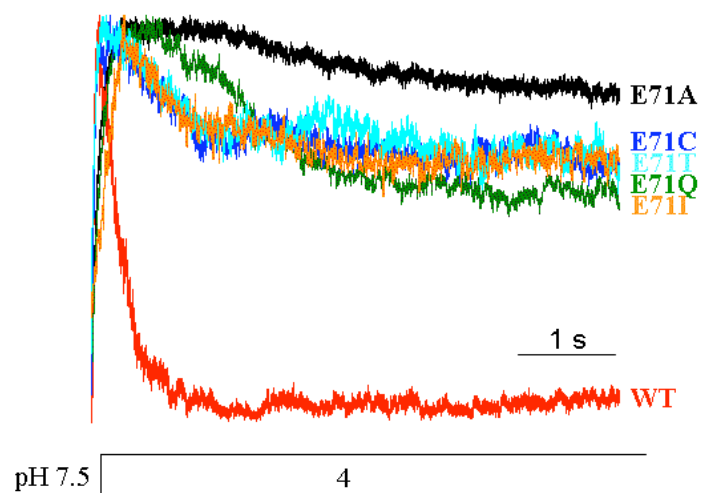
Figure 50 Glu71 side-chain substitutions affect the rate of inactivation. Macroscopic current traces elicited by a rapid pH jump demonstrate variations in the rate and steady-state level of inactivation similar to the non-inactivating E71A mutant.

6.4.3 Kinetic variability and modal gating of WT KcsA

Kinetic variability and modal gating at the single-channel level, under stationary conditions in WT KcsA gating is characterized by a highly variable and complex kinetic behavior. Steady-state single channel current traces reveal the presence of several different patterns of behavior or "modes". A representative single channel record from WT KcsA (Fig. 51) revealed three distinct populations based on the open probabilities and flicker kinetics, similar to the behavior observed in Glu71 mutants (Fig. 51, left panel). These results showed that the multiple gating regimes in WT KcsA are determined by the selectivity filter, since mutants were able to modulate the P_o, mean open and mean closed times by introducing different side chain volume and charge substitution at the 71 position. Furthermore, occupancy of the deep inactivated state demands the presence of Glu at position 71, because of the carboxyl-carboxylate interaction with Asp80 is required to assume the non-conductive conformation. However, once Glu71 is neutralized the inactivation process disappears, unmasking and stabilizing (depending of the side-chain substitution) distinct fast gating events that were present on WT KcsA (different flickering behavior, see figure 51), pointing to the role of local selectivity filter dynamics in determining single channel gating kinetics.
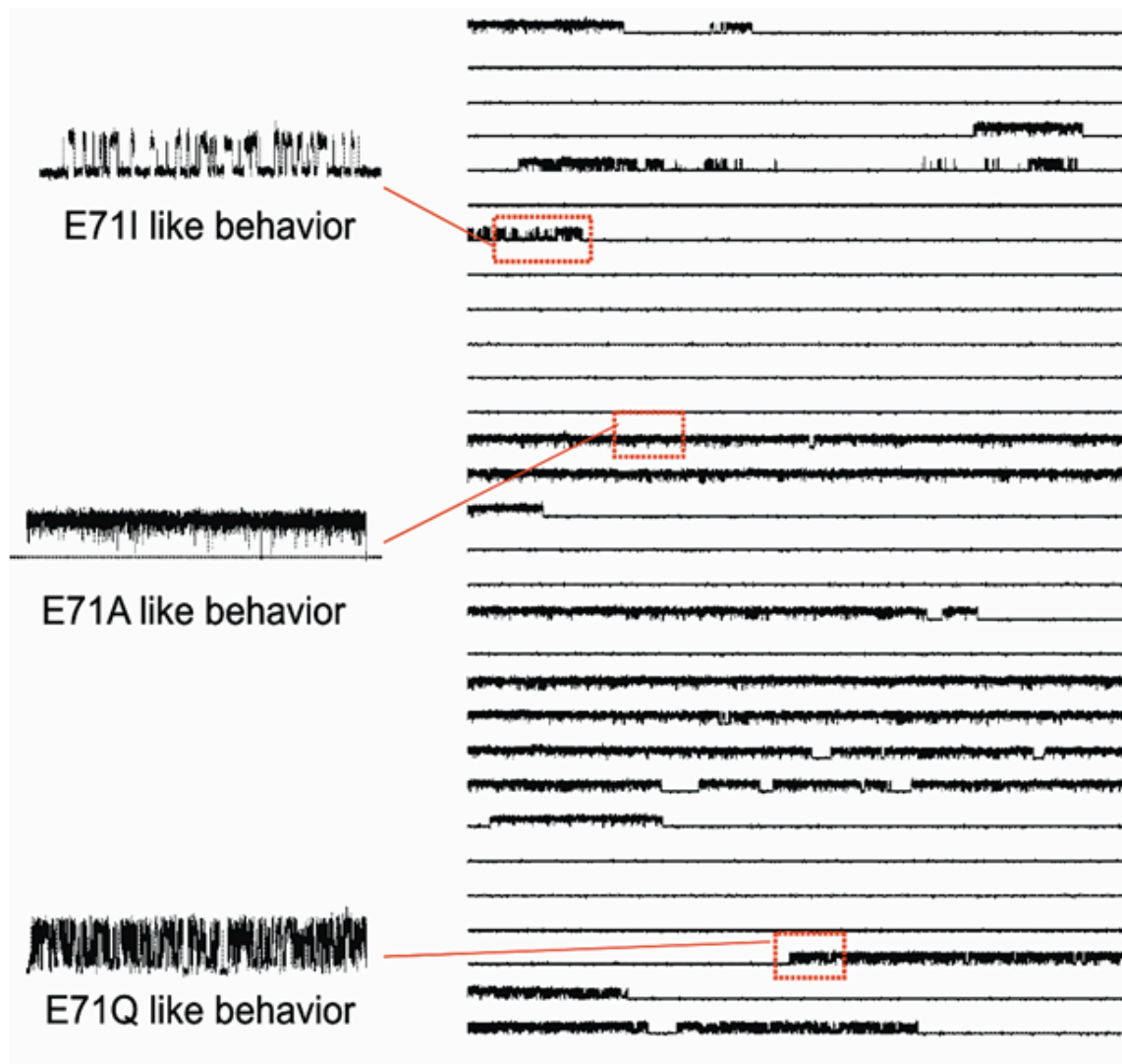
Figure 51 Modal behavior of WT KcsA. A continuous single channel recording of KcsA under steady state conditions at pH 3.0 with membrane potential at +100mV. WT KcsA displays a highly variable kinetic behavior which arises from a combination of three distinct modes of channels activity, the low P_o, high P_o and the flickery mode, similar to the ones observed in Glu71 mutants . Boxed areas are shown in expanded time scale on the left.

6.4.4 Crystal structures of Glu71 substitutions

In addition to the Glu71 functional studies, crystal structures of mutants in complex with Fab antibody in each representative group were solved at 2.2 Å (E71T), 2.5 Å (E71Q), 2.2 Å (E71I) and 2.5 Å (E71A) resolution (Fig. 51). In these structures no significant differences were observed (backbone and side chains) in comparison to the WT KcsA structure, suggesting that the conformational changes at the selectivity filter might occur only when the inner helix bundle is in the open conformation (channel open, pH 4) rather than the closed state trapped on the crystal structures (basic pH).

However, E71I crystal structure shows significant differences in the K^+ ion occupancy (Fig. 51) in comparison to the WT KcsA. The ion electron density at position S_2 was missing and reduced in position S_1. The decrease in K^+ occupancy might be due to the large side-chain of the isoleucine, which might interact with residues in the signature sequence of KcsA (i.e. Gly77), therefore inducing an increase in the diameter of the selectivity filter, and affecting the K^+ binding site S_1 and S_2.

E71T, 2.2 Å
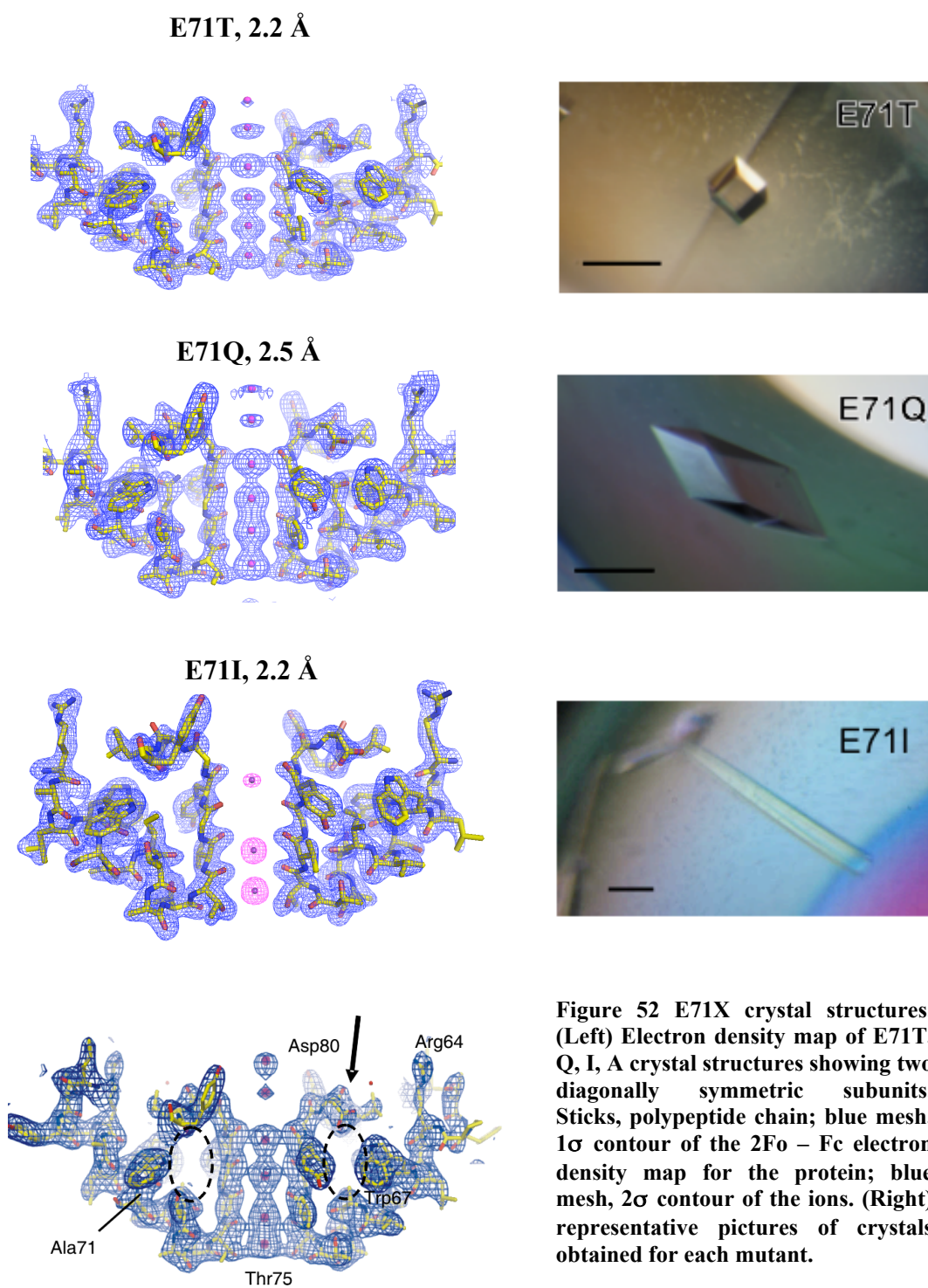

E71Q, 2.5 Å

E71I, 2.2 Å

Figure 52 E71X crystal structures. (Left) Electron density map of E71T, Q, I, A crystal structures showing two diagonally symmetric subunits. Sticks, polypeptide chain; blue mesh, 1σ contour of the 2Fo – Fc electron density map for the protein; blue mesh, 2σ contour of the ions. (Right) representative pictures of crystals obtained for each mutant.

On the other hand, E71G substitution has the same functional properties than E71A, displaying long openings interrupted only by very brief closures and as expected showing non-inactivating macroscopic currents (Fig. 52a, b). Unexpectedly, single channel currents were reduced (~ 10 times) from 15 pA for WT to 1.2 pA for E71G at +150 mV in symmetric condition, 200 mM K^+ (Fig. 52a). E71G crystal structure shows no significant differences when compared to the WT KcsA (Fig. 52c). This result suggests that in E71G major conformational changes occurred at the selectivity filter in the open state (pH 4), which can not be detected in the crystal structure (closed state).

This latest result is in disagreement with recent works published by Mackinnon's laboratory (Valiyaveetil et al., 2006b; Zhou and MacKinnon, 2004; Zhou and MacKinnon, 2003), where they suggested a correlation between the ion occupancy and the rate of ion conduction. For E71G, a decrease in ion conduction is not correlated with a decrease in ion occupancy, since not appreciable differences in the ion distribution were observed in the crystal structure when compared to the WT (closed state). Functional results of Glycine substitution at position 71 are not well understood, thus new experiments are required to determine the origin of the reduce ion conduction.

The results of this chapter provide new evidences suggesting that the fast gating transitions in KcsA channels are determined by the conformational dynamics at the selectivity filter. However, we are currently performing a deeper kinetic analysis in this set of mutants in order to have a more quantitative view of the selectivity filter modulation.

a

WT

o

c

20 pA

E71G

o
c

500 ms

b

+ 150 mV

E71G

1 s

WT

pH 8   4
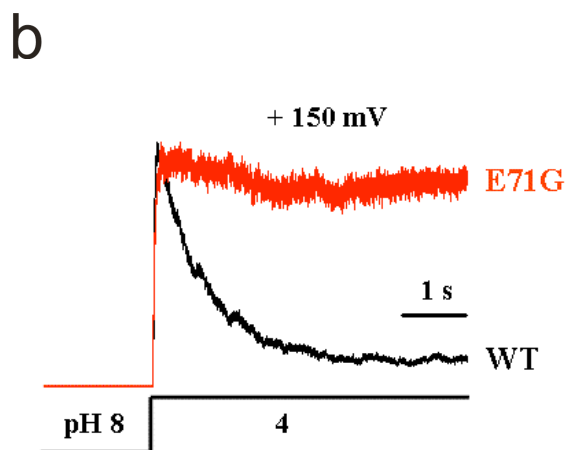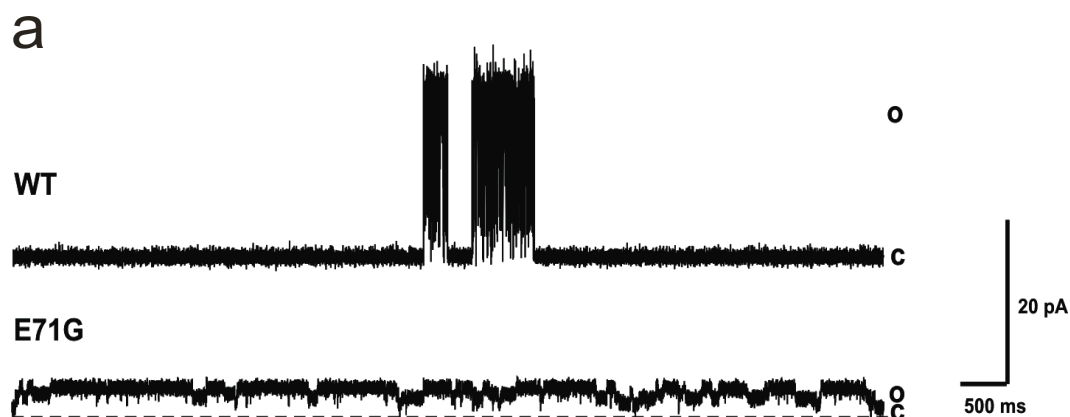
Figure 53 Glycine at position 71 reduced (~ 10 times) the single channel current. a) Comparison of the single channel current from E71G (3 channels, 1.2 pA) and WT KcsA (one channel, 15 pA). b) Normalized macroscopic currents activated by pH jump. c) E71G crystal structure at 2.5 Å resolution. Electron density map showing two diagonally symmetric subunits. Sticks, polypeptide chain; blue mesh, 3σ contour of the omit (Fo – Fc) electron density map for the protein; magenta mesh, 4σ contour of the ions. Water molecules are shown in red (mesh 1.5σ).

c
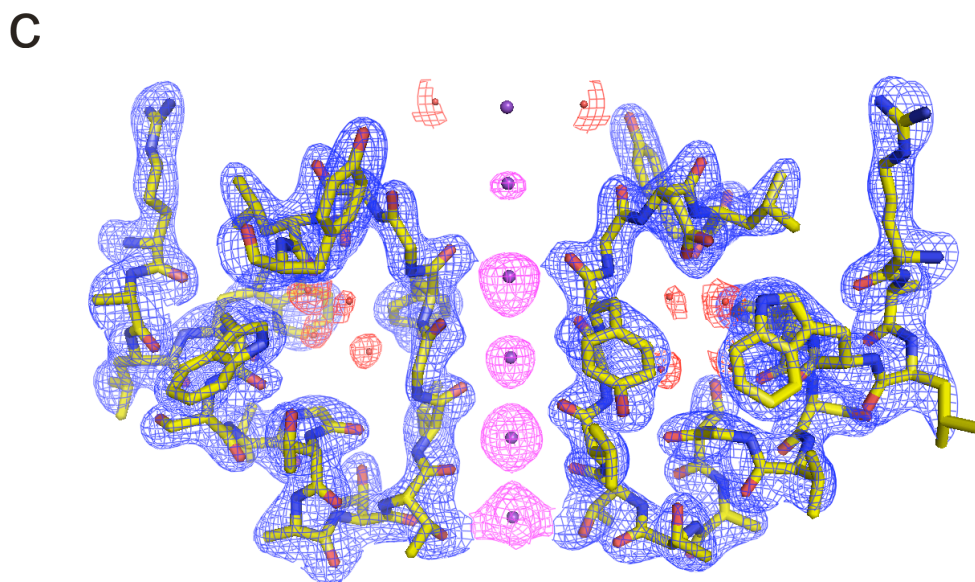
CHAPTER 7: Conclusions and Future Perspectives

7.1 Conclusions

We have used KcsA, a structural model of the pore domain of potassium channels, to characterize the functional and structural events that underlie gating. Using an spectroscopic technique (EPR) in combination with electrophysiological measurements (patch clamp), X-ray crystallography and theoretical analysis, we have gathered new information that would help to better understand the conformational changes during KcsA gating, which can be extrapolated to other K^+ channels, and therefore provide new insights into an unified model of gating.

The current model for the gating mechanism in KcsA is that the conductive conformation of the selectivity filter is intrinsically unstable. Thus, in the transition from the closed to the open state, movements of the TM2 gate allow the selectivity filter to fluctuate in a range of conformations, some conducting some not, before it undergoes a rearrangement that leads to a more stable inactivated state. The hydrogen-bond network at the selectivity filter (Glu71-Asp80 and Trp67-Asp80) is the driving force that promotes instability through a compression of the selectivity filter parallel to the permeation pathway, which energetically biases it towards the inactivated conformation. Subsequently, closing the intracellular gate resets the selectivity filter back into its conductive conformation. In the open state, different flickering behavior in KcsA, occurred through fast fluctuations at the selectivity filter. As shown from the kinetic analysis of various Glu71 mutants, once inactivation is eliminated, it is possible to unmask several of these kinetic modes of gating, depending on the side chain at position 71.

Analogous to KcsA, C-Type inactivation in Kv (Shaker and Kv1.2) channels can be modulated by the hydrogen bond interaction at the selectivity filter. This network of hydrogen bonds, involving residues Trp67, Tyr78 and Asp80 (conserved in most potassium channels) that comprise essential interactions between the selectivity filter and its adjacent pore helix, determines and modulates the rate and extent of C-type inactivation in eukaryotic K^+ channels. This thesis provides new functional insight into the KcsA inactivation mechanism, which might serves as the basis for C-type inactivation in the K^+ channel family. Therefore, KcsA is not only the archetypical structural pore domain of potassium channels, but also a functional model.

7.2 Future Perspectives

Based on our knowledge on KcsA, together with a multidisciplinary approach to study function, structure and dynamics offers new possibilities in the mechanistic analysis of K^+ channel gating. To this end, our efforts will focus on the following: First, we will pursue a systematic study of KcsA pore loop and external vestibule by EPR spectroscopy, in order to establish the role of this region during the gating process. Previous results have suggested that in eukaryotic voltage-dependent K^+ channels the outer mouth contributed to the inactivation and that during membrane depolarization the external loops from the tetramer channel come close to each other to occlude ion permeation (Liu et al., 2002; Liu et al., 1996). Through a cysteine scanning along with spin labeling, the pore loop and external vestibule will be evaluated for differences in probe mobility, solvent accessibility and changes in inter-subunit distances in order to reveal different types of conformational changes that occur during KcsA inactivation gating.

Second, the selectivity filter dynamics will be studyied using fluorescence polarization methods, which will help to characterize backbone dynamics and quantify the local motions in the KcsA selectivity filter in the conductive and non-conductive states. Each functional state will be stabilized by taking advantage of previously characterized mutants that represent important physiological conformations in KcsA. In all cases, we will focus on the dynamic behavior of Tyr78 at the selectivity filter, Tyr82 at the outer pore vestibule and Trp67 in the pore helix, all in a background of either WT-KcsA or the non-inactivating mutant (E71A). We will pursue the study of residues Asp80

and Trp67, given the large conformation changes observed in the two forms of the

E71A crystal structure (Cordero-Morales et al., 2006b).

Finally, we will pursue the study in more detail of the E71I and E71G substitutions. With the understanding of these mutants we expect to obtain more information of the ion conduction, permeation and selectivity mechanisms in K^+ channels.

REFERENCES

Aggarwal, S. K., and MacKinnon, R. (1996). Contribution of the S4 segment to gating charge in the Shaker K+ channel. Neuron *16*, 1169-1177.

Ahern, C. A., and Horn, R. (2004). Stirring up controversy with a voltage sensor paddle. Trends Neurosci *27*, 303-307.

Alagem, N., Yesylevskyy, S., and Reuveny, E. (2003). The pore helix is involved in stabilizing the open state of inwardly rectifying K+ channels. Biophys J *85*, 300-312.

Armstrong, C. M. (1971). Interaction of tetraethylammonium ion derivatives with the potassium channels of giant axons. J Gen Physiol *58*, 413-437.

Armstrong, C. M. (2003). Voltage-gated K channels. Sci STKE *2003*, re10.

Armstrong, C. M., and Bezanilla, F. (1973). Currents related to movement of the gating particles of the sodium channels. Nature *242*, 459-461.

Baker, K. A., Tzitzilonis, C., Kwiatkowski, W., Choe, S., and Riek, R. (2007). Conformational dynamics of the KcsA potassium channel governs gating properties. Nat Struct Mol Biol *14*, 1089-1095.

Baukrowitz, T., and Yellen, G. (1995). Modulation of K+ current by frequency and external [K+]: a tale of two inactivation mechanisms. Neuron *15*, 951-960.

Bean, B. P. (2007). The action potential in mammalian central neurons. Nat Rev Neurosci *8*, 451-465.

Berneche, S., and Roux, B. (2000). Molecular dynamics of the KcsA K(+) channel in a bilayer membrane. Biophys J *78*, 2900-2917.

Berneche, S., and Roux, B. (2002). The ionization state and the conformation of Glu-71 in the KcsA K(+) channel. Biophys J *82*, 772-780.

Berneche, S., and Roux, B. (2005). A gate in the selectivity filter of potassium channels. Structure *13*, 591-600.

Bezanilla, F. (2000). The voltage sensor in voltage-dependent ion channels. Physiol Rev *80*, 555-592.

Bezanilla, F. (2005). The voltage-sensor structure in a voltage-gated channel. Trends Biochem Sci *30*, 166-168.

Bezanilla, F., Perozo, E., Papazian, D. M., and Stefani, E. (1991). Molecular basis of gating charge immobilization in Shaker potassium channels. Science *254*, 679-683.

Blunck, R., Cordero-Morales, J. F., Cuello, L. G., Perozo, E., and Bezanilla, F. (2006). Detection of the opening of the bundle crossing in KcsA with fluorescence lifetime spectroscopy reveals the existence of two gates for ion conduction. J Gen Physiol *128*, 569-581.

Brammar, J. (1999). The Ion Channel, Facts Book, Voltage-gated Channels (San Diego CA, U.S.A**.**).

Brooks, B. R., Bruccoleri, R. E., Olafson, B. D., States, D. J., Swaminathan, S., and Karplus, M. (1983). CHARMM: a program for macromolecular energy, minimization, and dynamics calculations. Journal of Computational Chemistry *4*, 187-217.

Bruening-Wright, A., Schumacher, M. A., Adelman, J. P., and Maylie, J. (2002). Localization of the activation gate for small conductance Ca2+-activated K+ channels. J Neurosci *22*, 6499-6506.

Brunger, A. T., Adams, P. D., Clore, G. M., DeLano, W. L., Gros, P., Grosse-Kunstleve, R. W., Jiang, J.-S., Kuszewski, J., Nilges, M., Pannu, N. S*., et al.* (1998). Crystallography and NMR system: A new software suite for macromolecular structure determination. Acta Crystallography *sec D 54*, 905-921.

Cha, A., and Bezanilla, F. (1997). Characterizing voltage-dependent conformational changes in the Shaker K+ channel with fluorescence. Neuron *19*, 1127-1140.

Chakrapani, S., Cordero-Morales, J. F., and Perozo, E. (2007a). A quantitative description of KcsA gating I: macroscopic currents. J Gen Physiol *130*, 465-478.

Chakrapani, S., Cordero-Morales, J. F., and Perozo, E. (2007b). A quantitative description of KcsA gating II: single-channel currents. J Gen Physiol *130*, 479-496.

Chanda, B., Asamoah, O. K., Blunck, R., Roux, B., and Bezanilla, F. (2005). Gating charge displacement in voltage-gated ion channels involves limited transmembrane movement. Nature *436*, 852-856.

Chapman, M. L., Blanke, M. L., Krovetz, H. S., and Vandongen, A. M. (2006). Allosteric effects of external K(+) ions mediated by the aspartate of the GYGD signature sequence in the Kv2.1 K(+) channel. Pflugers Arch *451*, 776-792.

Chapman, M. L., Krovetz, H. S., and VanDongen, A. M. (2001). GYGD pore motifs in neighbouring potassium channel subunits interact to determine ion selectivity. J Physiol *530*, 21-33.

Chapman, M. L., VanDongen, H. M., and VanDongen, A. M. (1997). Activation-dependent subconductance levels in the drk1 K channel suggest a subunit basis for ion permeation and gating. Biophys J *72*, 708-719.

Choi, H., and Heginbotham, L. (2004). Functional influence of the pore helix glutamate in the KcsA K+ channel. Biophys J *86*, 2137-2144.

Choi, K. L., Aldrich, R. W., and Yellen, G. (1991). Tetraethylammonium blockade distinguishes two inactivation mechanisms in voltage-activated K+ channels. Proc Natl Acad Sci U S A *88*, 5092-5095.

Choi, K. L., Mossman, C., Aube, J., and Yellen, G. (1993). The internal quaternary ammonium receptor site of Shaker potassium channels. Neuron *10*, 533-541.

Claydon, T. W., Makary, S. Y., Dibb, K. M., and Boyett, M. R. (2003). The selectivity filter may act as the agonist-activated gate in the G protein-activated Kir3.1/Kir3.4 K+ channel. J Biol Chem *278*, 50654-50663.

Claydon, T. W., Vaid, M., Rezazadeh, S., Kwan, D. C., Kehl, S. J., and Fedida, D. (2007). A direct demonstration of closed-state inactivation of K+ channels at low pH. J Gen Physiol *129*, 437-455.

Cohen, B. E., Grabe, M., and Jan, L. Y. (2003). Answers and questions from the KvAP structures. Neuron *39*, 395-400.

Cordero-Morales, J. F., Cuello, L. G., and Perozo, E. (2006a). Voltage-dependent gating at the KcsA selectivity filter. Nat Struct Mol Biol *13*, 319-322.

Cordero-Morales, J. F., Cuello, L. G., Zhao, Y., Jogini, V., Cortes, D. M., Roux, B., and Perozo, E. (2006b). Molecular determinants of gating at the potassium-channel selectivity filter. Nat Struct Mol Biol *13*, 311-318.

Cordero-Morales, J. F., Jogini, V., Lewis, A., Vasquez, V., Cortes, D. M., Roux, B., and Perozo, E. (2007). Molecular driving forces determining potassium channel slow inactivation. Nat Struct Mol Biol *14*, 1062-1069.

Cortes, D. M., Cuello, L. G., and Perozo, E. (2001). Molecular architecture of full-length KcsA: role of cytoplasmic domains in ion permeation and activation gating. J Gen Physiol *117*, 165-180.

Cortes, D. M., and Perozo, E. (1997). Structural dynamics of the Streptomyces lividans K+ channel (SKC1): oligomeric stoichiometry and stability. Biochemistry *36*, 10343-10352.

Cuello, L. G., Cortes, D. M., and Perozo, E. (2004). Molecular architecture of the KvAP voltage-dependent K+ channel in a lipid bilayer. Science *306*, 491-495.

Cuello, L. G., Romero, J. G., Cortes, D. M., and Perozo, E. (1998). pH-dependent gating in the Streptomyces lividans K+ channel. Biochemistry *37*, 3229-3236.

De Biasi, M., Hartmann, H. A., Drewe, J. A., Taglialatela, M., Brown, A. M., and Kirsch, G. E. (1993). Inactivation determined by a single site in K+ pores. Pflugers Arch *422*, 354-363.

Delcour, A. H., Martinac, B., Adler, J., and Kung, C. (1989). Modified reconstitution method used in patch-clamp studies of Escherichia coli ion channels. Biophys J *56*, 631-636.

Demo, S. D., and Yellen, G. (1992). Ion effects on gating of the Ca(2+)-activated K+ channel correlate with occupancy of the pore. Biophys J *61*, 639-648.

Doyle, D. A., Morais Cabral, J., Pfuetzner, R. A., Kuo, A., Gulbis, J. M., Cohen, S. L., Chait, B. T., and MacKinnon, R. (1998). The structure of the potassium channel: molecular basis of K+ conduction and selectivity. Science *280*, 69-77.

Ficker, E., Jarolimek, W., Kiehn, J., Baumann, A., and Brown, A. M. (1998). Molecular determinants of dofetilide block of HERG K+ channels. Circ Res *82*, 386-395.

Gandhi, C. S., Clark, E., Loots, E., Pralle, A., and Isacoff, E. Y. (2003). The orientation and molecular movement of a k(+) channel voltage-sensing domain. Neuron *40*, 515-525.

Gao, L., Mi, X., Paajanen, V., Wang, K., and Fan, Z. (2005). Activation-coupled inactivation in the bacterial potassium channel KcsA. Proc Natl Acad Sci U S A *102*, 17630-17635.

Guidoni, L., Torre, V., and Carloni, P. (1999). Potassium and sodium binding to the outer mouth of the K+ channel. Biochemistry *38*, 8599-8604.

Hackos, D. H., Chang, T. H., and Swartz, K. J. (2002). Scanning the intracellular S6 activation gate in the shaker K+ channel. J Gen Physiol *119*, 521-532.

Heginbotham, L., LeMasurier, M., Kolmakova-Partensky, L., and Miller, C. (1999). Single streptomyces lividans K(+) channels: functional asymmetries and sidedness of proton activation. J Gen Physiol *114*, 551-560.

Heginbotham, L., Lu, Z., Abramson, T., and MacKinnon, R. (1994). Mutations in the K+ channel signature sequence. Biophys J *66*, 1061-1067.

Hille, B. (2001). Ion channels of excitables membranes, Third edn (Sunderland, MA: Sinauer Associates, Inc).

Hodgkin, A. L., and Huxley, A. F. (1952). A quantitative description of membrane current and its application to conduction and excitation in nerve. J Physiol *117*, 500-544.

Hoffmann, P., and Warner, B. (2006). Are hERG channel inhibition and QT interval prolongation all there is in drug-induced torsadogenesis? A review of emerging trends. J Pharmacol Toxicol Methods *53*, 87-105.

Hoshi, T., Zagotta, W. N., and Aldrich, R. W. (1990). Biophysical and molecular mechanisms of Shaker potassium channel inactivation. Science *250*, 533-538.

Hoshi, T., Zagotta, W. N., and Aldrich, R. W. (1991). Two types of inactivation in Shaker K+ channels: effects of alterations in the carboxy-terminal region. Neuron *7*, 547-556.

Humphrey, W., Dalke, A., and Schulten, K. (1996). VMD: visual molecular dynamics. J Mol Graph *14*, 33-38, 27-38.

Hunter, C. A. (1993). Sequence-dependent DNA structure. The role of base stacking interactions. J Mol Biol *230*, 1025-1054.

Hunter, C. A., Singh, J., and Thornton, J. M. (1991). Pi-pi interactions: the geometry and energetics of phenylalanine-phenylalanine interactions in proteins. J Mol Biol *218*, 837-846.

Hurst, R. S., Toro, L., and Stefani, E. (1996). Molecular determinants of external barium block in Shaker potassium channels. FEBS Lett *388*, 59-65.

Jiang, Y., Lee, A., Chen, J., Cadene, M., Chait, B. T., and MacKinnon, R. (2002). The open pore conformation of potassium channels. Nature *417*, 523-526.

Jiang, Y., Lee, A., Chen, J., Ruta, V., Cadene, M., Chait, B. T., and MacKinnon, R. (2003). X-ray structure of a voltage-dependent K+ channel. Nature *423*, 33-41.

Jin, T., Peng, L., Mirshahi, T., Rohacs, T., Chan, K. W., Sanchez, R., and Logothetis, D. E. (2002). The (beta)gamma subunits of G proteins gate a K(+) channel by pivoted bending of a transmembrane segment. Mol Cell *10*, 469-481.

Jones, T. A., Zou, J. Y., Cowans, S. W., and Kjeldgaard, M. (1991). Improved methods for building protein models in electron-density maps and the location of errors in these models. Acta Crystallography *sec 47*, 110-119.

Keating, M. T., and Sanguinetti, M. C. (2001). Molecular and cellular mechanisms of cardiac arrhythmias. Cell *104*, 569-580.

Kiss, L., LoTurco, J., and Korn, S. J. (1999). Contribution of the selectivity filter to inactivation in potassium channels. Biophys J *76*, 253-263.

Kumar, S., Bouzida, D., Swendsen, R. H., Kollman, P. A., and Rosenberg, J. M. (1992). The Weighted Histogram Analysis Method for Free-Energy Calculations on Biomolecules. I. The Methods. Journal of Computational Chemistry *13*, 1011-1021.

Kuo, A., Gulbis, J. M., Antcliff, J. F., Rahman, T., Lowe, E. D., Zimmer, J., Cuthbertson, J., Ashcroft, F. M., Ezaki, T., and Doyle, D. A. (2003). Crystal structure of the potassium channel KirBac1.1 in the closed state. Science *300*, 1922-1926.

Kurata, H. T., and Fedida, D. (2006). A structural interpretation of voltage-gated potassium channel inactivation. Prog Biophys Mol Biol *92*, 185-208.

Lange, A., Giller, K., Hornig, S., Martin-Eauclaire, M. F., Pongs, O., Becker, S., and Baldus, M. (2006). Toxin-induced conformational changes in a potassium channel revealed by solid-state NMR. Nature *440*, 959-962.

LeMasurier, M., Heginbotham, L., and Miller, C. (2001). KcsA: it's a potassium channel. J Gen Physiol *118*, 303-314.

Lenaeus, M. J., Vamvouka, M., Focia, P. J., and Gross, A. (2005). Structural basis of TEA blockade in a model potassium channel. Nat Struct Mol Biol *12*, 454-459.

Liu, J., Zhang, M., Jiang, M., and Tseng, G. N. (2002). Structural and functional role of the extracellular s5-p linker in the HERG potassium channel. J Gen Physiol *120*, 723-737.

Liu, Y., Holmgren, M., Jurman, M. E., and Yellen, G. (1997). Gated access to the pore of a voltage-dependent K+ channel. Neuron *19*, 175-184.

Liu, Y., and Joho, R. H. (1998). A side chain in S6 influences both open-state stability and ion permeation in a voltage-gated K+ channel. Pflugers Arch *435*, 654-661.

Liu, Y., Jurman, M. E., and Yellen, G. (1996). Dynamic rearrangement of the outer mouth of a K+ channel during gating. Neuron *16*, 859-867.

Liu, Y. S., Sompornpisut, P., and Perozo, E. (2001). Structure of the KcsA channel intracellular gate in the open state. Nat Struct Biol *8*, 883-887.

Lockless, S. W., Zhou, M., and MacKinnon, R. (2007). Structural and thermodynamic properties of selective ion binding in a K+ channel. PLoS Biol *5*, e121.

Long, S. B., Campbell, E. B., and Mackinnon, R. (2005a). Crystal structure of a mammalian voltage-dependent Shaker family K+ channel. Science *309*, 897-903.

Long, S. B., Campbell, E. B., and Mackinnon, R. (2005b). Voltage sensor of Kv1.2: structural basis of electromechanical coupling. Science *309*, 903-908.

Loots, E., and Isacoff, E. Y. (1998). Protein rearrangements underlying slow inactivation of the Shaker K+ channel. J Gen Physiol *112*, 377-389.

Lopez-Barneo, J., Hoshi, T., Heinemann, S. H., and Aldrich, R. W. (1993). Effects of external cations and mutations in the pore region on C-type inactivation of Shaker potassium channels. Receptors Channels *1*, 61-71.

Loussouarn, G., Phillips, L. R., Masia, R., Rose, T., and Nichols, C. G. (2001). Flexibility of the Kir6.2 inward rectifier K(+) channel pore. Proc Natl Acad Sci U S A *98*, 4227-4232.

Lu, T., Ting, A. Y., Mainland, J., Jan, L. Y., Schultz, P. G., and Yang, J. (2001). Probing ion permeation and gating in a K+ channel with backbone mutations in the selectivity filter. Nat Neurosci *4*, 239-246.

MacKinnon, R. (1991). Determination of the subunit stoichiometry of a voltage-activated potassium channel. Nature *350*, 232-235.

Mackinnon, R. (2004). Potassium channels and the atomic basis of selective ion conduction. Angew Chem Int Ed Engl *43*, 4265-4277.

Marban, E. (2002). Cardiac channelopathies. Nature *415*, 213-218.

McLaughlin, S. (1989). The electrostatic properties of membranes. Annu Rev Biophys Biophys Chem *18*, 113-136.

Meuser, D., Splitt, H., Wagner, R., and Schrempf, H. (1999). Exploring the open pore of the potassium channel from Streptomyces lividans. FEBS Lett *462*, 447-452.

Mienville, J. M., and Clay, J. R. (1996). Effects of intracellular K+ and Rb+ on gating of embryonic rat telencephalon Ca(2+)-activated K+ channels. Biophys J *70*, 778-785.

Miloshevsky, G. V., and Jordan, P. C. (2007). Open-state conformation of the KcsA K+ channel: Monte Carlo normal mode following simulations. Structure *15*, 1654-1662.

Molleman, A. (2002). Patch Clamping, An Introductory Guide to Patch Clamp Electrophysiology, Vol 1 (West Sussex, UK).

Murata, Y., Iwasaki, H., Sasaki, M., Inaba, K., and Okamura, Y. (2005). Phosphoinositide phosphatase activity coupled to an intrinsic voltage sensor. Nature *435*, 1239-1243.

Nishida, M., Cadene, M., Chait, B. T., and MacKinnon, R. (2007). Crystal structure of a Kir3.1-prokaryotic Kir channel chimera. Embo J *26*, 4005-4015.

Otwinowski, Z., and Minor, W. (1997). Macromolecular Crystallography, part A. Methods in Enzymology *276*, 307-326.

Panyi, G., and Deutsch, C. (2006). Cross talk between activation and slow inactivation gates of Shaker potassium channels. J Gen Physiol *128*, 547-559.

Peng, Y., Scarsdale, J. N., and Kellogg, G. E. (2007). Hydropathic analysis and comparison of KcsA and Shaker potassium channels. Chem Biodivers *4*, 2578-2592.

Perozo, E., Cortes, D. M., and Cuello, L. G. (1998). Three-dimensional architecture and gating mechanism of a K+ channel studied by EPR spectroscopy. Nat Struct Biol *5*, 459-469.

Perozo, E., Cortes, D. M., and Cuello, L. G. (1999). Structural rearrangements underlying K+-channel activation gating. Science *285*, 73-78.

Perozo, E., MacKinnon, R., Bezanilla, F., and Stefani, E. (1993). Gating currents from a nonconducting mutant reveal open-closed conformations in Shaker K+ channels. Neuron *11*, 353-358.

Posson, D. J., Ge, P., Miller, C., Bezanilla, F., and Selvin, P. R. (2005). Small vertical movement of a K+ channel voltage sensor measured with luminescence energy transfer. Nature *436*, 848-851.

Proks, P., Capener, C. E., Jones, P., and Ashcroft, F. M. (2001). Mutations within the P-loop of Kir6.2 modulate the intraburst kinetics of the ATP-sensitive potassium channel. J Gen Physiol *118*, 341-353.

Ranatunga, K. M., Shrivastava, I. H., Smith, G. R., and Sansom, M. S. (2001). Side-chain ionization states in a potassium channel. Biophys J *80*, 1210-1219.

Rasmusson, R. L., Morales, M. J., Wang, S., Liu, S., Campbell, D. L., Brahmajothi, M. V., and Strauss, H. C. (1998). Inactivation of voltage-gated cardiac K+ channels. Circ Res *82*, 739-750.

Roden, D. M., and Balser, J. R. (1999). A plethora of mechanisms in the HERG-related long QT syndrome. Genetics meets electrophysiology. Cardiovasc Res *44*, 242-246.

Ruta, V., Chen, J., and MacKinnon, R. (2005). Calibrated measurement of gating-charge arginine displacement in the KvAP voltage-dependent K+ channel. Cell *123*, 463-475.

Sanguinetti, M. C. (1999). Dysfunction of delayed rectifier potassium channels in an inherited cardiac arrhythmia. Ann N Y Acad Sci *868*, 406-413.

Schoppa, N. E., McCormack, K., Tanouye, M. A., and Sigworth, F. J. (1992). The size of gating charge in wild-type and mutant Shaker potassium channels. Science *255*, 1712-1715.

Schrempf, H., Schmidt, O., Kummerlen, R., Hinnah, S., Muller, D., Betzler, M., Steinkamp, T., and Wagner, R. (1995). A prokaryotic potassium ion channel with two predicted transmembrane segments from Streptomyces lividans. Embo J *14*, 5170-5178.

Seebohm, G., Sanguinetti, M. C., and Pusch, M. (2003). Tight coupling of rubidium conductance and inactivation in human KCNQ1 potassium channels. J Physiol *552*, 369-378.

Seoh, S. A., Sigg, D., Papazian, D. M., and Bezanilla, F. (1996). Voltage-sensing residues in the S2 and S4 segments of the Shaker K+ channel. Neuron *16*, 1159-1167.

Shapiro, M. S., and DeCoursey, T. E. (1991). Selectivity and gating of the type L potassium channel in mouse lymphocytes. J Gen Physiol *97*, 1227-1250.

Shealy, R. T., Murphy, A. D., Ramarathnam, R., Jakobsson, E., and Subramaniam, S. (2003). Sequence-function analysis of the K+-selective family of ion channels using a comprehensive alignment and the KcsA channel structure. Biophys J *84*, 2929-2942.

Smith, P. L., Baukrowitz, T., and Yellen, G. (1996). The inward rectification mechanism of the HERG cardiac potassium channel. Nature *379*, 833-836.

Spector, P. S., Curran, M. E., Zou, A., Keating, M. T., and Sanguinetti, M. C. (1996). Fast inactivation causes rectification of the IKr channel. J Gen Physiol *107*, 611-619.

Spruce, A. E., Standen, N. B., and Stanfield, P. R. (1989). Rubidium ions and the gating of delayed rectifier potassium channels of frog skeletal muscle. J Physiol *411*, 597-610.

Starkus, J. G., Kuschel, L., Rayner, M. D., and Heinemann, S. H. (1997). Ion conduction through C-type inactivated Shaker channels. J Gen Physiol *110*, 539-550.

Stuhmer, W., Ruppersberg, J. P., Schroter, K. H., Sakmann, B., Stocker, M., Giese, K. P., Perschke, A., Baumann, A., and Pongs, O. (1989). Molecular basis of functional diversity of voltage-gated potassium channels in mammalian brain. Embo J *8*, 3235-3244.

Sun, Z. P., Akabas, M. H., Goulding, E. H., Karlin, A., and Siegelbaum, S. A. (1996). Exposure of residues in the cyclic nucleotide-gated channel pore: P region structure and function in gating. Neuron *16*, 141-149.

Swenson, R. P., Jr., and Armstrong, C. M. (1981). K+ channels close more slowly in the presence of external K+ and Rb+. Nature *291*, 427-429.

Takeuchi, K., Takahashi, H., Kawano, S., and Shimada, I. (2007). Identification and characterization of the slowly exchanging pH-dependent conformational rearrangement in KcsA. J Biol Chem *282*, 15179-15186.

Torrie, G. M., and Valleau, J. P. (1977). Nonphysical sampling distributions in Monte Carlo free-energy estimation: umbrella sampling. J Comp Phys *23*, 187-199.

Valiyaveetil, F. I., Leonetti, M., Muir, T. W., and Mackinnon, R. (2006a). Ion selectivity in a semisynthetic K+ channel locked in the conductive conformation. Science *314*, 1004-1007.

Valiyaveetil, F. I., Sekedat, M., MacKinnon, R., and Muir, T. W. (2006b). Structural and functional consequences of an amide-to-ester substitution in the selectivity filter of a potassium channel. J Am Chem Soc *128*, 11591-11599.

VanDongen, A. M. (2004). K channel gating by an affinity-switching selectivity filter. Proc Natl Acad Sci U S A *101*, 3248-3252.

Yang, J., Yu, M., Jan, Y. N., and Jan, L. Y. (1997a). Stabilization of ion selectivity filter by pore loop ion pairs in an inwardly rectifying potassium channel. Proc Natl Acad Sci U S A *94*, 1568-1572.

Yang, Y., Yan, Y., and Sigworth, F. J. (1997b). How does the W434F mutation block current in Shaker potassium channels? J Gen Physiol *109*, 779-789.

Yellen, G. (1998). The moving parts of voltage-gated ion channels. Q Rev Biophys *31*, 239-295.

Yellen, G. (2002). The voltage-gated potassium channels and their relatives. Nature *419*, 35-42.

Yellen, G., Sodickson, D., Chen, T. Y., and Jurman, M. E. (1994). An engineered cysteine in the external mouth of a K+ channel allows inactivation to be modulated by metal binding. Biophys J *66*, 1068-1075.

Yifrach, O., and MacKinnon, R. (2002). Energetics of pore opening in a voltage-gated K(+) channel. Cell *111*, 231-239.

Zheng, J., and Sigworth, F. J. (1997). Selectivity changes during activation of mutant Shaker potassium channels. J Gen Physiol *110*, 101-117.

Zheng, J., and Sigworth, F. J. (1998). Intermediate conductances during deactivation of heteromultimeric Shaker potassium channels. J Gen Physiol *112*, 457-474.

Zhou, M., and MacKinnon, R. (2004). A mutant KcsA K(+) channel with altered conduction properties and selectivity filter ion distribution. J Mol Biol *338*, 839-846.

Zhou, M., Morais-Cabral, J. H., Mann, S., and MacKinnon, R. (2001a). Potassium channel receptor site for the inactivation gate and quaternary amine inhibitors. Nature *411*, 657-661.

Zhou, Y., and MacKinnon, R. (2003). The occupancy of ions in the K+ selectivity filter: charge balance and coupling of ion binding to a protein conformational change underlie high conduction rates. J Mol Biol *333*, 965-975.

Zhou, Y., Morais-Cabral, J. H., Kaufman, A., and MacKinnon, R. (2001b). Chemistry of ion coordination and hydration revealed by a K+ channel-Fab complex at 2.0 A resolution. Nature *414*, 43-48.

Zou, A., Xu, Q. P., and Sanguinetti, M. C. (1998). A mutation in the pore region of HERG K+ channels expressed in Xenopus oocytes reduces rectification by shifting the voltage dependence of inactivation. J Physiol *509 (Pt 1)*, 129-137.